TESI DI DOTTORATO

UNIVERSITÀ DEGLI STUDI DI NAPOLI "FEDERICO II"

DIPARTIMENTO DI INGEGNERIA ELETTRONICA
E DELLE TELECOMUNICAZIONI

DOTTORATO DI RICERCA IN
INGEGNERIA ELETTRONICA E DELLE TELECOMUNICAZIONI

CHARACTERIZATION OF HELIUM IMPLANTATION IN SILICON FOR THE OPTIMISATION OF STATIC AND DYNAMIC BEHAVIOUR OF POWER DIODES

LUIGI MELE

Il coordinatore del Corso di Dottorato
Ch.mo Prof. Giovanni POGGI

Il Tutore
Ch.mo Prof. P. Spirito

Anno Accademico 2006-2007

Index

Introduction

Research activity has been focused on experimental and numeric characterization of recombination lifetime control techniques in silicon power devices, with special attention to helium implantation. When power diodes have to switch off, the stored charge is to swept out before the current becomes zero. Reducing the recombination lifetime, this transient, termed *reverse recovery*, becomes faster but on the other hand forward voltage drop and leakage current increase. Damaging the lattice structure, the created defects can act as recombination centers for the free charge carriers. Lifetime control techniques aim just at creating recombination centers, whose effectiveness on the recombination process depends on the nature of the defects. There are two possible approaches: the reduction in the whole volume of the device (gold or platinum diffusion) or in a localised region (helium implantation). The latter technique allows the best trade-off between static and dynamic performances to be obtained and that is why it is the most attractive.

The aim of the activity was the extraction of a valid model for the description of the defects created by helium implantation in silicon. In fact although it is know that helium implantation is more effective in the performances optimization, a model to be used in a physically-based simulator would be suitable, in order to design the best device without manufacturing many test devices.

In order to reach our purpose, the differential measurement technique has been used. Making use of a special test structure, the technique is able to evaluate the in-depth recombination lifetime profile along a low-doped silicon layer. By means of measurement at different temperatures, it is possible to extract the energy level and the concentration of the introduced recombination centers.

Even though helium is a noble gas and it does not react with the lattice atoms, we found that it affects also the effective doping concentration around the penetration depth. By means the same test

structure, we propose a method which allows the evaluation the effective doping along a silicon layer starting from the measurement of the output static characteristic. The method is all electrical and the knowledge of the effective doping involves also an improvement of the resolution of the recombination lifetime technique.

A better comprehension of the helium implantation effects has been therefore possible and the dominant recombination centers have been identified, whose validity has been checked by means of the simulator.

Having a valid model for the defects distribution related to helium implantation, the numeric analysis of diodes with local control of lifetime has been possible.

In particular we tried to understand how helium implantation can improve the ruggedness of power diodes on the dynamic avalanche, which is one of the main failure mechanism in power diodes. During the switch, the voltage across the diode rises while charge carries are still present. It can happen that avalanche multiplication takes place even though the voltage is less than the breakdown value. If the diode is under avalanche multiplication condition, current through the device increases instead of decreasing and in the worst case this effect can lead to the device destruction. Since the dynamic avalanche onset is strictly related to the removal speed of charge carriers, we studied how the localised lifetime control can avoid the device reaching the dynamic avalanche condition.

Based on the results of the simulations, experimental power diodes have been manufactured.

List of publications

- S. Daliento, L. Mele, P. Spirito, B.N. Limata, L. Gialanella, R. Carta, L. Bellemo, "An experimental analysis of localized lifetime and resistivity control by Helium" , ISPSD 2005, Santa Barbara, June 2005, Page(s) 1-4
- L. Bellemo, R. Carta, S. Daliento, L. Gialanella, B.N. Limata, L.Mele, M. Romano, A. Sanseverino, P. Spirito, Electrical measurement of the lattice damage induced by alfa-particle implantation in silicon, Vacuum 78 (2005) 623-626
- S. Daliento, L. Mele, P. Spirito, B. N. Limata, All electrical resistivity profiling technique for ion implanted semiconductor materials, Materials Science and Engineering B, 124-125 December (2005) 310-313
- S. Bellone, G.D. Licciardo, S. Daliento, L. Mele, Experimental measurements of majority and minority carrier lifetime profile in SI eplilayers by the use of an improved OCVD method, IEEE Electron Device Letters, Vol. 26, No. 7, July 2005
- S. Daliento, L. Mele, P. Spirito, B.N. Limata, L. Gialanella, R. Carta, L. Bellemo, "Helium implantation in silicon: detailed experimental analysis of resistivity and lifetime profiles as a function of the implantation dose and energy" , ISPSD 2006, Naples, June 2006, Page(s): 259-262
- S. Daliento, L. Mele, L. Lancelotti, P. Morvillo, E. Bobeico, F. Roca, L. Pirozzi, "Performances characterization of concentration solar cells by means of I-V and lifetime measurements made with the QSSPC technique" 21th European Photovoltaic Solar Energy Conference and Exhibition, Dresden, September 2006
- S. Daliento, L. Mele, P. Spirito, L. Gialanella, B. N. Limata, M. Romano, Experimental measurement of in-depth secondary defects distribution produced by helium implantationin silicon, Materials Science and Engineering B, 90-93 253 December (2006)

- S.Daliento, L. Mele, Approximate closet-form analytical solution for minority carrier transport in opaque heavily doped regions under illuminated conditions, IEEE Transactions on Electron Devices, Vol. 53, No. 11, November 2006
- S. Daliento, L. Mele, E. Bobeico, L. Lancellotti, P. Morvillo, Analytical modelling and minority current measurements for the determination of the emitter surface recombination velocity in silicon solar cells, Solar Energy Materials and Solar Cells, Solar Energy Materials and Solar Cells Volume 91, Issue 8, 4 May 2007, Pages 707-713
- S. Daliento, L. Mele, P. Spirito, L. Gialanella, B. N. Limata , Lifetime and resistivity modifications induced by helium implantation in silicon: experimental analysis with the ac profiling technique, Journal of Applied Physics, accepted

Chapter 1

Lifetime tailoring in power diodes

Modern switching applications need a freewheeling diode as a security-device, in order to avoid abrupt current variations, which could cause dangerous voltage overshoots, due to the stray inductances in the circuit [1,2].

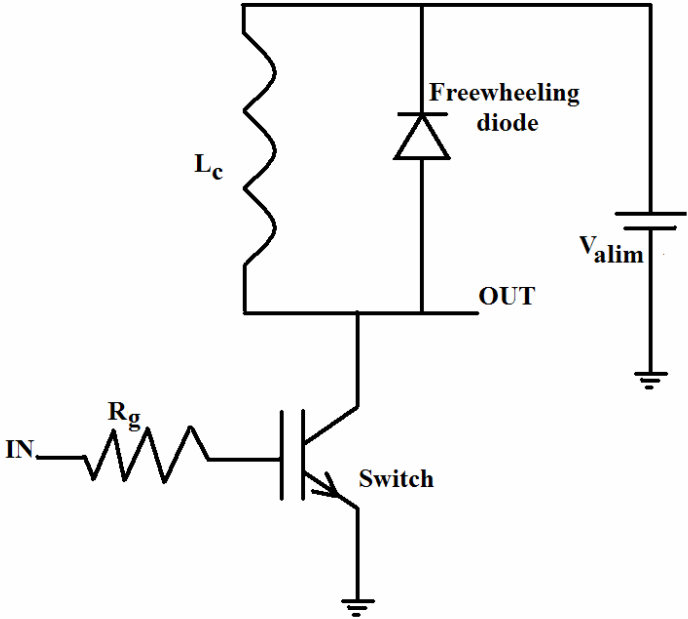A simple example of switching circuit is shown in Fig 1:

Fig. 1 Schematic of the switching circuit

It is the switching stage of a dc-dc converter with chopper configuration.

This topology is no isolated, that is, input and output voltages share a common ground.

When the state of the switch is ON, a large current flows through the inductor, depending on the different applications.

When the switch is turned-off, if the current which flows into the inductor reduces abruptly to zero, a large voltage spike would be produced, recalling the relation between the current and the voltage across the inductor:

$$V = L\frac{di}{dt} \tag{1}$$

This overshoot could destroy the circuit components and, therefore, an alternative path is needed where the inductor current can flow. That is why a freewheeling diode is used in parallel to the inductor. Turning-off the switch, the diode works in forward mode and the current can flow freely through it. On the contrary, when the switch is turned-on again, the diode becomes reverse biased. Nevertheless, current does not reach the zero value outright, but a transient occurs, during which it decreases to a negative peak and after it drops gradually to the leakage value. This transient is termed reverse recovery [3] and represents one of the most critical restrictions for the performances of these circuits.

Today switching applications make a wide use of IGBTs, which combine the structures of both MOS and bipolar devices, allowing a low power loss (both static and dynamic) and a large current density to be obtained. Unluckily, IGBT is a unidirectional conducting device and, as above described, an antiparallel diode is needed. Nevertheless, the freewheeling diode, which is essential anyway, can reduce the performances, determining a switching velocity reduction and a power loss increase. Furthermore the diode reverse current has to flow through the IGBT, the total current of which can also become two or three times bigger than the ON-state value, leading the device to work over the SOA limits. Therefore, nowadays, the freewheeling diode represents the weak component of the power electronic circuits.

The aim is to design a power diode with a reverse recovery which is on the one hand fast, in order to increase the switching frequency and reduce the dynamic power loss, and on the other hand soft in order to avoid the snappy phenomenon and the consequent voltage spikes[4].

To achieve this goal and make the power diode engineered, we have to find out the physical parameter from which the reverse recovery strongly depends and try to modify it conveniently for our purpose.

1.1   Reverse Recovery

Power diodes have the typical PIN structure shown in Fig. 2:
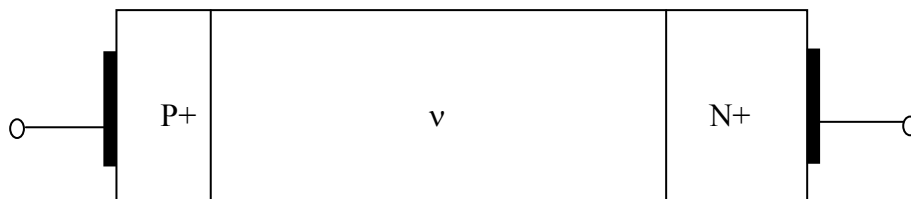
Fig. 2 Basic structure of a P-ʋ-N diode

The drift layer allows the depletion region to extend when a negative voltage is applied and the doping concentration is low in order to sustain high breakdown voltage. The drawback of the low doping concentration is a high series resistance. But in forward mode these devices work at high injection level and charge carriers fill the drift region: the effect is called conductivity modulation and allows the series resistance to be reduced. Nevertheless, during the turn-off these carriers become an issue, because they have to be swept out before the diode exhibits its blocking capability.

The structure can be obtained in two different ways:

- •   For low thickness a low-doped layer is grown epitaxially on a high-doped substrate, and at the end the anode region is created by implantation.
- •   If the thickness is too large, as well as in the high power applications, the epitaxial grown is not suitable. In this case the starting material is low doped and both the anode region and the high-doped cathode region are created by implantation.

By means of the ATLAS-Silvaco simulator, we can analyse the internal physics of the device when it is switched-OFF. It is a 700V power diode: the drift region thickness is 58μm and its doping concentration $2x10^{14}$ cm^{-3}. The active area is $3.46x10^{-2}$ cm^2.

The typical reverse recovery waveform is shown in Fig. 3, for a forward current of 10A and a reverse voltage of 200V:
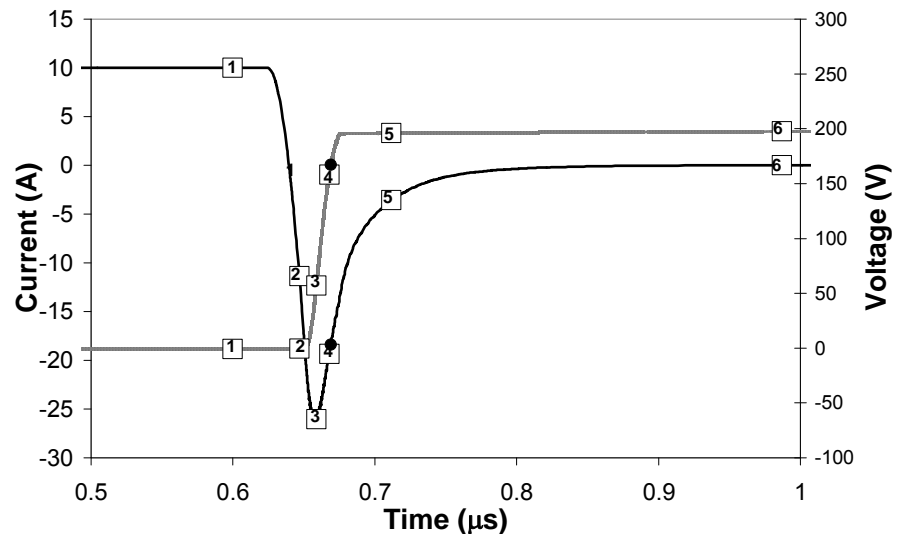

Fig. 3 Reverse recovery of power diodes simulated by ATLAS-Silvaco

Firstly, a positive voltage is applied across the junction and a constant current I_F flows through the device. The carrier amount is greater than the doping concentration and it is almost uniform along the drift region, as depicted in Fig. 4 at the instant (1). As the switch

starts, the current does not become zero at once, because the charge can not disappear instantaneously.

On the contrary the current drops at a constant rate di/dt, which depends on both stray inductance and charging velocity of the input capacitance of the switch.

The stored charge starts to decrease near the PN junction, while the voltage across the diode keeps almost constant. At the instant (2) the sign of the slope of the hole distribution near the junction changes and the current becomes negative.
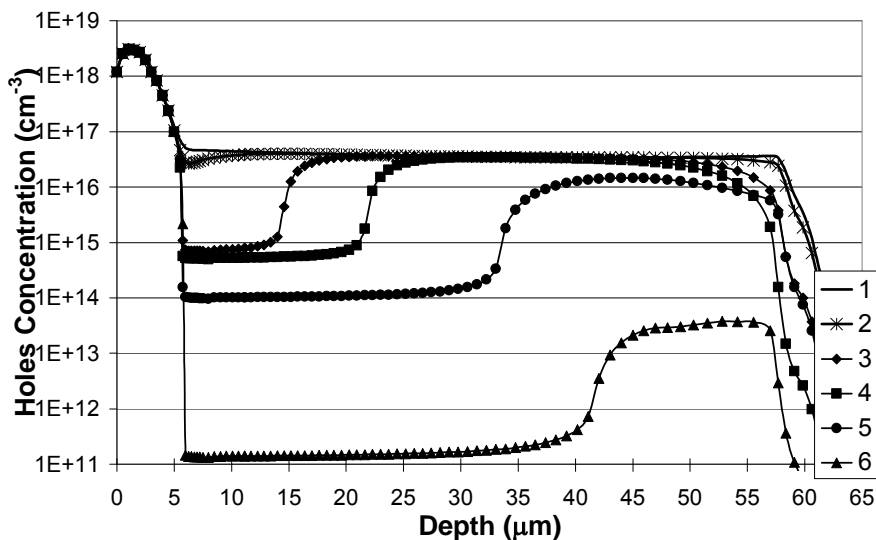

Fig. 4 Holes concentration at the time instants showed in Fig.3

At the instant (3), the current reaches a negative peak and the depletion region extends into the drift layer and thereby the reverse voltage across the diode rises at a rate dV/dt. Into the depletion region an electric field appears (Fig. 5) which speeds up the holes toward the anode and the electrons toward the cathode. The charge concentration is almost constant and, recalling the Poisson's equation, the shape is triangular. In this phase the carrier concentration holds high at the bottom, near the substrate, while the excess carriers progressively reduce in the depletion region, which is widening into the drift region. From the instant (3) onwards the current drops to the zero value.

The black circle in Fig.3 represents the instant of the maximum power dissipation and the electric field has got its largest value near the PN junction (instant 4). Afterwards the depleted region extends more and more and the maximum value of the electric field starts to decrease.
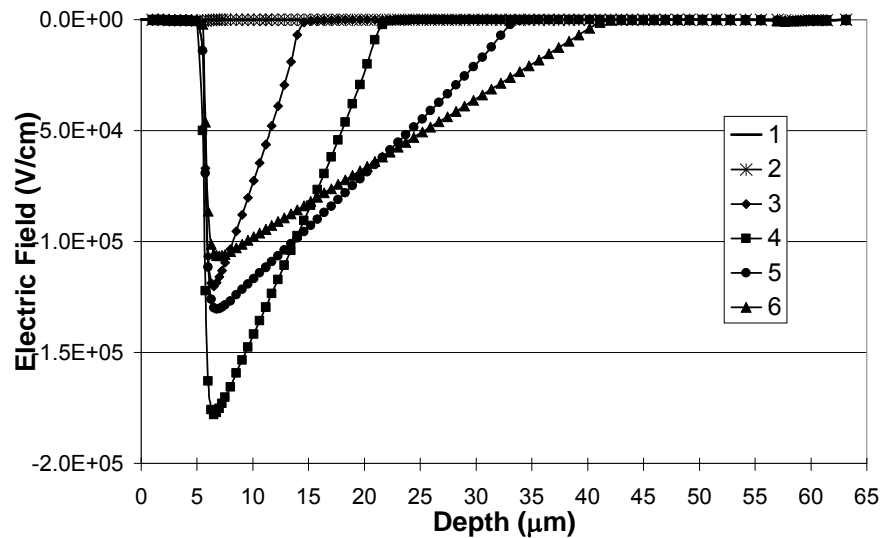
Fig. 5 Electric field strength at the time instants showed in Fig.3

At the instant (5) the voltage has already reached the final value, but the current is not zero yet. At the instant (6) only the leakage current flows through the device, whereas the hole number is decreasing toward the equilibrium concentration. The electric field still has the typical linear shape, being constant the doping into the drift region.

1.1.1 Dependence on the recombination lifetime

The time interval between the instant when the current crosses the zero and the instant when it reaches the negative peak depends on both circuit parameters and diode structure.

We can write the charge control equation:

$$\frac{dQ}{dt} = -i(t) - \frac{Q(t)}{\tau_{eff}} \qquad (2)$$

where Q is the charge stored in the drift region and is related to the forward current value I_F, τ_{eff} is the effective lifetime and i(t) is the diode current, whose expression is:

$$i(t) = I_F - (V_R / L_C)t \qquad (3)$$

where L_C is the circuit inductance and V_R the applied reverse voltage.

We can observe that the rate of change dQ/dt is sum of two components: the reverse recovery current, which sweeps out charge carriers from the drift region and the recombination current.

For a given forward current (and then an initial charge Q) and a rate di/dt (and then a fixed reverse recovery current), from (2) the rate of change dQ/dt depends only on the minority carrier recombination lifetime. The lower its value, the faster the charge disappears near the junction and the lower the reverse current peak is.

Fig. 6 plots the reverse recovery of the same diode structure with a lower lifetime value into the drift region. The lower the lifetime, the faster hole and electron recombine each other and thereby the charge disappears.
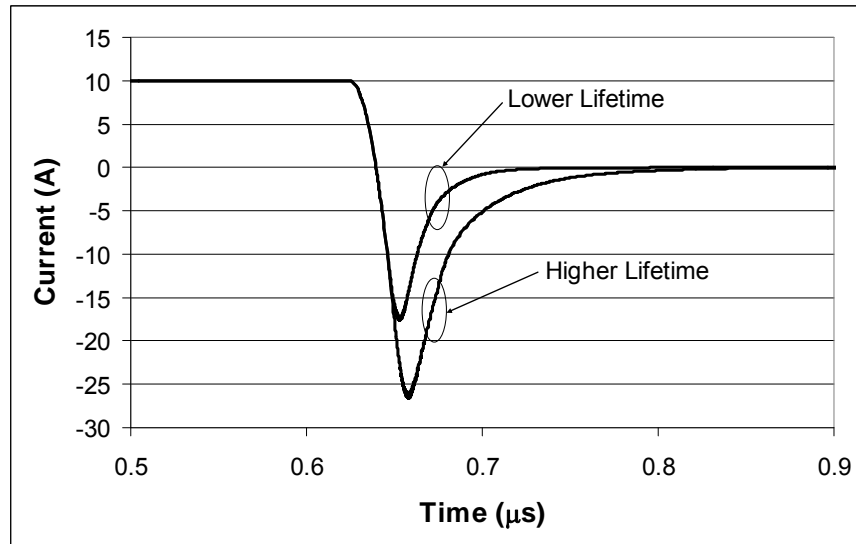
Fig. 6 Reverse recoveries evaluated setting two different recombination lifetime within the drift region

In order to obtain fast diodes, the reverse recovery has to be as fast as possible.

After the reverse current peak, also the rate of change of the current becomes dependent on the device characteristics. This phase is very critical for the circuit: if the charge concentration is too low at the current peak, carriers could disappear too fast causing an abrupt reduction of the current. This condition must be avoided, because either oscillations or voltage spikes could occur, leading the system in a non-safety condition: a soft recovery is suitable, event though the transient is slower. The charge amount left in the drift region after the reverse peak depends on the lifetime in the drift region, far from the junction edge, and carriers disappear faster if the recombination lifetime is low.

Therefore the charge carrier recombination process strongly weights on the dynamic behaviour and the recombination lifetime is the main parameter to take under control in order to improve it.

1.2   Recombination lifetime

As observed, the recombination lifetime is one of the most critical parameter in power diodes and therefore we need to recur to special control techniques.

The recombination is a process by which an electron-hole pair disappears into semiconductor devices.

As know, the silicon is an indirect bandgap semiconductor and the electrons at the bottom of the conduction band have a different momentum in respect to the holes at the top of the valence band. Therefore the direct transition is not very likely and the dominant recombination mechanism occurs via recombination centres within the bandgap [5].

Any impurity or lattice defects can introduce allowed energy levels within the bandgap. The trap-assisted recombination is a two-steps process. If a trap is empty, an electron can fill it and the centre is unavailable to capture another electron, but it can catch a hole. If this event occurs, the recombination centre is empty again, but an electron-hole pair is missing. It is worth noting that the hole capture is equivalent to the falling of an electron to the valence band. The energy lost in the process is given up as heat to the lattice.

The recombination rate U is described by the SRH model [6]:

$$U = \frac{v_{th}\sigma_n\sigma_p N_t \left(p_n n_n - n_i^2\right)}{\sigma_p\left[p_n + n_i e^{(E_i - E_t)/kT}\right] + \sigma_n\left[n_n + n_i e^{(E_t - E_i)/kT}\right]} \qquad (4)$$

In (4) v_{th} is the thermal velocity, N_t the recombination centre concentration and σ_n and σ_p the capture cross-section of respectively electron and hole. The capture cross-section takes into account the capability of capturing an electron or a hole.

Typically, the recombination mechanism described by the SRH model is dominant when the carrier concentration is less than 10^{18} cm^{-3}. When the concentration becomes four times greater than the background doping, the Auger recombination takes place. Unlike the SRH mechanism, the Auger recombination is not dependent on the material property.

From (4), we can see that the recombination rate strongly depends on the position of the centre into the forbidden energy gap: the nearer to the intrinsic Fermi level the centre is, the higher the recombination rate is and therefore the more effective the trap is in reducing the carrier lifetime.

To better understand the dependence on both the energy level and the temperature, it is worth recalling the occupancy probability of an electronic state within the forbidden bandgap, described by the Fermi-Dirac distribution function [6]:

$$F(E) = \frac{1}{1 + \exp[(E - E_F)/kT]} \tag{5}$$

where k is the Boltzmann constant, E_F the energy of the Fermi level, E the energy level of the recombination centre and T the absolute temperature in Kelvin degrees. If the energy of a recombination centre is equal to E_F, its occupancy probability is 0.5.

For a given recombination centre, if its energy E* is lower than the Fermi energy level, the probability that it catches an electron is high and thereby it takes part in the recombination process, capturing a free hole. On the contrary, if E* is greater than E_F, the probability of capturing an electron is low.

In intrinsic silicon, the Fermi energy level corresponds to the intrinsic Fermi level, lied in the centre of the forbidden bandgap. When a semiconductor is doped by impurities, the position of E_F approaches to either the edge of the conduction band or the valence one, depending on type and concentration of the impurity. The position of the Fermi energy level within the forbidden band in N-doped material is given by [6]:

$$E_C - E_F = kT \ln(N_C/N_D) \tag{6}$$

where N_C is the effective density of states in conduction band and N_D is the doping concentration.

At low temperature E_F is near to the conduction band edge and, hence, the recombination process is most likely: the deeper the energy level E*, the greater the occupancy probability F(E*) is and the centre can take part in the recombination process. Increasing the temperature,

E_F approaches to the middle of the bandgap and the semiconductor tends to become intrinsic.

As the Fermi energy level passes under the level E*, the probability of capturing an electron decreases and the effectiveness of the recombination centre reduces.

Therefore, we can conclude that deep centres are more suitable, because they take part in the recombination process in a wider temperature range and power devices usually work at temperature greater than 100°C.

Nevertheless, there is another dominant mechanism called generation, which interests the charge carriers: it is the process by which an electron-hole couple is created. A common expression of the generation lifetime is [5]:

$$\tau_g = \frac{2\cosh\left(\dfrac{E_i - E_t}{kT}\right)}{v_{th}\sigma_0 N_t} \qquad (7)$$

where the hole and the electron capture cross-section are assumed equal to σ_0.

The generation lifetime is a function of the centre energy level as well as the recombination lifetime: an energy level is more effective as generation centre if it is near to the midgap.

Recombination lifetime and generation lifetime can differ up to two orders of magnitude.

Basically in power diodes recombination lifetime affects the forward voltage drop and the dynamic behaviour, whereas the generation lifetime controls the leakage current and, consequently, the breakdown voltage value.

Theoretically into the forbidden energy gap of semiconductors there are not allowed energy levels, but any defects in the lattice introduce new energy levels within the bandgap. The lifetime control techniques aim at damaging opportunely the crystal lattice. The created defects act as recombination centres, the relevant parameters of which, as energy level, concentration and capture cross-section, depend on the defect typology. The nature of the centre can change according to the particular technique and the specific element used for the defects creation.

In way of improving the dynamic behaviour of power diodes, a technique which creates deep levels would be desirable, because the recombination rate is higher and the charge carriers disappear faster. Nevertheless, at the same time we must take into account the generation lifetime: when temperature increases, power devices with deep levels suffer from high leakage current which strongly affects the avalanche breakdown onset and, in general, lifetime killers which introduce deep levels should be avoided.

Therefore we need a good characterization technique, in order to find out the typology of the introduced centres by means of the different lifetime tailoring techniques and pick out that one which allows the best trade-off to be obtained.

1.1.2 Lifetime tailoring techniques

Basically, the lifetime engineering has got two different approaches:

- Reducing the lifetime in the whole device volume, by means the introduction of noble metals, like platinum or gold
- Reducing the lifetime in a narrow region of the device, by means ionic implantation

The most well-established technique is the noble metals diffusion which introduces recombination centres in the entire device [7,8]. The chosen species is deposited on the back of the device and let it diffuse into the device at high temperature. The diffusion temperature determines the solid solubility of the species into the silicon. The typical diffusion temperature range is from 800°C to 1000°C. This step must precede the realization of the contacts, because the diffusion temperature is greater than the eutectic one.

This technique is well-known and is used in the industry for ages.

In general the lifetime control techniques on the one hand allow the dynamic behaviour to be improved but on the other hand cause a

worsening of the static performances. In fact the forward voltage drop inversely depends on the recombination lifetime, while the energy levels in the bandgap act as generation centre during the reverse biasing, with consequent increase of the leakage current. So the best trade-off between static and dynamic behaviour is always to aim.

The drawback of platinum and gold diffusion is that, increasing too much the defects concentration, the static power loss could become dominant in respect to the dynamic one and therefore no longer suitable.

Moreover, the diffusion velocity in the temperature range 700°C-1000°C is very fast, making the control of the defects distribution almost difficult [9].

It is worth mentioning that platinum and gold introduce electrical active defects [10]. These centres tend to compensate the background doping due to the energy levels lied near either the conduction band edge or the valence one. If the defects concentration becomes comparable to the number of shallow impurities, compensation effects take place and the resistivity of the starting material changes. If the number of the defects overcomes the doping concentration, the material is overcompensated and its conductivity type inverts. The number of the defects introduced by platinum diffusion is typically less than one order of magnitude in respect to gold. Therefore the platinum is more suitable as lifetime killer, because the smaller defects concentration prevents doping compensation effects.

The other tailoring technique is the ion implantation and allows the lifetime to be modified in a localized region into the device [11,12]. The energy implantation and the dose determine respectively the position and the concentration of the defects distribution, which typically has got a gaussian shape.

This technique gives a new degree of freedom to the designers [13]: in fact, due to the localisation, the properties of the lattice are not completely modified and then the static behaviour is not drastically worsened [14,15]. On the other hand, by choosing the best defects position the dynamic performances can be improved considerably[16].

The defects created by helium implantation, called primary defects, are unstable and, hence, an annealing process is needed. At about 250°C-300°C the primary defects recombine each others or with other impurities, leading to a stable defects distribution within the device. The typical lifetime killers are either helium or hydrogen.

Being a noble gas, helium tends to leave the lattice and therefore there are not defects related to the implanted species. Moreover, as it is heavier than hydrogen it localises in a narrower region increasing the spatial selectivity of the lifetime control. For this reasons, helium is often preferred to hydrogen.

The greatest advantage of ionic implantation is that the lifetime control technological step is carried out after the complete realization of the device, while the gold or platinum diffusion is realized before the metal contacts, due to the high needed temperature, getting the manufacturing process more complex. Furthermore it is a reproducible process and therefore it is more reliable than the noble metals diffusion. Nevertheless the ionic implantation requires very expensive equipment and therefore it is not used for all the applications, but the metals diffusion often allows satisfactory performances to be obtained keeping low the production cost.

1.2   Experimental analysis of platinum diffused diodes

At the beginning of our work, we carried out several test devices, in order to study the effects of the lifetime engineering processes on the power diodes performances.

Firstly, we have analysed metal diffused devices: as lifetime killer we used platinum, because gold introduces deeper recombination centres, causing a leakage current up to ten times greater than platinum and the greater defects concentration can affect considerably the electrical properties of the diffused device [17].

The platinum has been diffused for 40 minutes at three different temperatures, 880°C, 920°C and 940°C, which correspond to three different defects concentrations. Below we term the untreated device STD (standard device), and the platinum diffused device Pt880, Pt920 and Pt940, according to the diffusion temperature.

Fig.7 shows the comparison of the reverse recoveries measured on untreated device and platinum diffused devices. The switching

conditions are not particularly stressed, being the forward current 8A, the reverse voltage 200V and the rate di/dt 250A/μs.
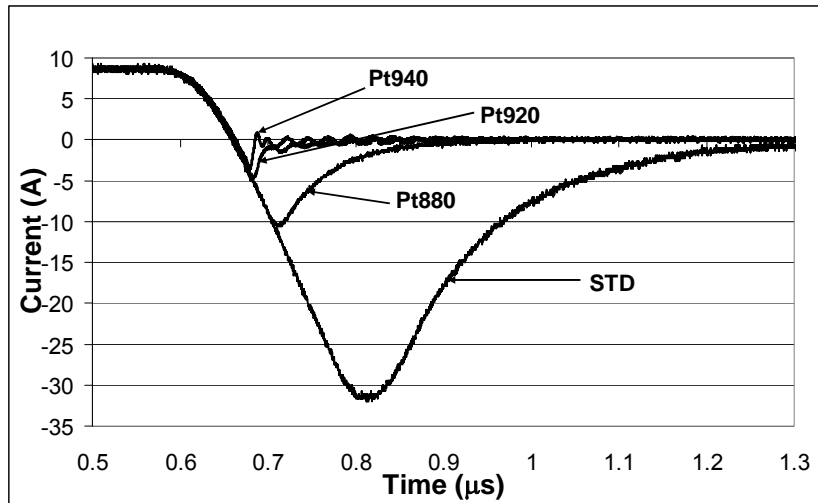

Fig. 7 Comparison between the reverse recoveries of untreated diode (STD) and diodes diffused by platinum at different temperatures

We can observe how remarkable the effect of the platinum is. The untreated device has a reverse peak of 31A, which is nearby four times as large as the value of the forward current. In more stressful conditions it would be quite impossible to measure the reverse recovery of this diode without damaging the circuit components.

The lowest platinum concentration (Pt880) allows the reverse peak to be reduced at about 33% in respect to the STD device and its value becomes comparable to the forward current. Increasing the defects concentration the peak reduces further on, becoming half of the forward current for a diffusion temperature of 940°C.

Reducing the reverse peak, also the reverse recovery time becomes shorter, varying from 400ns for the untreated device to 40ns for the device diffused at 940°C. As the platinum concentration increases, the reverse recovery becomes snappier and in Pt940 some small oscillations appear. In this case the switching conditions are not stressful and thus this effect is not dangerous.

From this curves, we could guess the temperature of 940 is the more suitable, but we have not taken into account the static behaviour

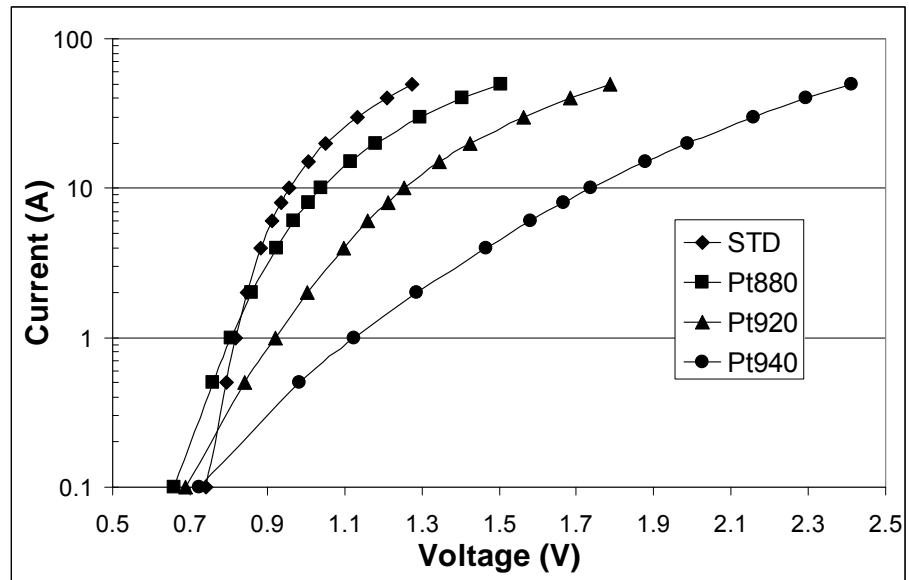yet. Fig. 8 shows the forward IV characteristic of the analyzed devices.

Fig. 8 Forward characteristic of untreated diode (STD) and diodes diffused by platinum at different temperatures

Increasing the temperature diffusion and, hence, the defects concentration, the voltage drop rises due to two effects: the carrier concentration is reduced because of the lower recombination lifetime and the resistivity is increased because of the doping compensation effect. The worsening of the forward behaviour is very drastic and at 10A the ON-state voltage across Pt940 is about twice as much that one measured on the untreated device.

Typically trade-off curves are traced, in order to observe the effects on both the dynamic and static behaviour at the same time. These trade-off curves report the forward voltage drop as a function of either the reverse current peak or the reverse recovery time, according to the more critical constraint.

The trade-off curve V_{ON}-I_{RR} of Fig. 9 has got a typical hyperbolic shape: using only the platinum diffusion we are bound to stay along this curve and then we can not improve the dynamic behaviour without worsening the ON-state voltage drop.

From this curves we can see that increasing the diffusion temperature from 920°C to 940°C the reverse current peak decreases about 25%, while the voltage drop rises about 38% and the forward behaviour worsening seems to become dominant.
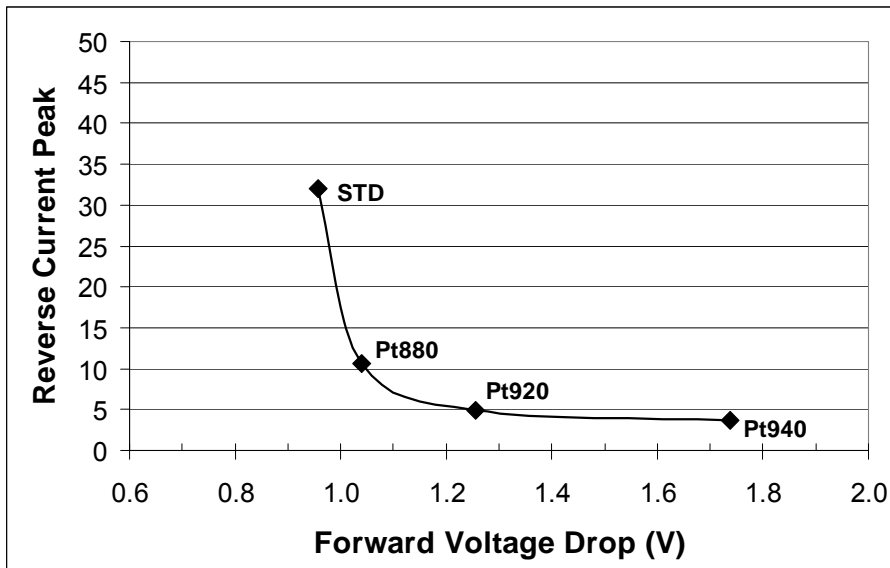

Fig. 9 Trade-off curves of diodes diffused by platinum

A straightforward analysis can be done evaluating the total power loss, as a sum of both static and dynamic contribution.

Typically, the diodes under test work with a duty cycle of 0.6 and a switching frequency from 10kHz to 100kH.

The static power loss is evaluated as:

$$V_{ON} \cdot I_F \cdot \Delta T \tag{8}$$

where I_F is the forward current, V_{ON} the forward voltage drop and ΔT the duty cycle.

Instead we can evaluate the dynamic power loss as

$$E_{RR} \cdot f \tag{9}$$

where f is the switching frequency and E_{RR} is the energy loss during a single turn-OFF.

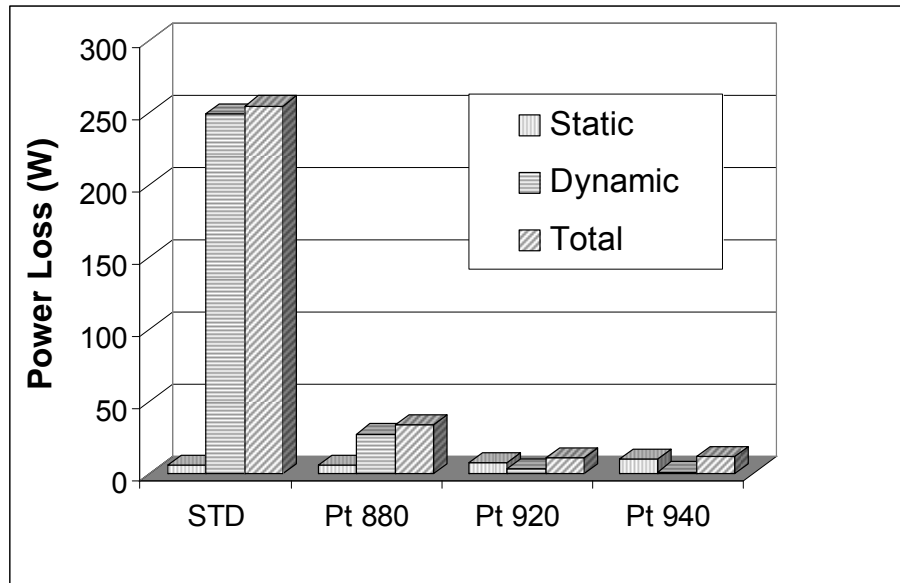The results for the diodes above analysed are depicted in Fig. 10.

Fig. 10 Dynamic and static power loss of untreated device and diodes diffused by platinum (I_F=10A)

It stands to reason how the untreated device can not be used at all in switching applications. In fact the dynamic power loss is 254W, while the static one is only 5.7W and the total power loss is nearby 8 times as big as that one of the Pt880 device. Therefore the lifetime reduction is essential and in platinum diffused devices the dynamic power loss becomes comparable to the static one.

In order to study with a greater detail the effect of the lifetime control process, in Fig. 11 we report only the power loss of the platinum diffused devices.
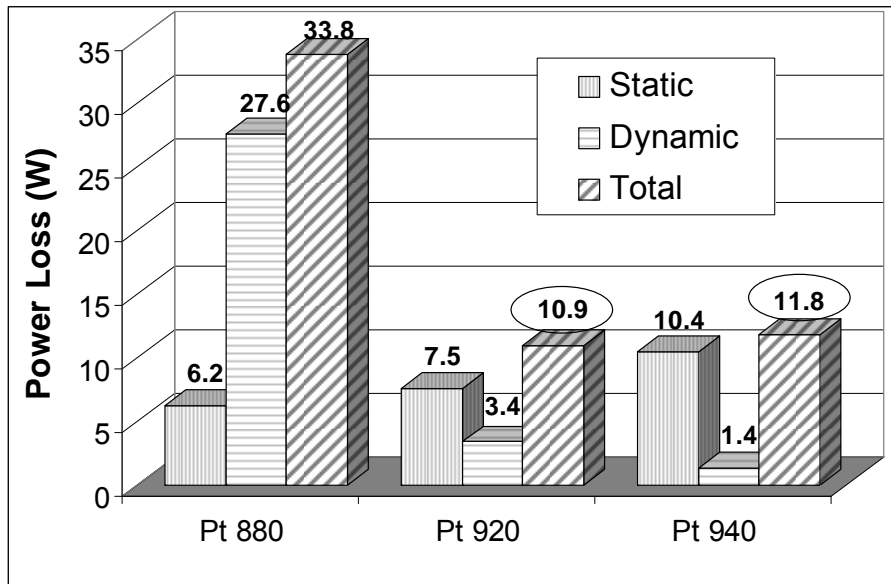
Fig. 11 Dynamic and static power loss of diodes diffused by platinum (I_F=10A)

The device diffused at the lowest temperature (880°C) has got the greatest static and dynamic losses and, consequently, the greatest total power loss in respect to the two others devices.

The most relevant observation is found out by the comparison between Pt920 and Pt940.

First of all, in respect to STD and Pt880, in these switching conditions the static loss becomes the dominant effect.

As shown in Fig.12 Pt940 has the best dynamic behaviour and the dynamic power loss is only 1.4W, less than half than the one of Pt920. But on the other hand the Pt920 ON-state voltage drop is smaller as well as its static power loss. The total power loss of the Pt920 device is 10.9W and it is smaller than the power loss of the Pt940 (11.8W), even though the latter exhibits a better dynamic behaviour.

Making more stressful the switching conditions, Pt940 still has the best dynamic behaviour, as shown in Fig.12 for I_F=30, V_R=300V and di/dt about 600A/μs.
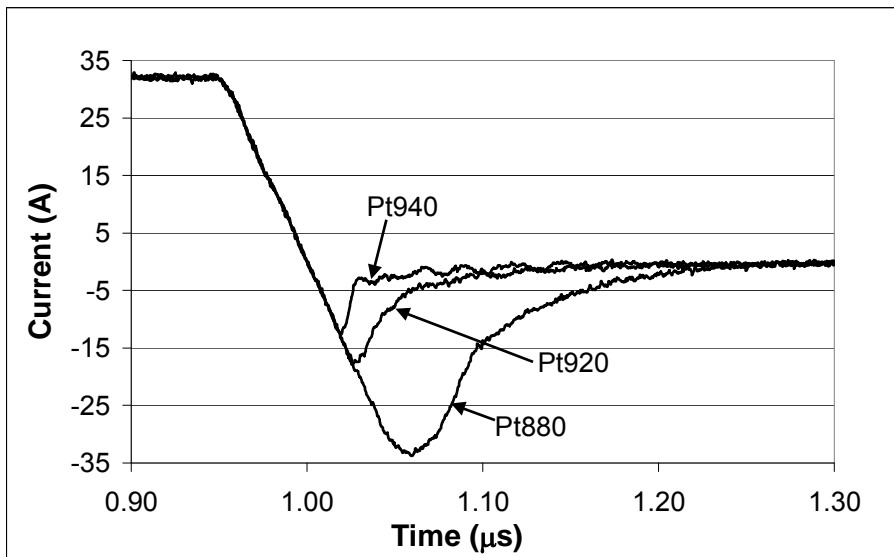
Fig. 12 Comparison between the reverse recoveries of diodes diffused by platinum at different temperatures (I_F=30A)

On the other hand the weight of the static loss becomes more and more dominant, as depicted in Fig. 13
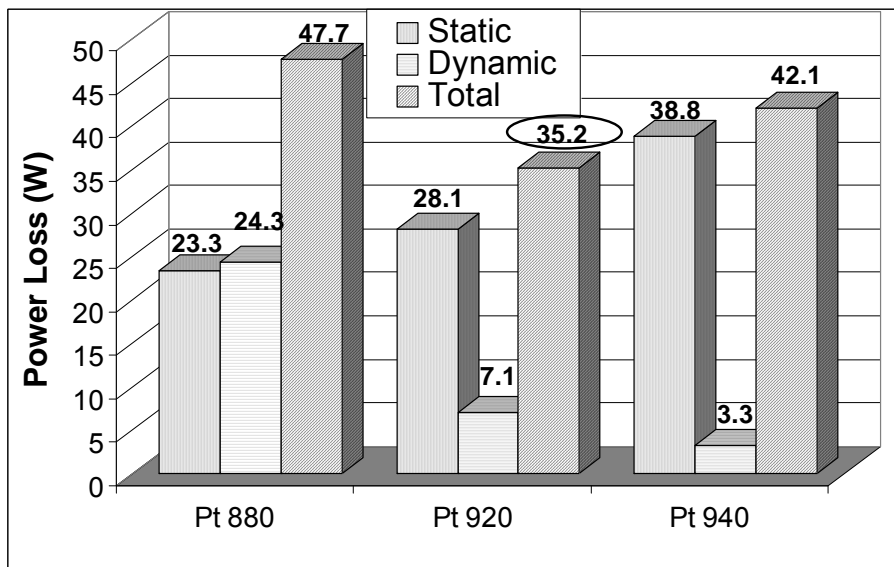

Fig. 13 Dynamic and static power loss of diodes diffused by platinum (I_F=30A)

Unlike observed in Fig.11, in this case the total power loss of Pt920 is less than 17% (about 7W) in respect the Pt940, even though the dynamic power loss of the latter device is much less.

Therefore it is not always convenient to reduce the recombination lifetime as much as possible. In this specific case, if we are interested in minimizing the total power dissipation, the optimum is reached by means of the diffusion temperature of 920°C. This example shows clearly how the aim of the power diode designers must be the pursuit of the best trade-off and not only the optimization of the reverse recovery phenomenon.

1.3   Experimental analysis of helium implanted diodes

As described, we can not avoid the forward voltage drop increase when we improve the transient behaviour. Furthermore, by using platinum diffusion, the V_{ON}-I_{RR} couple is always a point belonging to the trade-off curve of Fig. 9. The only solution for improving further on the trade-off is to recur to a different lifetime control technique.

In the same devices already analysed, we have implanted helium at three doses (10^{11} cm^{-2}, $2x10^{11}$ cm^{-2}, $5x10^{11}$ cm^{-2}) and energy 2.3MeV, which places the defects into the anode region, near the junction.

One of the most favourable position for introducing defects is the anode [18], near the space charge region. The doping concentration of the anode is much greater than the drift region one and, hence, the depletion region extends mostly in the low-doped layer. Therefore defects always lie outside the space charge region, not affecting the leakage current, but on the other hand they allow the carrier concentration to be reduced near the junction, improving the dynamic behaviour.

The Fig. 14 reports the reverse recoveries of Pt880 devices implanted by helium.
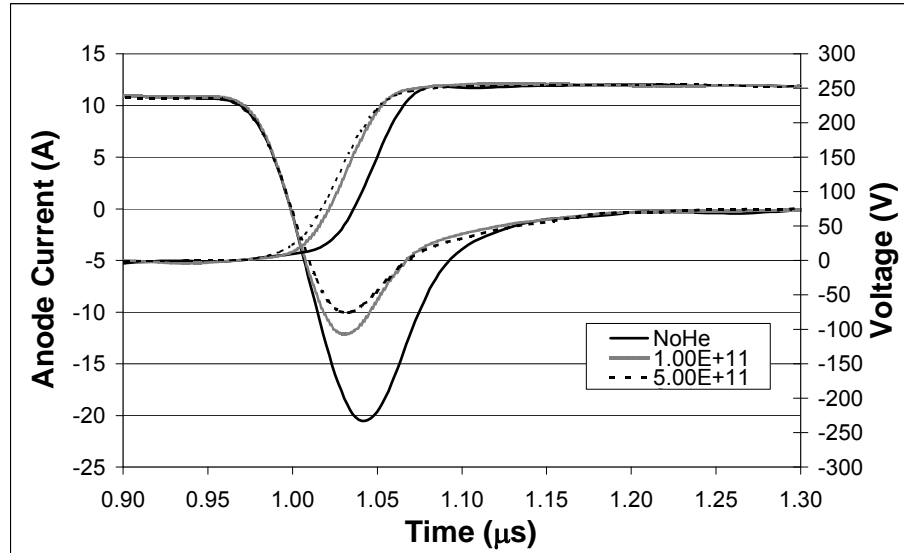
Fig. 14 Comparison between Pt880 diode and Pt880 diodes implanted by He

Helium implantation involves a further reduction of the reverse current peak (about 40% with dose 10^{11} cm^{-2} and about 50% with dose 5×10^{11} cm^{-2}), even though the reverse recovery time holds almost steady.
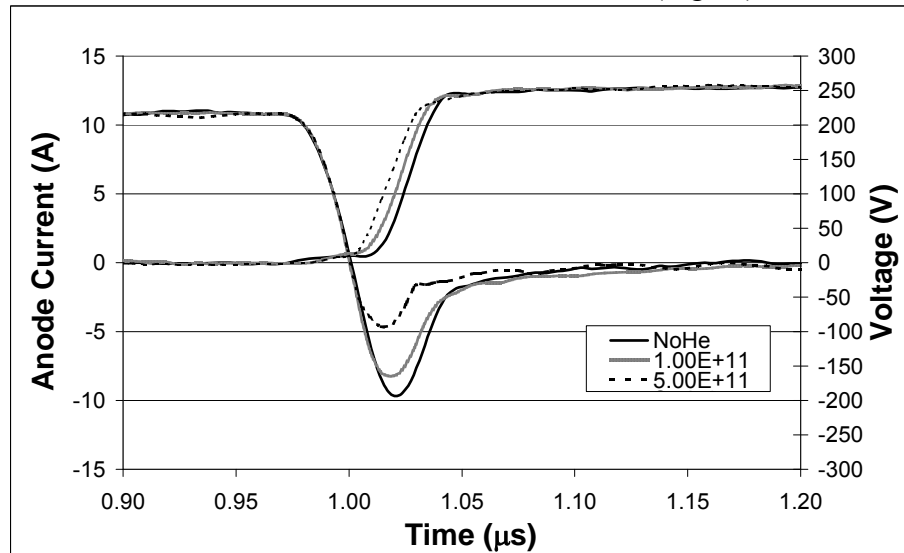
The same effect is measured on Pt920 devices (Fig.15).

Fig. 15 Comparison between Pt920 diode and Pt920 diodes implanted by He

Adding the new V_{ON}-I_{RR} couples measured on the heliun implanted diodes, we obtain the new trade-off graph of Fig. 16.
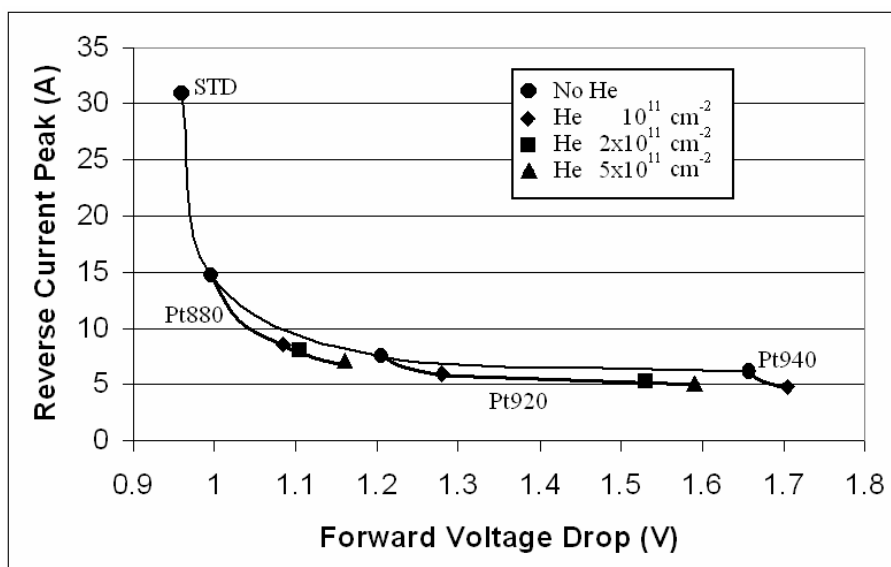

Fig. 16 Trade-off curves of He implanted diodes

The helium implantation clearly improves the trade-off: for a given diffusion temperature, the helium implanted devices show a less V_{ON} for the same reverse current, compared to a device treated only by platinum. As example, a Pt880 implanted by Helium with dose $5x10^{11}$ cm^{-2} has roughly the same reverse current peak of Pt920, but the forward voltage drop is reduced of 50mV. The same observation can be made on Pt920 diode implanted by helium with dose either $2x10^{11}$ cm^{-2} or $5x10^{11}$ cm^{-2}: these devices have got a lower reverse peak and forward voltage drop in respect to Pt940.

Therefore the trade-off is actually improved by means of helium implantation, but we have to take into account that the production cost of these diodes increases.

As shown in Fig. 9 helium implantation allows the reverse current peak to be reduced further, keeping down the forward voltage drop increase and, therefore, it is suitable for the improvement of the V_{ON}-I_{RR} trade-off.

Fig. 17 plots the static and dynamic power dissipation of the Pt880 device implanted by Helium. The unimplanted device has the largest power loss, both dynamic and static. Instead implanted devices show an unexpected behaviour. We have seen that the Pt880 implanted with dose 5×10^{11} cm^{-2} exhibits the lowest reverse current peak, which is reduced of about 17% in respect to the dose 10^{11} cm^{-2}. Nevertheless the dynamic power loss of the latter device is lower, even though the difference is only 0.2W, as well as the total power dissipation.
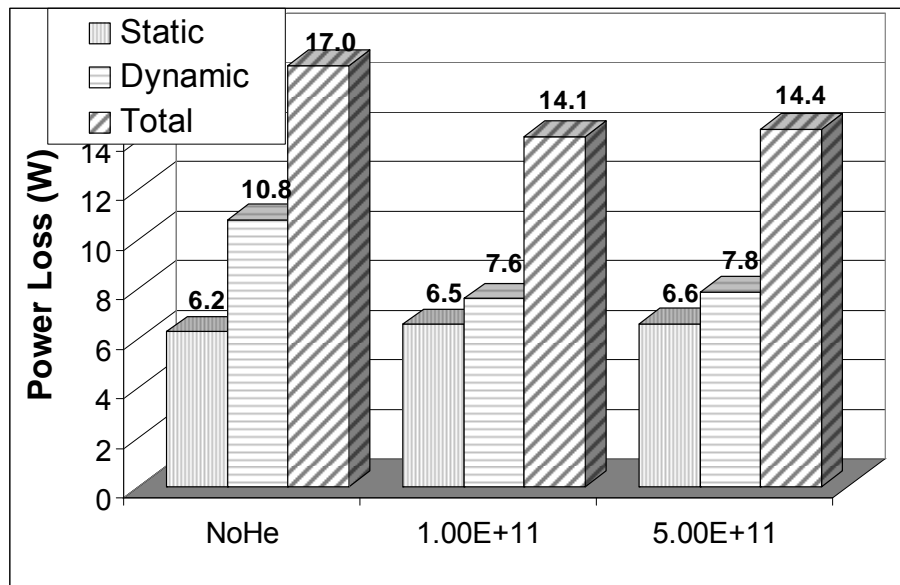

Fig. 17 Static and dynamic power loss of diodes of Fig.14 (Pt880)

In order to understand the reason of this strange behaviour, it is worth observing the instantaneous power loss, evaluated as the product between the current and the voltage for each time instant (Fig. 18).
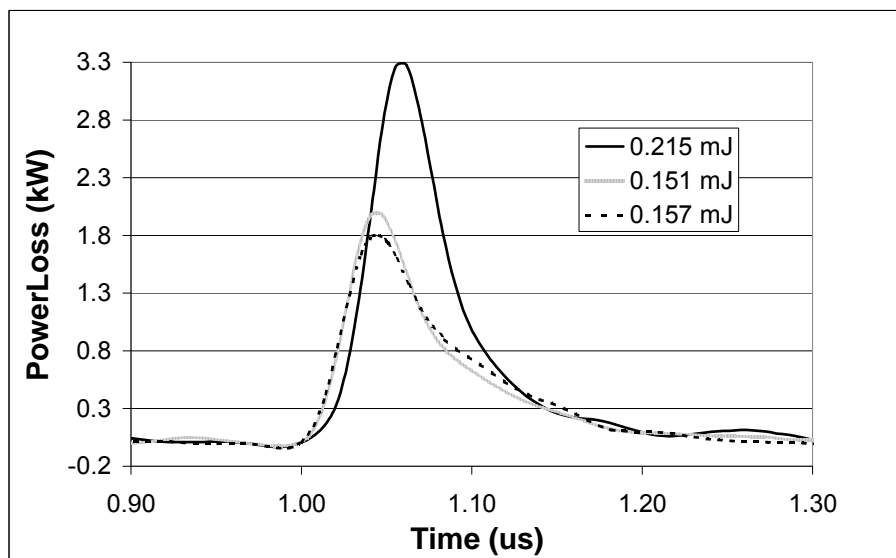
Fig. 18 Instantaneous power loss of diodes of Fig.14

The Pt880 implanted with dose 5×10^{11} cm^{-2} has got the lowest peak of the instantaneous power loss. When the current reaches its minimum, the voltage across the device is still low and, hence, the power dissipation in these instants keeps reduced. Both helium implanted devices present a soft behaviour and the power dissipation in the final instant is not negligible, because the voltage has reached its maximum value. As we can see in Fig. 18, in the final instants of the switch the device implanted with dose 5×10^{11} cm^{-2} has got the instantaneous power dissipation greater than the one of the device implanted with dose 10^{11} cm^{-2}.

Repeating the same analysis at two different temperatures, 25°C and 125°C, and for different switching condition (I_F=15A, V_R=400V, f=50kHz, duty cycle 0.6), we can observe that the device implanted with dose 10^{11} cm^{-2} always exhibits the lowest power dissipation (Fig. 19-20).
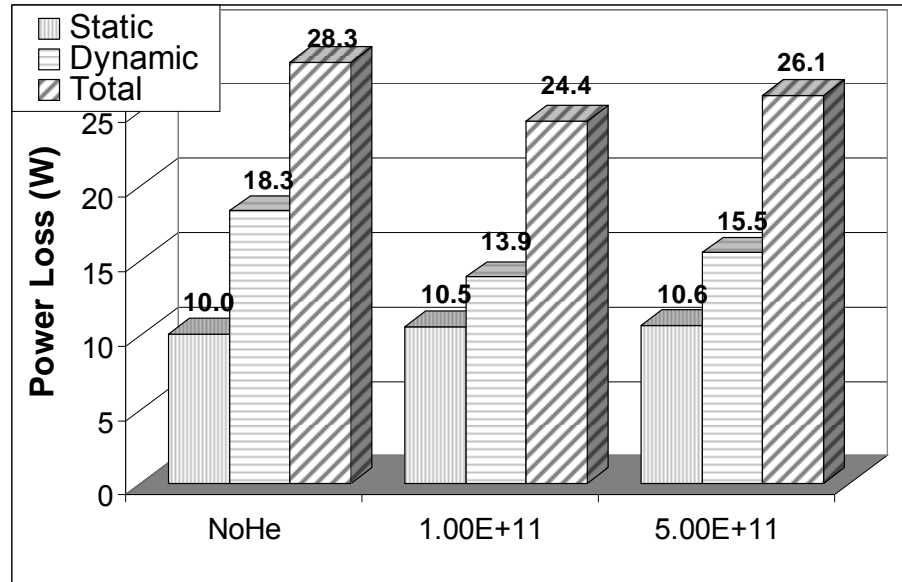
Fig. 19 Static and dynamic power loss of Pt880 diodes (T=25°C)

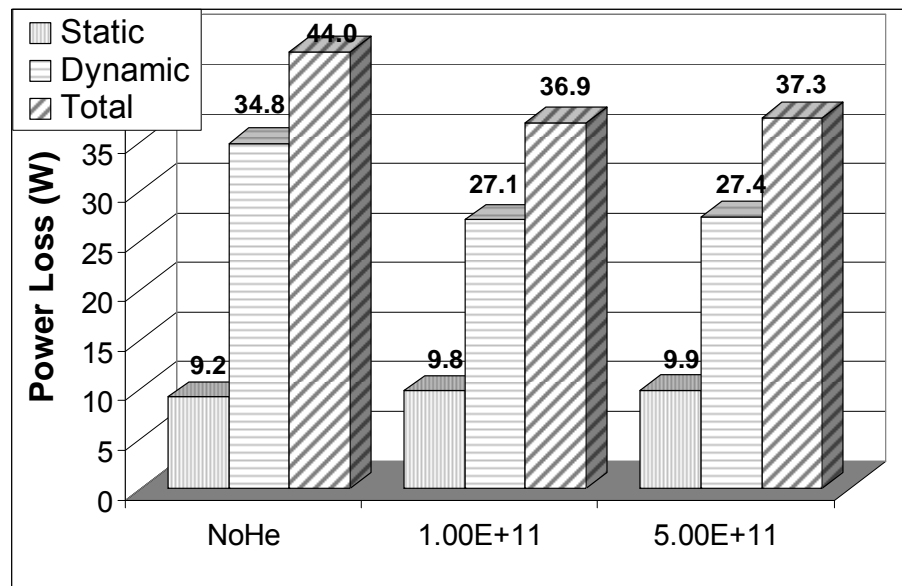**Fig. 20 Static and dynamic power loss of Pt880 diodes (T=125°C)**

Pt920 exhibits a much stranger behaviour. In this case the unimplanted device has got the lowest power loss, because in this device the static power loss becomes dominant (Fig. 21).
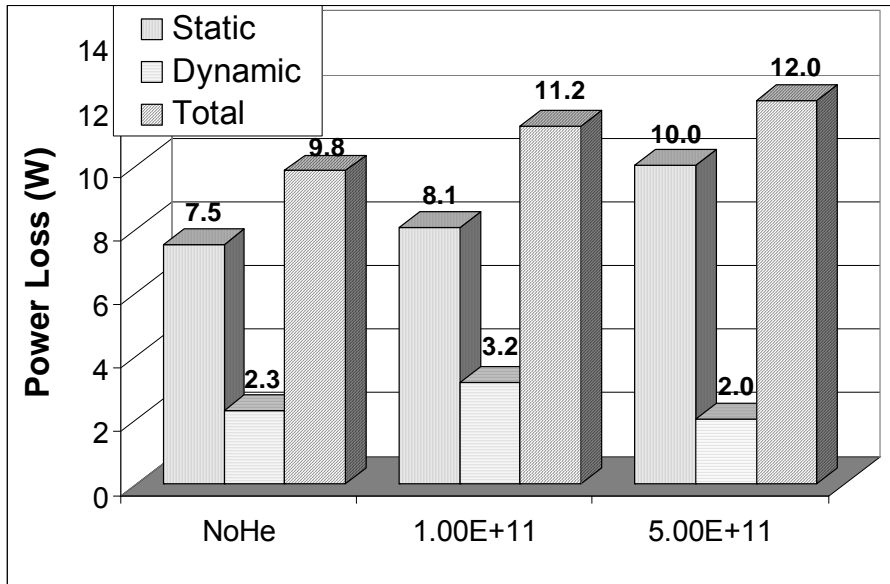
Fig. 21 Static and dynamic power loss of diodes of Fig.14 (Pt920)

The device implanted with dose 10^{11} cm^{-2} has the largest dynamic loss. The explanation can be found again observing the instantaneous power loss (Fig. 22). The reverse recovery of this device is very soft and a pronounced tail current appears, as depicted in Fig. 15. The voltage has already reached the final value and, therefore, in the final instant the instantaneous power loss is greater than that one of Pt920, whereas the power loss peak is roughly the same.
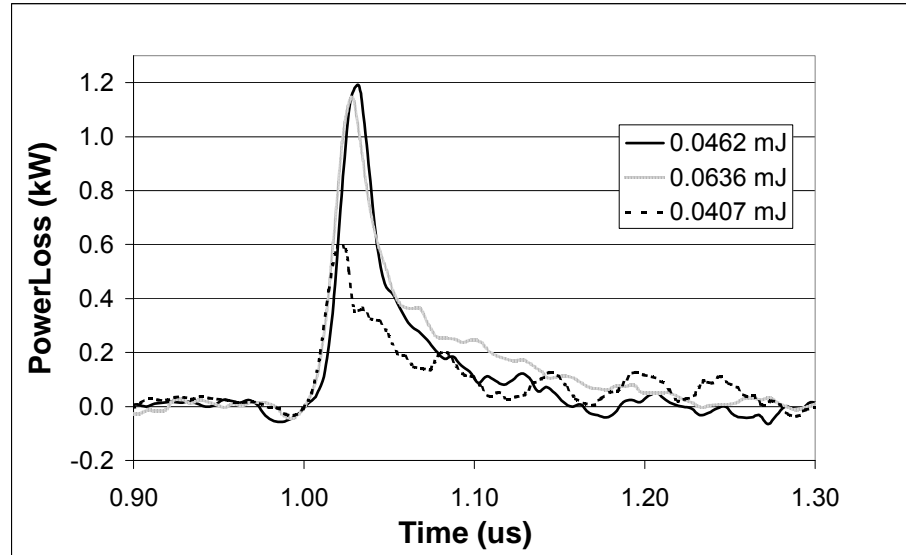
Fig. 22 Instantaneous power loss of diodes of Fig.15

From Fig. 21 the helium implantation could be supposed to be not suitable, because it causes an increase of the power loss, even thought the V_{ON}-I_{RR} is improved. Nevertheless, we must take into account that these devices usually work at high temperature.

Fig. 23-24 report the power dissipation at respectively 25°C and 125°C, for I_F=15A, V_R=400V, f=50kHz, duty cycle 0.6.
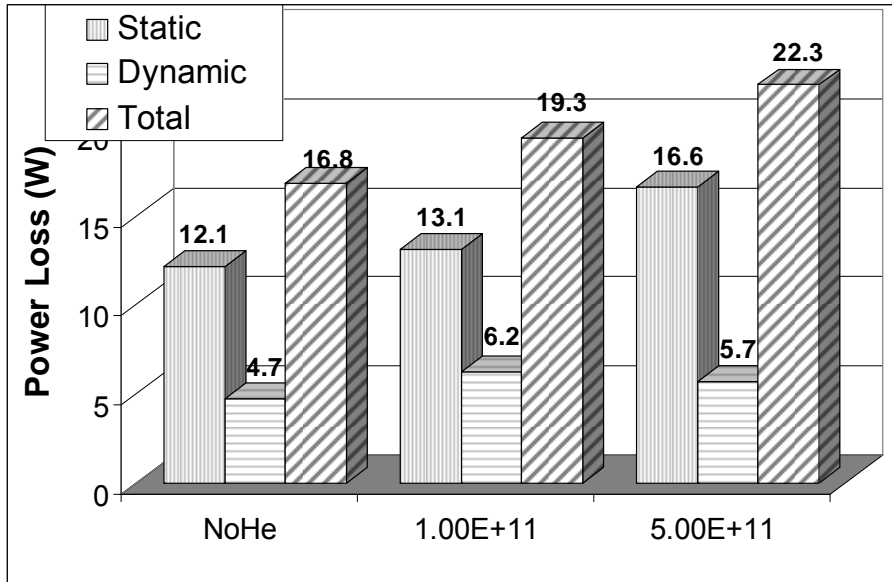
Fig. 23 Static and dynamic power loss of Pt920 diodes (T=25°C)

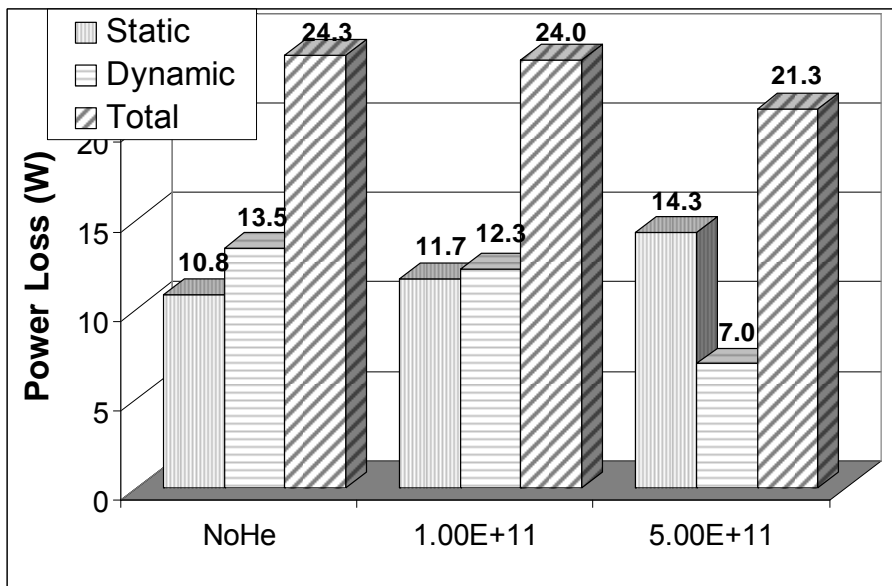**Fig. 24 Static and dynamic power loss of Pt920 diodes (T=125°C)**

At 25°C Pt920 still has the lowest power dissipation, but at 125°C the device implanted with dose 10^{11} cm^{-2} exhibits the best behaviour, because of the drastic dynamic power loss reduction.

Finally, helium implantation involves many benefits, because it allows the V_{ON}-I_{RR} trade-off to be improved and the total power loss to be reduced.

Nevertheless, the behaviour which helium implanted devices exhibit is not so obvious. In fact, if on the one hand we can expect the reduction of the reverse current peak increasing the implantation dose, on the other hand it is not so easy to explain why the helium implantation causes an increase of the power loss in particular switching condition.

As an example, in Pt880 device the dose 10^{11} cm^{-2} allows the lowest power dissipation to be obtained, even though the dose 5×10^{11} cm^{-2} seems to exhibit the best V_{ON}-I_{RR} trade-off.

Even helium implantation could be supposed to worsen the device performance in Pt920 diodes, but the benefits become clearly visible at high temperature. In this case the diodes implanted with dose 5×10^{11} cm^{-2} have the lowest power dissipation.

Therefore the helium implantation effects are somewhat complicated to understand by means of simple experimental measurement and, hence, we need to study more carefully the matter, in order to explain the helium implanted device behaviour.

1.4 Final comments

The above results show how attractive the helium implantation is in the optimisation of power diodes performances. Nevertheless, these are merely experimental results and the test devices have been manufactured by using the basic theory of the recombination process in semiconductor devices and finding out the results obtained in other works present in the scientific literature.

In order to project a device with the best performances, we could recur to this approach, termed *trial and error*, manufacturing a large set of test samples, with different combination of implantation energy and dose, and picking out the one which allows the best trade-off to be obtained. By using this method, we can only claim that the device is the best among all the test devices, without knowing if it represents the best possible choice. Furthermore, we can not explain clearly why the device exhibits the best behaviour compared to the other test samples. Moreover the entire productive cycle becomes more expensive. Indeed we need to manufacture several test devices and we must take into account the cost of silicon wafers growing, helium implantation, bonding and packaging.

The best approach is the analysis and the physics comprehension of the matter. At the beginning, it could appear much harder, but on the other hand if we are able to describe effectively the problem by means of a mathematical model, we could recur to physically-based simulation software. Thus we could use the simulator to find out the optimum combination for the performances improvement, provided that the derived model is valid with a satisfactory approximation.

Referring to our specific problem, we need a measurement technique by means of which we can study the effect related to the helium implantation and find out the parameters of interest, that is, the number of the recombination centres, their energy levels and their capture cross-section. Obviously, because of the nature of the ionic implantation, the chosen technique must be capable to extract the in-depth profile of the defects distribution.

We started our research activity improving the lifetime differential measurement technique, developed into the Electronic Engineering Department of the University of Naples Federico II, wishing to obtain a description of the helium defects distribution as accurate as possible.

Once the effectiveness of the extracted parameters has been checked, we used the model in the ATLAS-Silvaco simulator and observed how the helium implantation affects charge carrier and electric field distribution during the reverse recovery, in order to improve the power diodes performance, with reference to a particular effect called *dynamic avalanche*. This phenomenon consists in the onset of the avalanche breakdown under particular switching condition even though the voltage across the diode is less than the static breakdown value. The dynamic avalanche can be very dangerous, leading to the device destruction. We aim at using the model obtained by means of the differential measurement technique for optimisation of the dynamic avalanche ruggedness of the power diodes.

Chapter 2

The lifetime measurement technique

In the scientific literature many techniques have been proposed for the measurement of the recombination lifetime, which is a critical parameter for the performances optimisation in several power electronic applications. Among all these techniques, which use different approaches, it is worth mentioning OCVD and DLTS.

OCVD technique [19] can furnish just an average value of the lifetime and, in general, it is more suitable for low injection levels, whereas power devices work at high injection level in forward mode.

DLTS technique [20] is the most widely used for defects characterization in semiconductor devices. It allows the energy of recombination centres and their capture cross-section to be obtained and by means of recent improvements the extraction of the in-depth profile of the centres can be done. The technique is based on the measurement of the emission velocity of the carriers trapped in the defects. It needs a reverse biased diode, to which a positive pulse is applied in order to fill the recombination centres into the depletion region. From the knowledge of the velocity needed to recover the equilibrium value of the depletion capacity, it is possible to evaluate the emission velocity and thus both energy level and capture cross-section of the centres.

Nevertheless, the technique can evaluate only the generation lifetime, being the junction reverse biased, and it does not work properly if the defects number is 10% greater than the doping concentration and, therefore, it is less effective when electrical compensation effects take place. Furthermore it can reveal only deep levels.

We focus our attention on the differential measurement technique, which offers several advantages in respect to the above mentioned techniques.

2.1 The lifetime differential measurement technique

In the Electronic Engineering Department of the University of Naples Federico II it has been proposed in [21] the differential technique for the measurement of the recombination lifetime. Using a special test device, the technique can extract the lifetime profile in a low-doped layer, measuring currents and voltages at the device terminals.

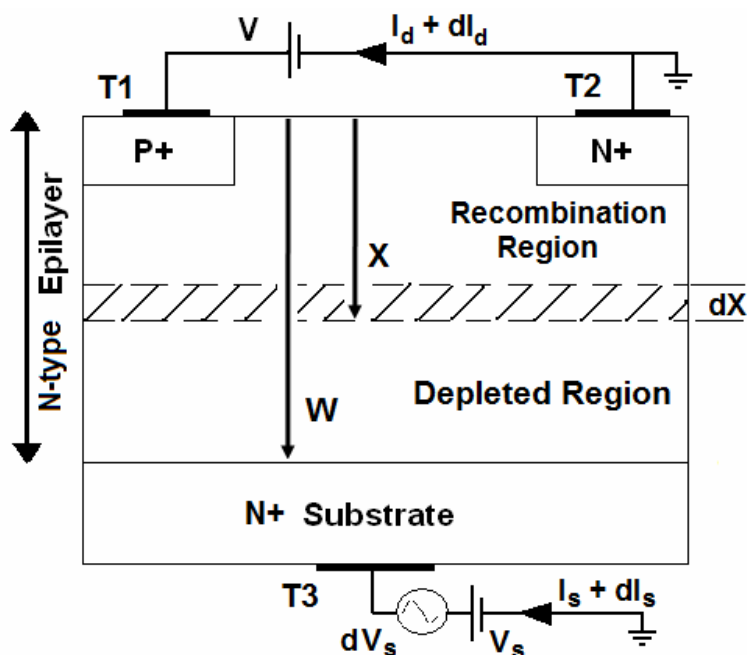The schematic of the structure is shown in Fig. 1.

Fig.1 Cross section schematic of the elementary cell of the test structure

It is a three terminal device: by applying a positive voltage to the base (T1), the surface diode works in forward mode and carriers are injected into the drift region. A positive voltage at the collector terminal (T3) repeals minority carriers toward the surface up to a

depth X_C: the epilayer is split in a plasma region, filled with both minority and majority carriers, and in an ohmic region, with only majority carriers.

By applying a small signal voltage to the collector, there's a modulation effect of the recombination region. The a.c. current value of the lateral diode is related to the recombination lifetime in the epilayer. The value of X_C depends on the collector voltage and the recombination lifetime is evaluated at this depth X_C. The scansion of the whole epilayer can be performed varying the collector voltage. The technique results very effective because it allows being free from the recombination effects in the high doped regions. The other recombination components in the high doped region are constant, being fixed the diode voltage. Therefore, due to the differential behaviour of the technique, these contributions do not appear in the small signal current, which only depends on the recombination in the modulated region [22]. This feature represents the main point of the technique, which is able to detect only the SRH recombination term.

Eq.1-2 report the depth X_C [23] where minority carriers are confined and the lifetime at the position X_C [21]:

$$X_C = W \frac{2(1 + P_{ON})}{(V_S/V_T + 2(1 + P_{ON}))} \qquad (1)$$

$$\tau(X_C) = \frac{X_C}{D_n^*} \frac{1}{\dfrac{d}{dX_C}\left(\dfrac{i_d}{i_s}\right)} \qquad (2)$$

In the above equations P_{ON} is the normalised injection level, defined as the ratio between the surface hole concentration and the epilayer doping N_D, W the epilayer thickness, V_S the substrate voltage, V_T the thermal voltage, while i_d and i_s are the small signal currents respectively of the base-emitter diode and collector. The expressions are compact and stylish.

2.2 Improvements needed for the differential measurement technique

The technique is very effective, as shown in [23], but it is required that the doping is constant along the epilayer.

Using the technique on helium-implanted test device, we have revealed an incorrect operation. Fig. 2 plots the lifetime profile extracted using the classic theory into a helium-implanted test device, with dose 10^{11} cm^{-2} and energy 5.8MeV. We are able to measure a variable lifetime profile, but the lifetime minimum lies at 26.5μm and it does not agree with the energy implantation. Indeed, with the energy of 5.8MeV the maximum damage is placed around 30μm from the surface and, congruently, the lifetime minimum should be located at the same depth of the maximum defects concentration.

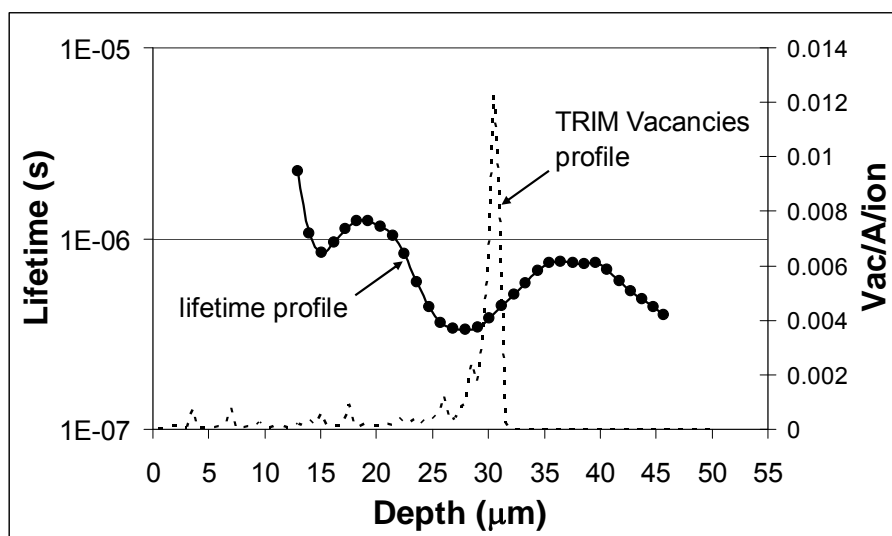**Fig.2 Lifetime profile evaluated on device implanted by He in dose 10^{11}cm^{-2}**

Increasing the implantation dose to 2×10^{11} cm^{-2} we cannot observe any localisation effect, but only a profile which decreases toward the surface (Fig. 3).
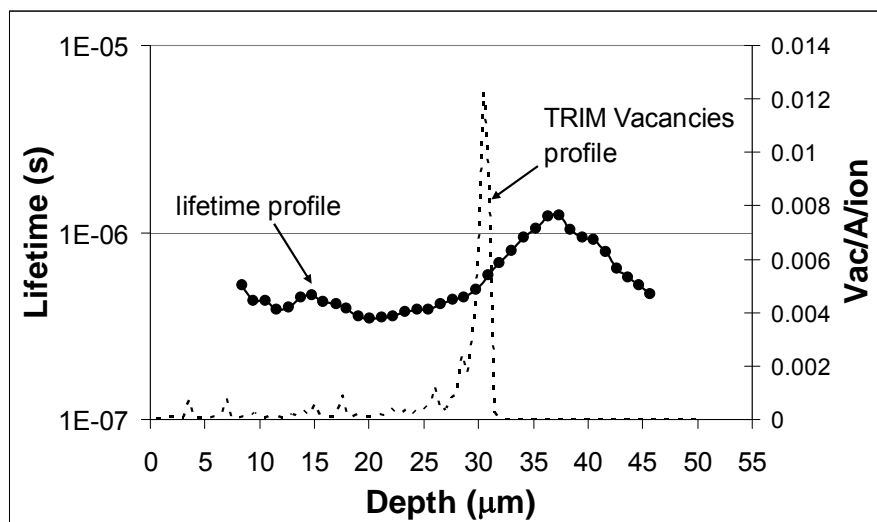
Fig.3 Lifetime profile evaluated on device implanted by He in dose 2x10^{11}cm^{-2}

We can deduce that the technique fails in this case, probably in the evaluation of the abscissa X_C.

By a spreading resistance measurement on a device implanted with energy 4.4MeV and dose 2x10^{11} cm^{-2} (Fig. 4) we have noticed that helium implantation affects also the effective doping distribution, which we will discuss in the next chapter about.
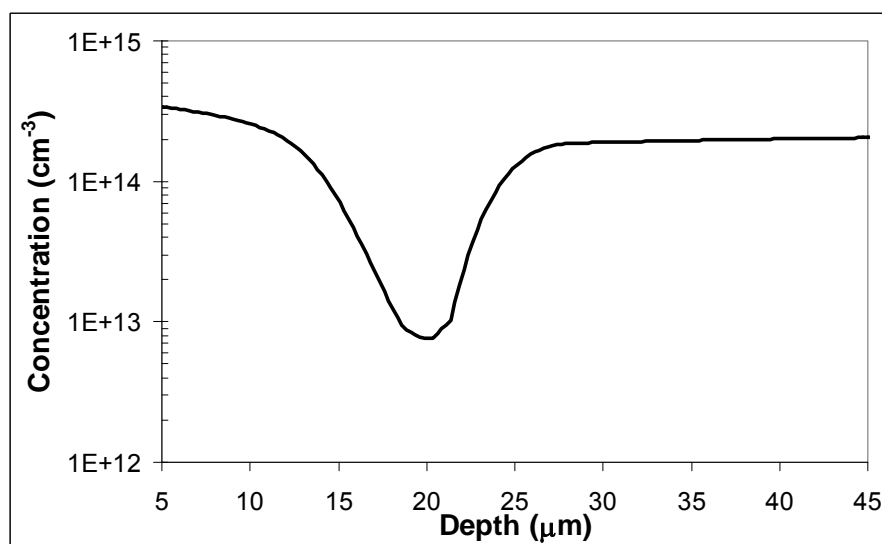

Fig.4 SRP measurement on device implanted by helium in dose 2x10^{11}cm^{-2}

This effect is not so obvious and there are not many works in the literature which discuss about the doping compensation involved by helium implantation. Nevertheless this effect seems to be not negligible for a correct lifetime profile analysis. Indeed if the doping concentration is not constant, the Eq. (1) is no longer valid, and, therefore, using the expression (1), the evaluation of the depth X_C gets wrong.

In order to obtain a correct evaluation of the lifetime profile, we need to modify the X_C calculation, taking into account that doping concentration could be variable. Obviously, as previously shown, this information is not known a priori, but it has been acquired by a SRP measurement. Nevertheless, SRP involves the destruction of the analysed sample and then the measurement of the lifetime profile can not be done on the same device. Moreover SRP is performed only at room temperature, making impossible the recombination centres extraction procedure, which needs measurements at different temperatures.

The aim is to obtain information about the effective doping on the same device whose lifetime profile is measured, in order to carry out temperature measurements and properly extract the defects distribution related to the helium implantation.

As described in the next section, it has been proposed a technique which, starting from the measurements of the device output characteristic, allows the doping distribution along the epilayer to be evaluated by means of an iterative algorithm. This is a considerable result, because the technique is completely electric and it is possible to measure on the same device the effects on both recombination lifetime and effective doping, for different operating temperatures.

2.3   Measurement of a variable resistivity profile

As it has been already described, by applying a positive voltage V_S to the collector terminal of the test structure of Fig.1, an electric field appears and it pushes the minority carriers toward the surface up to a

depth X_C, function of the voltage V_S. Therefore the drift layer is divided in two regions: a plasma region, from the surface to X_C, with both minority and majority carriers, and an ohmic region, from X_C to the substrate, where there are only majority carriers. If the injection level is high enough, the resistivity of the plasma region is almost zero and, therefore, the resistivity between emitter and collector terminals is only due to the region depleted of minority carriers and it can be evaluated as the ratio between the voltage V_S and the current I_S flowing trough the collector terminal (Fig. 5).

Increasing the voltage V_S of a value ΔV_S, minority carriers are confined up to a depth $X_C + \Delta X_C$ and the resistance of the ohmic region increases of ΔR. From the difference between $R + \Delta R$ and R we can evaluate the resistance of the region ΔX_C and, taking into account the device geometry, we are able to obtain the localised resistivity around the depth X_C.

As previously said, at high injection levels, we can evaluate the resistance R_C of the epilayer as:

$$R_C = \int_{X_C}^{W} \frac{1}{q\mu_n n(x)} \frac{dx}{A} = \frac{1}{q\mu_n A} \int_{X_C}^{W} \frac{dx}{n(x)} = \frac{V_S}{I_S} \qquad (3)$$

where W is the epilayer thickness, V_S the collector voltage, A the device area, I_S the collector current, μ_n the electron mobility and $n(x)$ the majority carriers concentration. From Eq. (3) we can see that R_C can be evaluated by a simple I-V measurement.

For a fixed injection level the abscissa X_C is a function of the voltage V_S, as reported in [23]

$$X_C = \frac{2(1 + P_{ON})}{1 + 2P_{ON}} \frac{qD_n p_0}{I_S} \left(2 + \frac{1}{P_{ON}}\right) A \qquad (4)$$

where D_n is the electron diffusion coefficient, p_0 the surface hole concentration and P_{ON} the normalised injection level.

From (1) the value of the area A is:

$$A = \frac{I_S}{q\mu_n V_S} \int_{X_C}^{W} \frac{dx}{n(x)} \qquad (5)$$

Replacing (5) in (4), we obtain a new expression of X_C which does not depend on the active area of the device:

$$X_C = \frac{V_T}{V_S} \frac{p_0}{P_{ON}} 2(1 + P_{ON}) \int_{X_C}^{W} \frac{dx}{n(x)} \qquad (6)$$

where V_T is the thermal voltage.

If the doping along the epilayer is constant, the integral in (6) can be easily solved and X_C becomes [23]:

$$X_C = 2 \frac{W(1 + P_{ON})}{V_S/V_T + 2(1 + P_{ON})} \qquad (7)$$

Nevertheless, if the doping concentration is variable, we can not find a closed expression as well as (7). In this case the evaluation is somewhat complicated, because X_C depends on both the voltage V_S and the doping concentration.

Therefore, measuring the lifetime profile in the event of variable doping concentration, the technique could be inaccurate, because of the wrong evaluation of X_C and from (2) we can see how the lifetime value strongly depends on the X_C precision.

To overcome this problem, it has been proposed an iterative procedure for the doping concentration evaluation along the epilayer, in order to correct numerically the value of X_C [25].

2.3.1 Procedure description

In order to describe the procedure, we assume a generic doping profile $N_D(x)$, which gives rise to a variable resistivity along the epilayer.

The first step of the procedure is the measurement of the I_S-V_S static characteristic, for a given high injection level, by applying a constant voltage to the surface diode.

The iterative procedure starts assuming, at the first step, that the doping is constant, hence, for each V_S, we evaluate X_C from (5), let $X_C(i)$ the value of X_C corresponding to a particular $V_S(i)$ ($I_S(i)$ is kwon form the I_S-V_S characteristic).
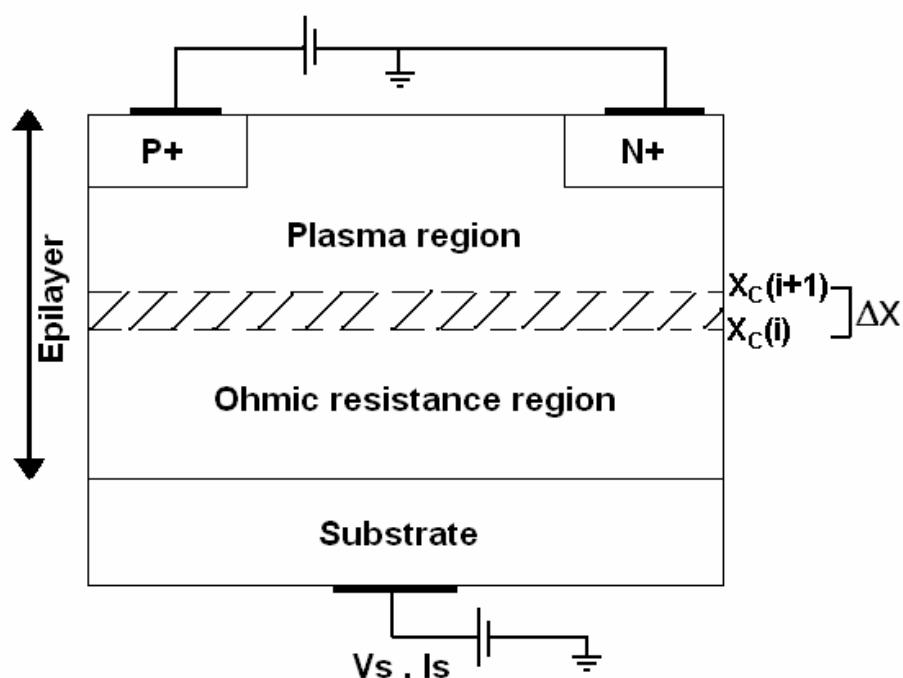
Fig.5 Cross section schematic of the test structure for the doping profile evaluation

With reference to Fig.5 we define the differential resistance of the region ΔX, from depth $X_C(i)$ to $X_C(i+1)$, as:

$$R_{diff} = R(i+1) - R(i) = \frac{V_S(i+1)}{I_S(i+1)} - \frac{V_S(i)}{I_S(i)} \qquad (8)$$

from which the mean value of the doping into the region ΔX can be written as:

$$N_D(x) = \frac{1}{q\mu_n R_{diff}} \frac{\Delta X}{A} \qquad (9)$$

Obviously the wrong estimation (from Eq. 7) of X_C gives a wrong reconstruction of $N_D(x)$. Fig. 6 shows two dimensional numerical simulations of the test structure, performed with the program ATLAS-Silvaco [26], in which a step variable doping profile (dashed curve) has been assigned in the epilayer. The curve labelled step1 is the doping profile we reconstruct assuming a constant N_D for the evaluation of X_C. From this curve we have a first rough estimation of the doping profile.
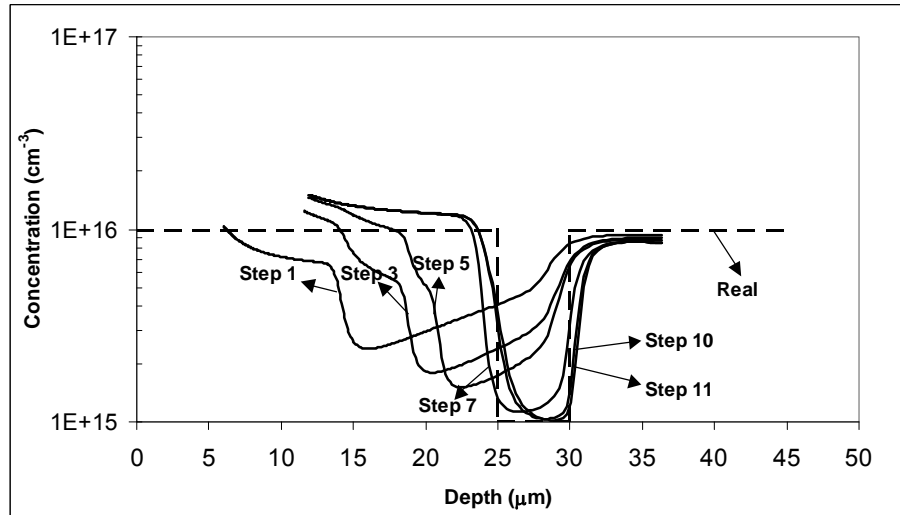

Fig.6 Simulated results illustrating the measurement procedure. The step variable curve is the doping profile set in the numerical simulator. Curves labelled from 1 to 11 represent the reconstruction of such profile obtained after 1 to 11 iteration steps respectively.

The second step of the procedure makes use of a discrete form of Equation (4) obtained by replacing the integral term with a numerical sum:

$$X_C(i) = \frac{V_T}{V_S(i)} \frac{p_0}{P_{ON}} 2(1 + P_{ON}) \sum_{j=i}^{k} \frac{X_C(j+1) - X_C(j)}{N_D(j)} \qquad (10)$$

where k is the number of the intervals in which the epilayer has been divided.

By using in Equation (10) the couples $X_C(i)$, $N_D[X_C(i)]$ obtained in the previous step (see curve step1 in Fig. 6) we obtain a new estimation of the substrate voltage $V_S(i)$ needed to obtain a particular $X_C(i)$:

$$V_S(i) = V_T \frac{N_D}{X_C(i)} 2(1 + P_{ON}) \sum_{j=i}^{k} \frac{X_C(j+1) - X_C(j)}{N_D(j)} \qquad (11)$$

By using again Equations (8) and (9) we obtain a new $N_D(x)$ and hence new couples $X_C(i)$, $N_D[X_C(i)]$, which can be used again for evaluating again the voltages $V_S(i)$ related to the depths $X_C(i)$ from (11) and, hence, a new profile $N_D(x)$. The iterative procedure ends when $N_D(x)$ gets stable. Fig. 6 shows the profiles obtained after the steps 3, 5, 7 10 and 11. After about 10 steps we reach a stable solution which is in good agreement with the profile imposed in the simulator. A schematic representation of the algorithm is shown in Fig. 7.

It is worth noting that the used step variable profile has got very abrupt variations and this case represents the hardest operation condition. For smoother profile we can expect a faster convergence and a more accurate estimation of the doping concentration

Fig. 8 plots an example of doping distribution evaluation when the doping shape is gaussian along a small region of the epilayer. The fit is almost good.
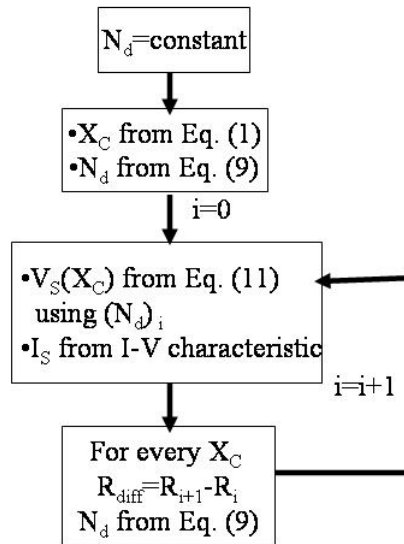
Fig.7 Schematic representation of the iterative algorithm used when the resistivity profile is non constant.
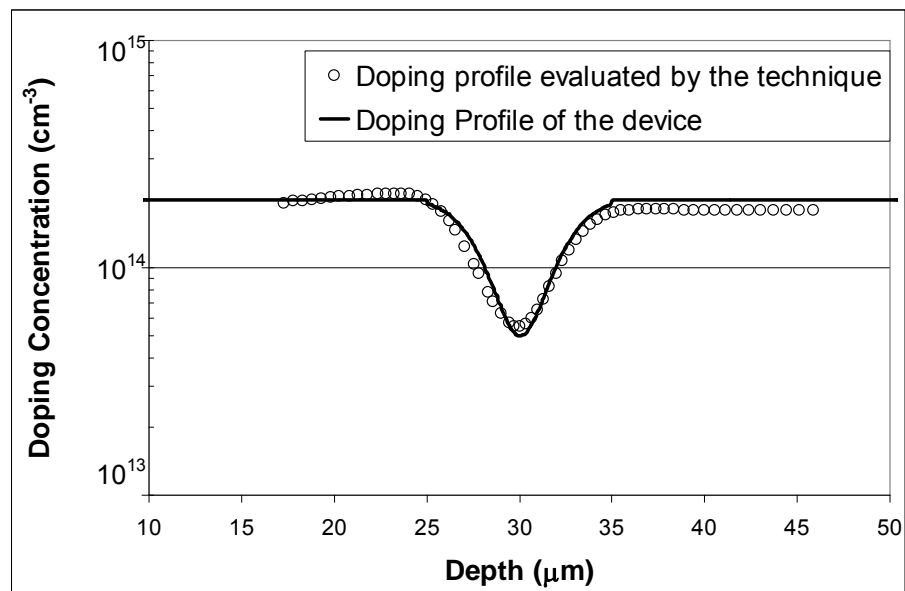

Fig.8 Comparison with a doping profile set in the simulation and the one evaluated by means of the proposed technique

The technique has been applied to unimplanted device and to a device implanted with dose $2x10^{11}$ cm^{-2}, whose SRP doping profile has been shown in Fig.4. The thickness of the epilayer is 58μm and its doping concentration is $2x10^{14}$ cm^{-3}. The doping profile of the untreated device is almost constant and equal to $2x10^{14}$ cm^{-3}, as expected. The comparison between the SRP profile and the one evaluated by means of our technique shows the effectiveness of the proposed procedure. Indeed the two profiles matches with an acceptable precision. Therefore our technique allows the same doping compensation effect to be observed without involving the destruction of the device.
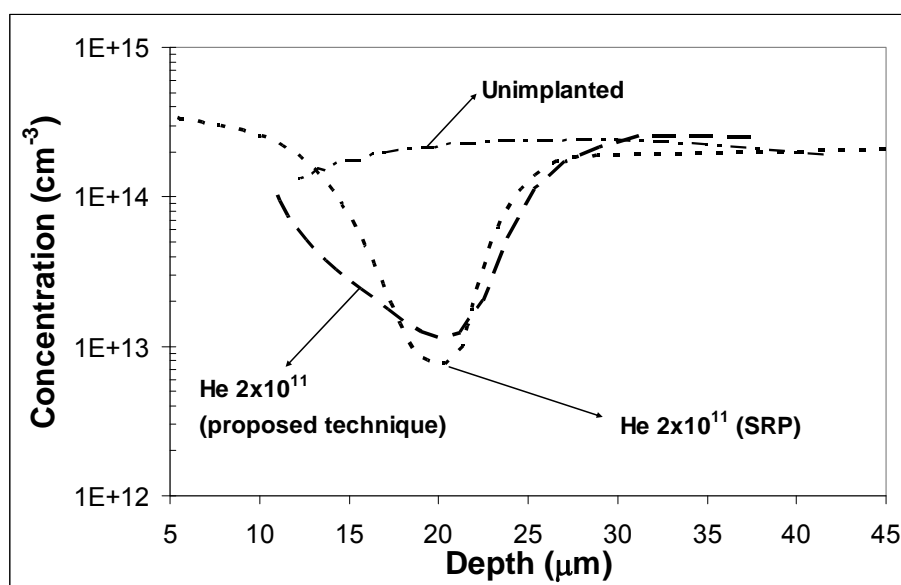

Fig.9 Comparison between the doping profile evaluated by SRP and the one by the proposed technique on a device implanted by He in dose $2x10^{11}$cm^{-2}

2.4   Complete simulation of the technique

The differential measurement technique has been simulated taking into account the correction of the abscissa proposed above [26], in the event that recombination centres affect both lifetime and effective

doping. Simulations have been performed for several temperatures, as to extract also the recombination centres distribution.

The epitaxial region has got a thickness of 58μm and a constant doping of 2×10^{14} cm^{-3}.

The defects profile of Fig.10 has been imposed: the shape is gaussian, with a peak value of 10^{15} cm^{-3} around 30μm and the energy level is X_C-0.23eV, where E_C is the lowest edge of the conduction band.
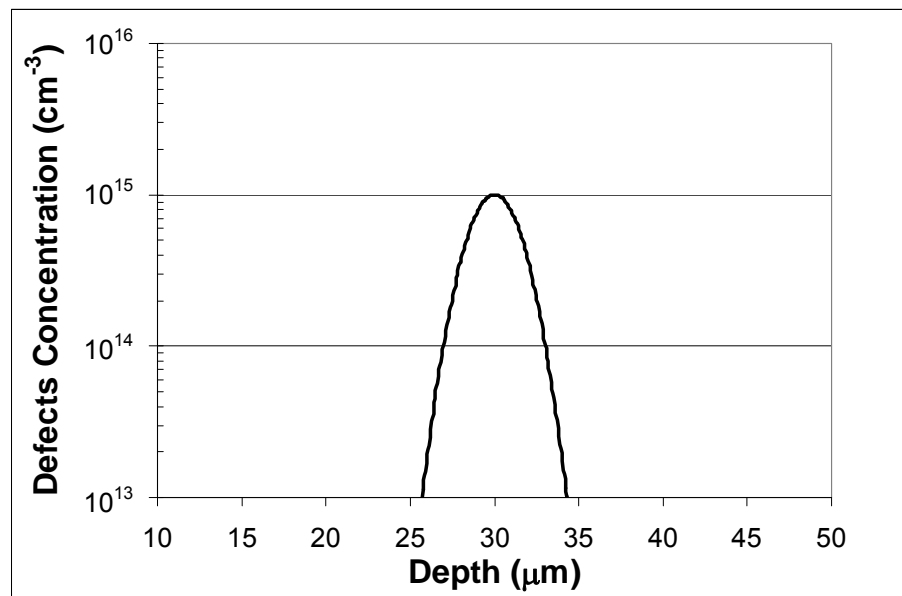

Fig.10 Defects profile used in the test device for two dimensional simulation

The lifetime of the starting material, without defects, is 2 μs.

Ad described above, by measuring the static characteristic we have extracted the shape of the resistivity (Fig. 11) at 300K from (8), relative to the defects profile of Fig. From the localised resistivity, we have evaluated the effective doping concentration (Fig. 12) from (9). The effective doping has got a minimun around the position of the maximun defects concentration and the shape is roughly Gaussian.
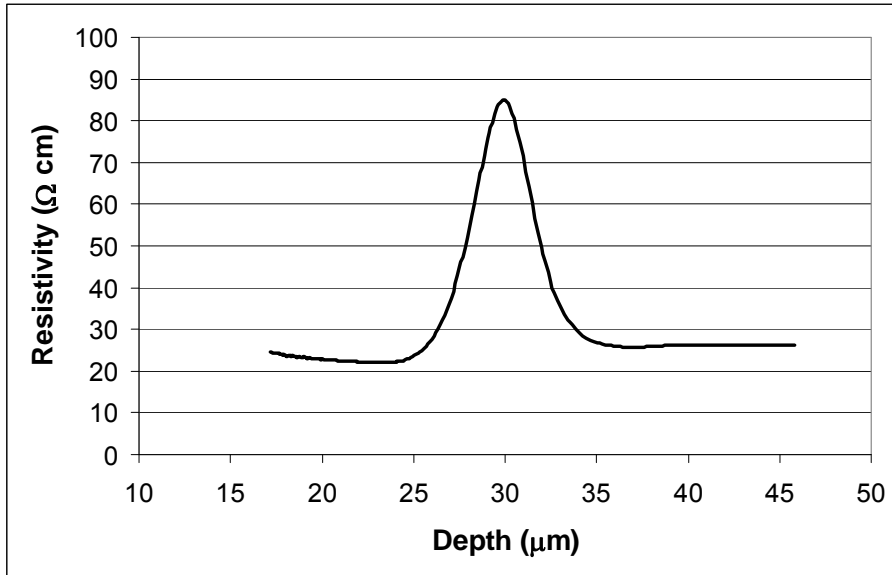
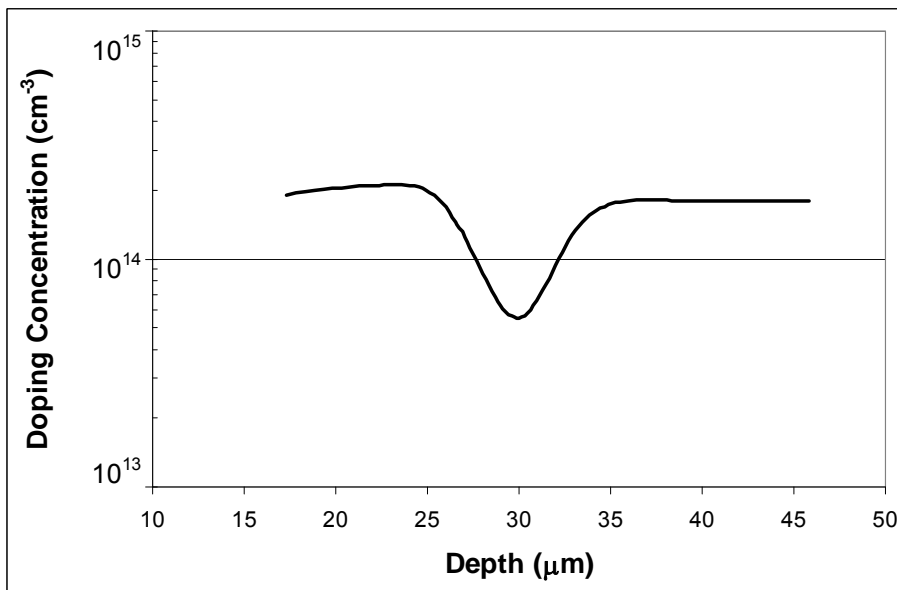**Fig.11 Resistivity profile evaluated by means the iterative procedure**

Fig.12 Effective doping concentration evaluated from the resistivity profile of Fig. 11

Fig.13 shows the comparison between the lifetime profile evaluated without taking into account the doping compensation and the one evaluated by using the technique improvement.
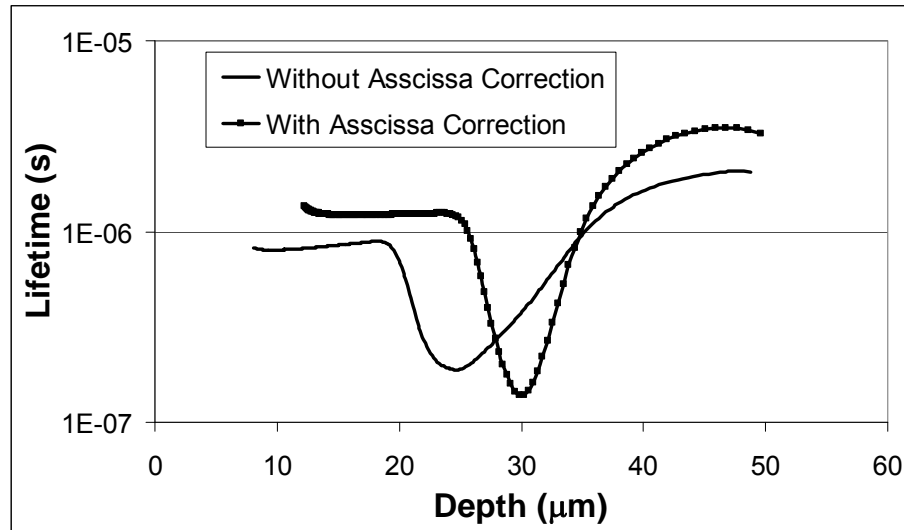

Fig.13 Comparison between the lifetime profile evaluated by means ATLAS simulation with or without abscissa correction

Without correcting the abscissa the minimum of the lifetime is not located around the penetration depth of 30μm, but closer to the surface, as already observed in the experimental measurement of Fig.2. Taking into account the doping variation, the lifetime profile becomes narrower around its minimum, which now corresponds exactly with the position of the maximum defects concentration. The result is through-and-through congruent with the Eq.10. Indeed if the effective doping concentration reduces, applying the same voltage V_S the minority carriers are confined at a greater distance from surface and the evaluated profile shifts towards the substrate.

Fig. 14 shows the recombination lifetime as a function of the temperature. In agreement with the SRH theory, increasing the temperature the Fermi level moves toward the midgap and the semiconductor material starts to become intrinsic. As soon as the Fermi level becomes lower than that one of the recombination centre, according to the Fermi-Dirac statistics, the occupancy probability of the centre decreases and, therefore, it results less effective in the

recombination process. Consequently the lifetime rises, as we can see in Fig. 14, in the region where defects have been introduced. The deeper the centre is, the less the lifetime depends on the temperature, as it happens in the external region, where the energy level has been imposed equal to the midgap.
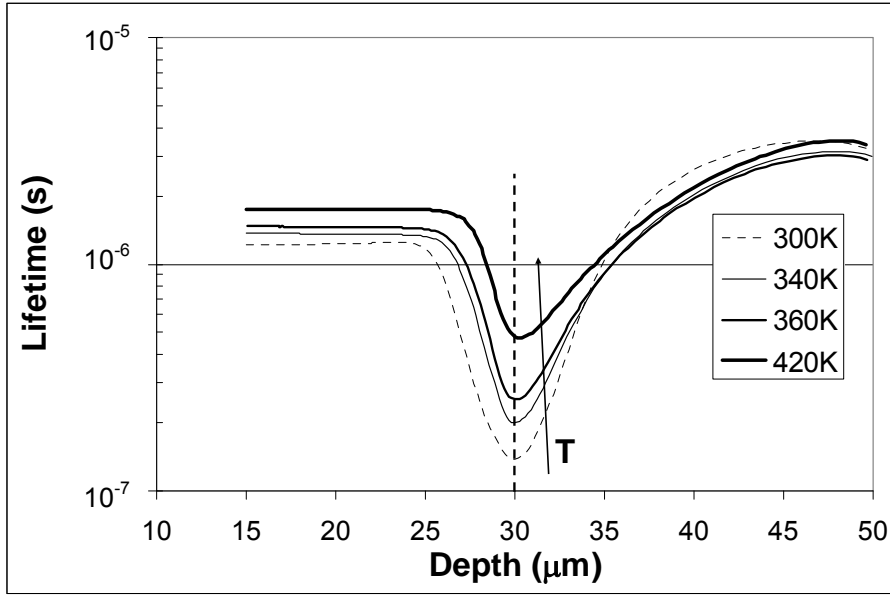

Fig.14 Simulated lifetime profiles as a function of the temperature

This behaviour is clearer in Fig.15, where the circles represent the Arrhenius plot drawn at the depth of 30μm. The graph reports the lifetime, normalised to the thermal velocity v_{th}, in order to remove the further temperature dependence of this parameters, as a function of the inverse of the temperature.

The diagram can be explained by means of SRH theory, which expresses the lifetime as [27]:

$$\tau = \tau_{p0}\left[1 + \frac{1}{1+I}\exp\left(\frac{E_T - E_F}{kT}\right)\right] + \tau_{n0}\left[\frac{I}{1+I} + \frac{1}{1+I}\exp\left(\frac{2E_i - E_T - E_F}{kT}\right)\right] (12)$$

where I is the injection level, E_i the intrinsic Fermi energy level, E_F the Fermi energy level and T the temperature in Kelvin degrees.

From (12), the lifetime τ reduces to $1/\sigma N_t v_{th}$ at low temperatures and, therefore, we can evaluate the term σN_t from the value of this plateau. As soon as the centre deactivates, the lifetime starts to linearly increase in logarithmic scale and the slope depends on the energy level of the centre.

The best fit of the simulated points (solid curve) is obtained with the energy level E_C-0.23eV, equal to the value settled in the simulation (Fig. 15).
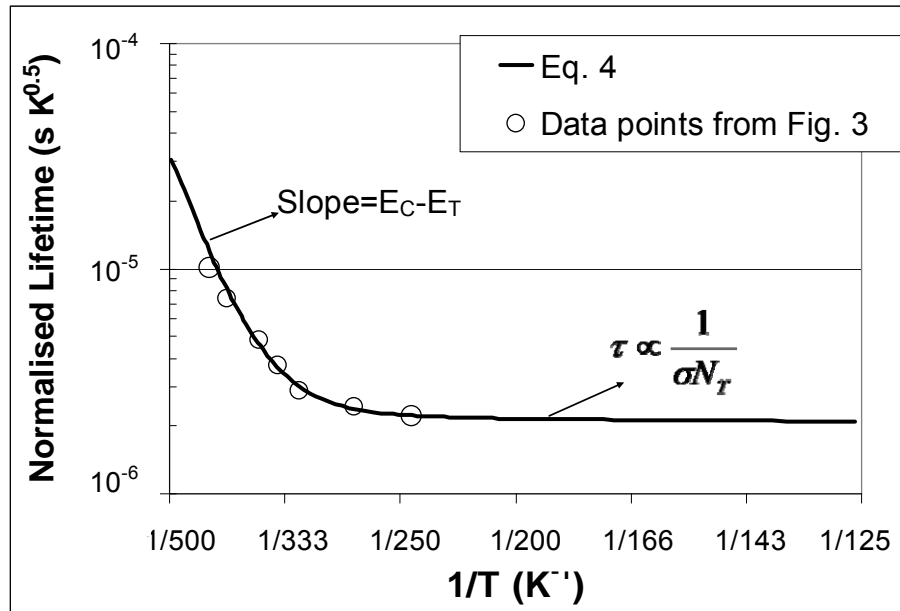

Fig.15 Arrhenius plot at the depth of 30μm, evaluated from lifetime profiles of Fig. 14

Plotting the Arrhenius diagram for many depths, it is possible to trace the concentration of each detected centre. The defects concentration can be easily evaluated by dividing the term σN_t for the capture cross-section, assumed constant with the temperature.
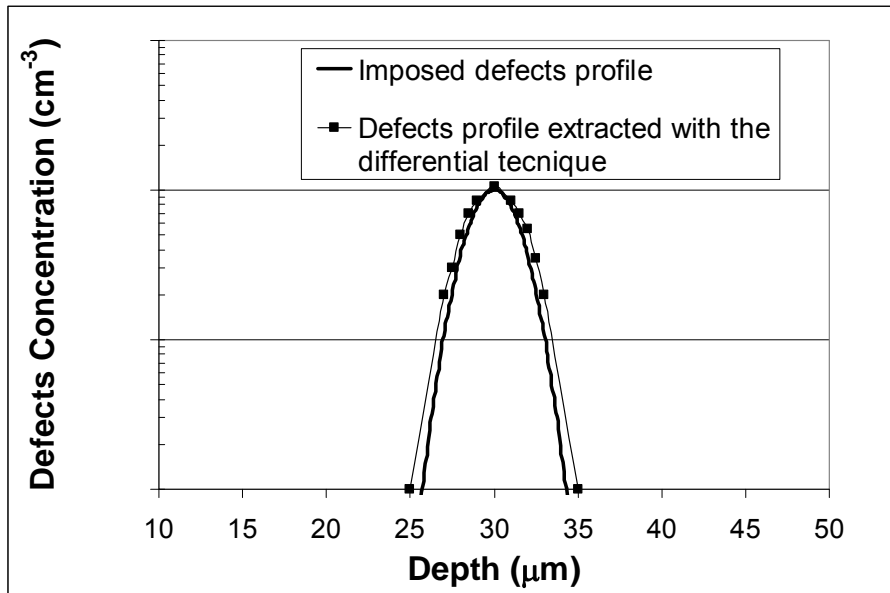
Fig.16 Comparison between the defects profile evaluated by means of our technique and this one imposed in the device

Fig.16 shows the comparison between the imposed centres distribution and that one extracted by means of the technique, starting form the lifetime profile of Fig.14 and tracing the Arrhenius plot for each depth.

The agreement is quite good and, therefore, taking into account the improvements for variable doping concentration, we can resolve that the technique properly works even when the recombination centres acts on the localised resistivity of the material.

As shown in Fig.13, by means of the knowledge of the effective doping we achieve two important improvements: the evaluation of the abscissa X_C is now correct, so that the minimum of the lifetime corresponds to the maximum defects concentration, and the technique resolution enhances.

In Fig. 2 and 3 we have observed that we were unable to evaluate with a good precision the penetration depth for low implantation dose (10^{11} cm^{-2}), whereas we could not reveal any localised reduction for higher dose ($2x10^{11}$ cm^{-2}).

Evaluating the lifetime profile on the same device implanted with dose 10^{11} cm^{-2} by recurring the technique improvement, we obtain the

curve of Fig.17. As well as depicted in the simulation of Fig.13 the lifetime profile shifts toward the substrate and its minimum corresponds to the ion stopping range predicted by TRIM simulation. The straggle around the penetration depth is reduced, leading to a resolution enhancement.
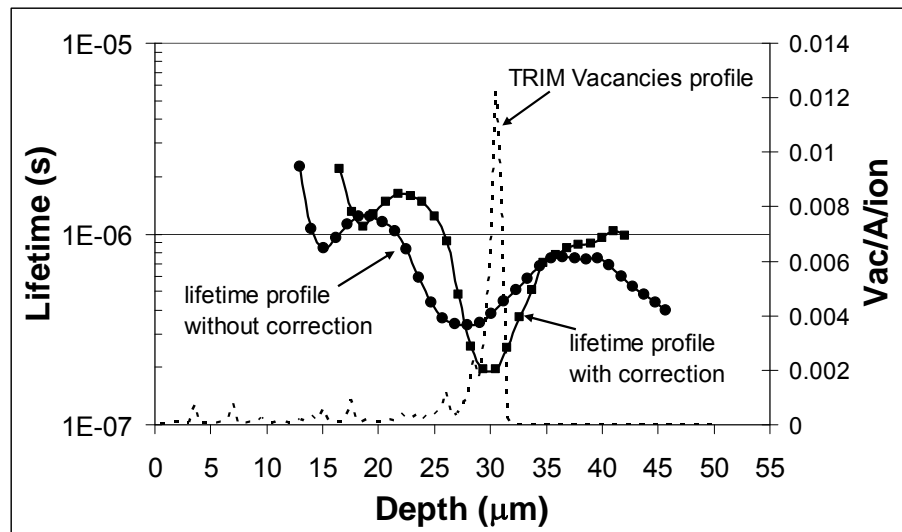

Fig.17 Comparison between the lifetime profile evaluated with or without abscissa correction on device implanted by He in dose 10^{11}cm^{-2}

Applying the technique to the device implanted with dose 2×10^{11} cm^{-2} we can note how drastic the improvement involved by the abscissa correction is (Fig. 18). Without taking into consideration the effective doping modification, we could not reveal any noteworthy lifetime profile; introducing the abscissa correction, a gaussian shape appears whose minimum lies around the penetration depth. In this case the effective doping reduces up to one order of magnitude (Fig. 4) and, hence, neglecting the effective doping variation, the analysis would be completely wrong.
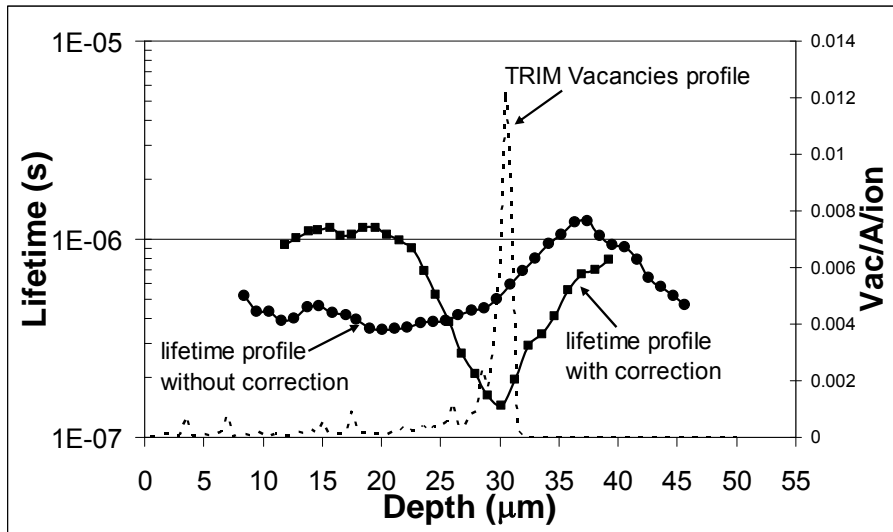
Fig.18 Comparison between the lifetime profile evaluated with or without abscissa correction on device implanted by He in dose $2x10^{11}cm^{-2}$

2.5   Final comments

The analysis of helium implanted devices is not so easy to achieve, because of the combined effect on both recombination lifetime and doping compensation. Helium implantation was not supposed to modify strongly the effective doping, but lifetime measurements showed unexpected results. By means an SRP measurement, we found out that helium implantation involves a localised doping compensation, which affects the depth evaluation of the technique.

In order to measure the correct lifetime profile, we have proposed an all electrical measurement technique which allows the effective doping concentration to be revealed in helium implanted devices. The results are in good agreement with the SRP measurements, but being a non-destructive technique it is possible to measure on the same device both recombination lifetime and effective doping concentration.

The technique has been checked by ATLAS simulation and its application to helium implanted device leads to a noteworthy improvement on the recombination lifetime evaluation.

Therefore we can now recur to the differential lifetime measurement technique to study with a greater detail the effects of helium implantation in low-doped silicon layer, aiming at extracting a valid model to be used in the simulator for high power diodes design.

Chapter 3

Helium implantation: effects on recombination lifetime and effective doping

Ionic implantation is used in many electronic fields to introduce new species into the crystal lattice, in order to modify its structure or composition, either as a simple technological step or with the intent of improving the features of electronic devices.

According to the implanted species, ionic implantation can be used to create high doped regions, i.e. thin emitters in BJTs, or to modify the local doping, i.e. for the optimization of the threshold voltage in MOSFETs, or to control the local recombination lifetime, i.e. in high power devices.

Usually ionic implantation requires a post thermal treatment, the temperature and the duration of which vary with the particular application.

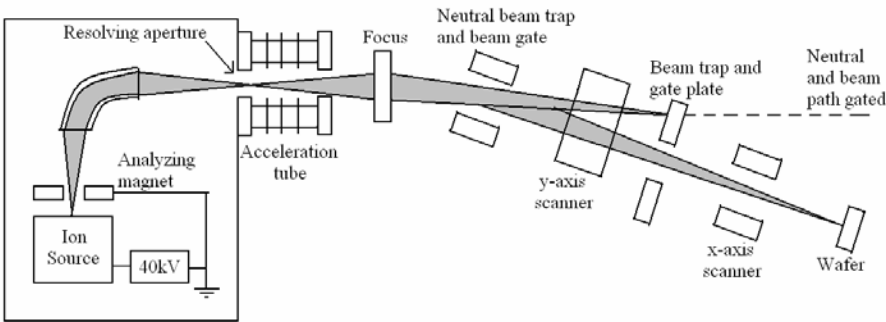The implantation system is very complex and the schematic is shown in Fig.1 [6]:

Fig.1 Schematic of ionic implantation system

The first stage is the ion source, where the ions of the desired species are created. It consists of a heated filament, which allows a gas source to be broken up into charged ions. If the desired species does not exist in a gaseous form, it can be heated in an oven inside the ion source in order to generate a vapor.

By means of an extraction voltage of around 40kV, the charged ions are extracted from the ion source and moved into the mass analyzer, which selects the ions with the specified mass-to-charge ratio.

After having crossed the mass analyzer, ions reach the acceleration tube, where they are accelerated to the chosen implantation energy. By means of electrostatic deflection plates and lens the ion beam is oriented toward the target and collimated opportunely.

Ions are implanted into the material with a given energy, but they lose their own energy progressively inside the lattice. The process has got a random nature and thereby the energy loss is described by a statistical model. The shape of the defects distribution is Gaussian [6], with a maximum lied around the projected range R_P and a certain projected straggle σ_P. The distribution has got also a fluctuation along the direction perpendicular to the implantation axis, termed lateral straggle $\sigma_\perp$. All these parameters are a function of the energy implantation, the implanted species mass and the mode how the ions lose their initial energy.

The mechanisms which cause the energy loss are fundamentally two: electronic interaction and nuclear interaction.

In the former case, electrons can be viewed as a viscous drag where implanted ions move. The collisions are inelastic and they seldom involve atomic displacement. This interaction can be regarded as a mere friction term and it is likely when the ion energy is very high.

As the ions go deeply inside the target, the probability of nuclear interaction increases. In this case the incident ions and the atoms of the lattice can be treated as hard spheres: the interactions are elastic and the classic scattering theory can be applied. The nuclear interaction is more effective for heavy ions and becomes dominant when the ion energy is low. Indeed if the ion is too fast, there's not

enough interaction time for the energy transfer. If the needed energy (about 15eV) is transferred to an atom of the lattice, this latter is displaced from its equilibrium position. A Frenkel-pair defect is created, which consist of an interstitial, related to the dislodged atom, and a vacancy that is the place left vacant into the lattice.

If the transferred energy is much greater than 15eV, the displaced atom can in turn create new defects, giving rise to a cascade generation.

Both electronic and nuclear interactions determine an energy loss of the implanted ions, reducing their penetration depth.

If ions are implanted along a crystallographic direction, where atoms density is low, they can be steered down the channel, without losing energy by nuclear interaction, but only by electronic interaction. The ions which travel along the channel can reach a larger depth and the defects distribution shows an undesired tail.

The channeling effect can be minimized growing an amorphous surface layer or misorientating the wafer. In the first case the direction of ions which pass through the amorphous layer is randomized, while the misorientation of the wafer prevents that ions travel through a crystallographic direction. Usually the implantation machines tilt the wafer to be implanted by 7°.

The migration activation energy of the primary defects created by ionic implantation, which can acquire different charge states, is very low [28,29]; thereby their diffusivity is high and, hence, they are extremely unstable at room temperature [30].

Primary defects tend to interact each other or with other impurities present in the material, leading to the formation of new stable defects, called secondary defects, as divacancy or clusters [31]. The impurities concentration plays a fundamental role in this phase and the mainly present species in silicon are oxygen, which lies in the interstitial site, and carbon, which instead occupies substitutional positions.

The stable defects creation is enhanced by means of thermal annealing, which increases the migration velocity of the primary defects and thereby their interaction probability [32].

Due to the oxygen presence [33], it is very likely the formation of oxygen-vacancy pairs, which consist in the capture of a vacancy by interstitial oxygen.

Another typical secondary defect is the divacancy that is the combination of two near vacancies. Sometimes divacancies already

exist as primary defects, but they are usually created after the thermal annealing of vacancies. Divacancies can have four different charge states (VV++,VV0, VV-,VV--).

The defects introduce new allowed energy level within the bandgap: if the centers are shallow they act as donor or acceptor, depending on their position, while deep centers act as generation/recombination centers.

Varying the implanted species, both energy level and capture cross-section can change and thereby their effectiveness in the recombination process, according to the SRH theory.

In this chapter we analyze the effect of the helium implantation in a low-doped silicon layer, in a wide range of energy and dose. We will study the effect on both recombination lifetime and local resistivity.

Helium is a noble gas and it tends to move out from the lattice. Thereby it could be supposed that the electric properties of the material are not affected, being not active electrical centers related to the implanted species, but only centers caused by the lattice damage. Nevertheless we found out that helium implantation can change the effective doping of the implanted material.

3.2   Experimental samples

Test structures, done as illustrated in the Chapter 2 and designed by us, have been manufactured by IRCI (International Rectifier Corporation Italian) and the wafers diameter is 5" (Fig.2).
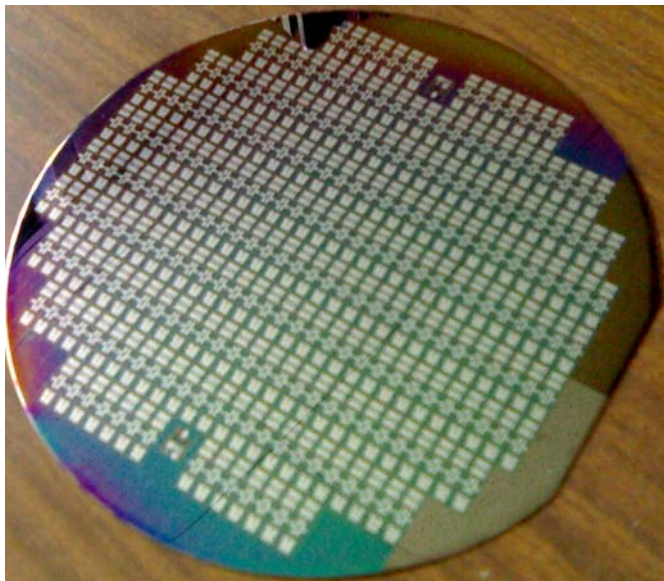

Fig. 2 Wafer with test structures for recombination lifetime measurement

Helium implantations have been carried out in the Dynamitron Tandem Laboratory of Bochum, in collaboration with the Department of Physics of University of Naples Federico II. Table I reports the energies and the doses used for our analysis.

Helium Implanation	
Energy (MeV)	*Dose (cm^{-2})*
5.8	1×10^{10}, 1×10^{11}, 2×10^{11}, 5×10^{11}
3.5, 4.4, 5.1, 5.8	10^{11}

Table 1 Implantation energies and doses used for test devices

Cutting, bonding and packaging have been executed in the characterization Laboratory of the Electronic Engineering Department of University of Naples Federico II. The chosen package is TO-5 (Fig.3).
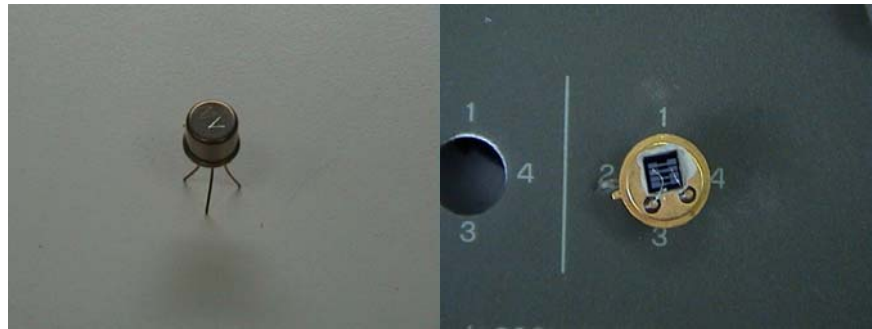

Fig. 3 Packaged device

As proofed in [34], since the defects created by ionic implantation are mainly vacancy-related, and therefore quite unstable, a thermal annealing is needed in order to stabilise the defects distribution. All the implanted devices have been annealed at 250°C for 2 hours.

3.3 Effective doping

We start our analysis from the study of the effects on the local resistivity. Indeed, as described in the second chapter, the knowledge of the effective doping profile is necessary for a correct evaluation of the recombination lifetime.

3.3.1 Experimental characterization of the series resistance in implanted layers

It is well known that in semiconductor materials the resistivity is a function of both doping concentration and carrier mobility.

We know that the mobility can be viewed as the parallel of two terms: impurity scattering and lattice scattering [6]. In the former case, as charge carriers approach to the ionized impurity, they can be deflected because of coulombic interactions. Increasing the impurity concentration the mobility reduces, whereas for high temperatures the carriers speed increases and thereby the scattering effect is less effective because the interaction time becomes shorter.

Lattice scattering is due to the vibrations of the atoms lattice around their equilibrium position. At high temperature, the vibrations increase and, hence, the mean free path reduces, as well as the carrier mobility.

In general at around the room temperature the lattice scattering becomes dominant and the mobility reduces when the temperature increases. Therefore, for a given doping concentration, the resistivity of a silicon layer increases with the temperature (Fig.4). Obviously, for a fixed temperature, the resistivity reduces increasing the doping concentration.

Recalling the schematic of the test structure (Fig. 5), if the surface diode is zero-biased, no charge carriers are injected into the epilayer and, hence, by applying a positive bias to the control terminal we have a resistivity path between the emitter and the collector. Therefore we

can find out the resistivity of the layer measuring the static IV
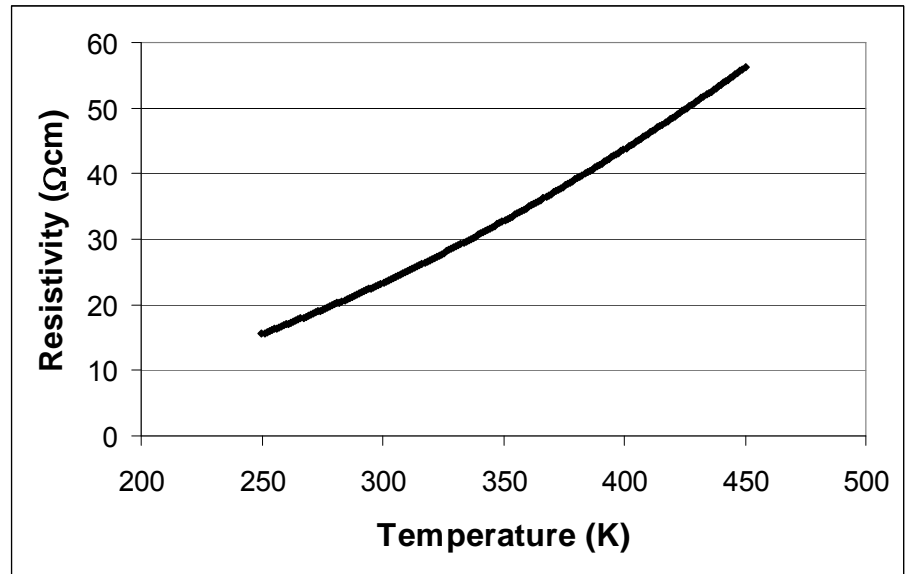characteristic.

**Fig.4 Dependence of the resistivity on the temperature, in a $2x10^{14}$ cm^{-3}
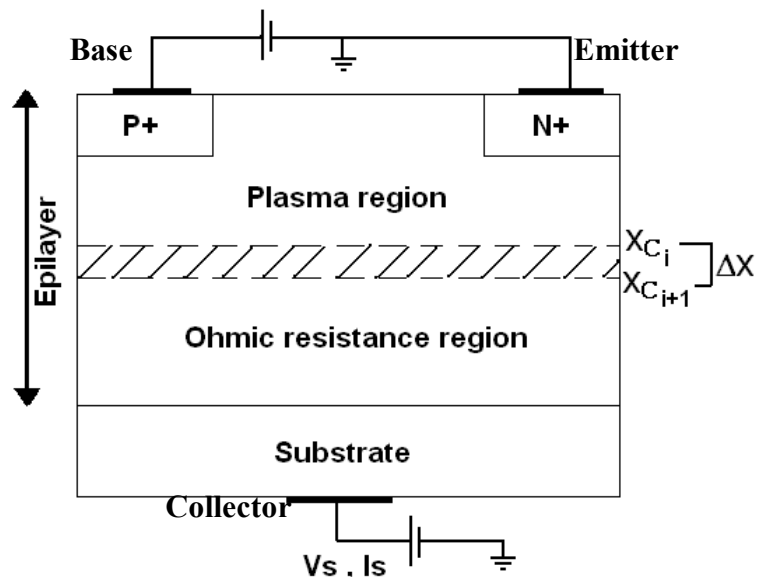N-doped silicon layer, using the Arora model for the carrier mobility**

Fig. 5 Cross section schematic of the test structure

Firstly, we have analyzed the untreated device (STD), without any lifetime control step. The Emitter-Collector characteristic with the base grounded exhibits a linear shape (Fig. 6) and we can easily obtain the doping concentration from its slope, by knowing the dimension of the device. Increasing the temperature, also the resistivity increases, according to the Arora model for constant doping concentration.
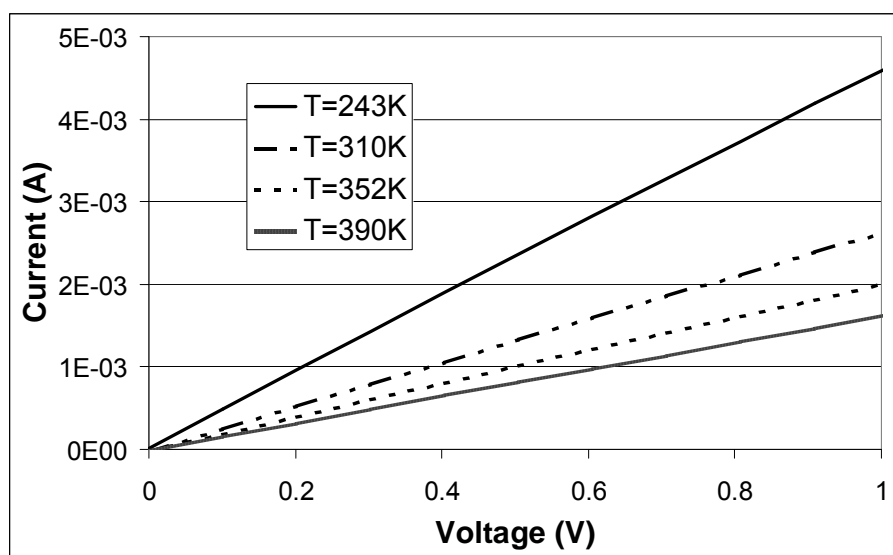

Fig. 6 Ohmic characteristic of STD device as a function of the temperature

The structure diffused by platinum at 920°C shows the same behaviour of the STD (Fig.7). The characteristic is linear and the resistivity increases with the temperature.

The STD device implanted by helium in dose $2x10^{11}$ cm^{-2} exhibits an apparently anomalous behavior (Fig.8): the resistivity reduces, when we increase the device temperature from 327K to 395K, unlike already observed for the other devices, but from 395K onwards the resistivity starts to increase.

This behavior cannot be explained using the classical mobility model with a constant doping concentration.
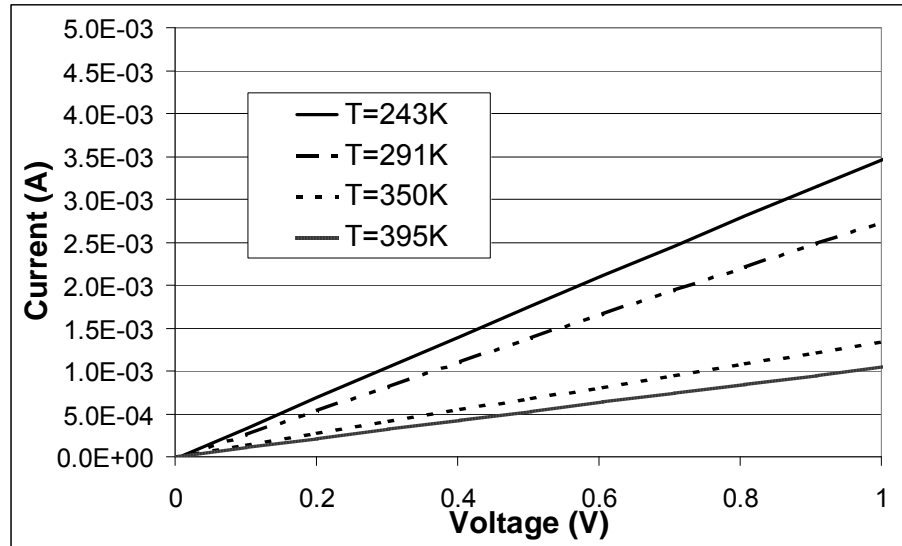
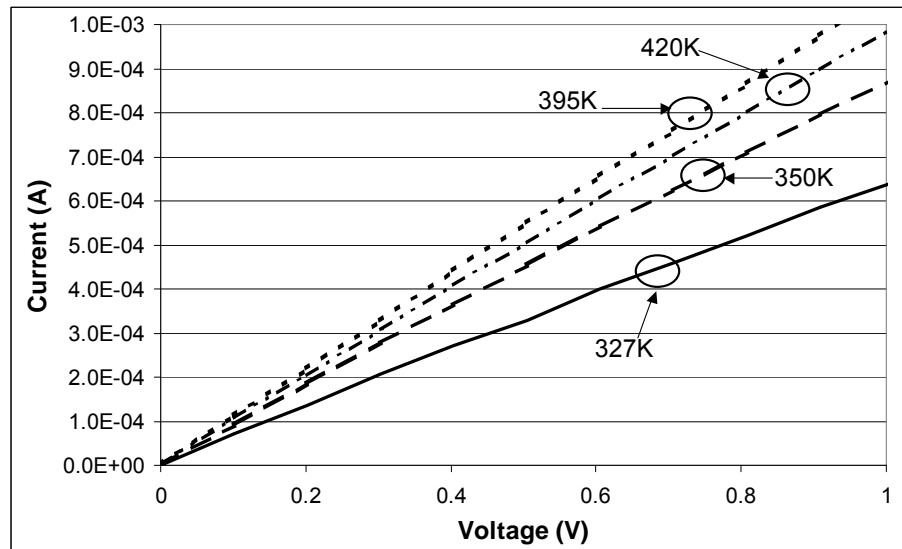**Fig.7 Ohmic characteristic of Pt920 device as a function of the temperature**

Fig.8 Ohmic characteristic of helium implanted device (dose $2x10^{11}$ cm^{-2}) as a function of the temperature

We can recall the general expression of the resistivity ρ, given by:

$$\rho = \frac{1}{q\mu_n(T)N} \tag{1}$$

where q is electronic charge, N the doping concentration and $\mu_n(T)$ the carrier mobility, function of the temperature. We do not take into consideration the weak dependence of the mobility on the doping for values less than 10^{15} cm^{-3}, being the doping concentration of the epilayer equal to 2×10^{14} cm^{-3}.

Tracing the product (R μ) between the resistivity R and the mobility μ, we can be free from the temperature dependence of ρ from the mobility $\mu(T)$ and, therefore, if the doping concentration is constant, also Rμ should be constant with the temperature.

In Fig. 9 the function Rμ is depicted as a function of the temperature for the STD device and helium implanted device, in the dose range from 10^{10} cm^{-2} to 5×10^{11} cm^{-2}.

The quantity Rμ holds actually steady in the STD device and, hence, the doping concentration is constant as expected. From the value of Rμ we can easily evaluate the doping concentration of the epilayer.

The implantation dose of 10^{10} cm^{-2} does not change the behaviour and Rμ is constant with the temperature. The implantation dose 10^{11} cm^{-2} involves a small increase of Rμ for temperature less than 300K. This effect becomes more evident in the devices implanted with doses 2×10^{11} cm^{-2} and 5×10^{11} cm^{-2}, even for temperature greater than 300K. Increasing the device temperature, the value of Rμ progressively reduces, recovering the one of the STD device.
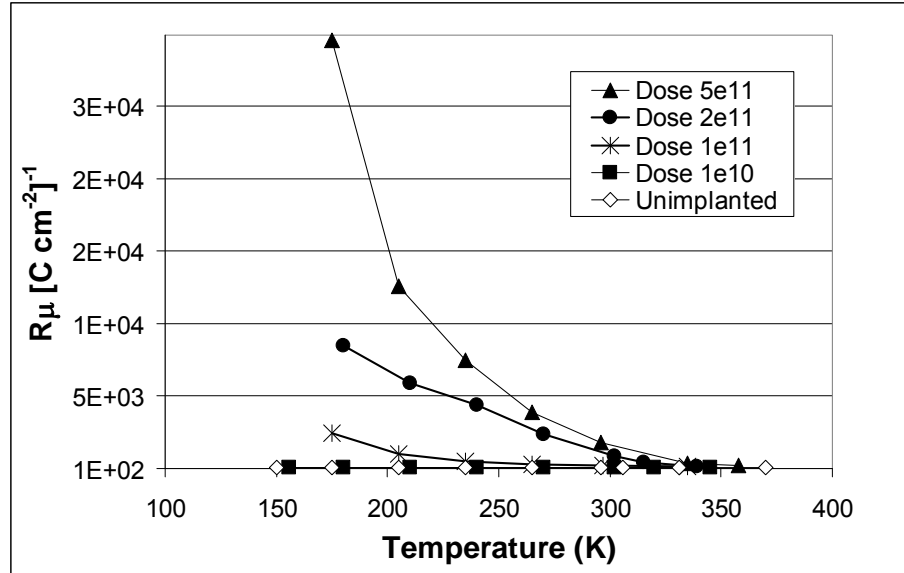
Fig.9 Product between ohmic resistance R and electron mobility μ_n measured as a function of temperature (for unity Area)

It is worth recalling the definition of $R\mu$:

$$\rho\mu_n(T) = \frac{1}{qN} \qquad (2)$$

Being q the magnitude of the electronic charge, the only dependence on the temperature should be owing to the doping concentration. As observed for STD and helium implanted device with dose 10^{10} cm^{-2}, $R\mu$ is constant and therefore effective doping does not change varying the temperature. For doses greater than 10^{11} cm^{-2}, $R\mu$ becomes strongly dependent on the temperature and from Eq.(2) the explanation can be found only in the doping concentration variation. Since $R\mu$ tends asymptotically to the value of the STD, we can conclude that for temperature greater than 400K the effective doping concentration is $2x10^{14}$ cm^{-3} even in the implanted devices.

This kind of analysis can give us only "global" information on the epilayer resistivity, but we are not able to say if the doping variation

affects the entire layer or just the region around the projected range, considering the nature of the implantation process.

3.3.2 Electrical extraction of the in-depth resistivity profiles in implanted devices

In order to find out more detailed information about the doping variation in helium implanted silicon, we can recur to the technique proposed in the second chapter, which makes use of the same test structure for the recombination lifetime measurement.

Before starting the analysis by means of our technique measurement, we carried out a SRP measurement on a test device implanted with dose $2x10^{11}$ cm^{-2} and energy 4.4MeV (Fig.10), which allows a projected range of 20μm to be obtained. As shown, the effective doping compensation becomes noteworthy at room temperature for dose $2x10^{11}$ cm^{-2}.

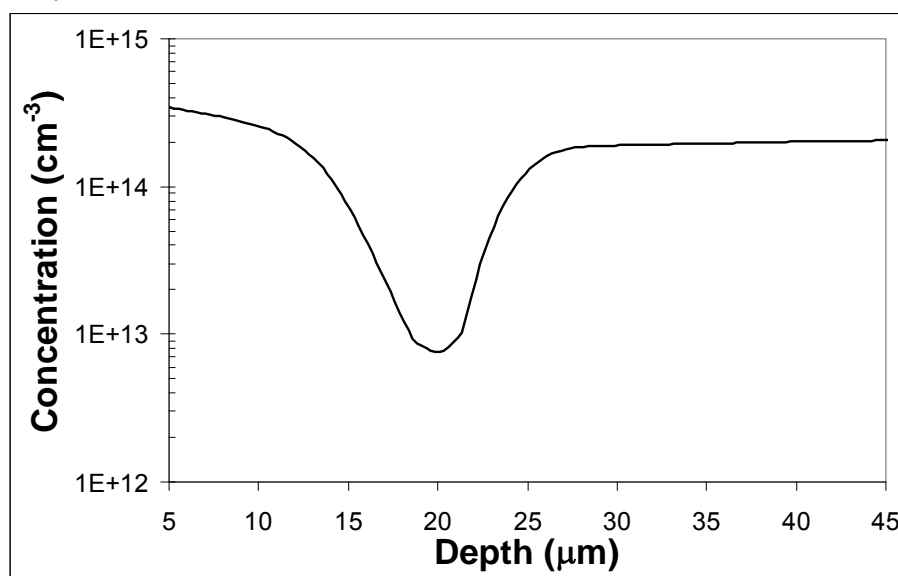**Fig.10 SRP measurement on test device implanted by helium in dose $2x10^{11}$cm^{-2}**

This mere experimental measurement evidences a strong modification of the resistivity profile (actually the Fig.10 reports the effective doping calculated from the measured resistivity profile). The doping concentration is strongly reduced by helium implantation and around the projected range the doping is one order of magnitude less than the bulk concentration ($2x10^{14}$ cm^{-3}). Nevertheless, although the SRP is a well-known and reliable technique, the analysis of the resistivity, performed by using SRP, does not help to understand the physical mechanisms underlying the changes induced by ion implantation. Carriers trapping, in fact, strongly depends on operation condition, such as temperature and injection level. Moreover, SRP is a destructive method which requires special prepared samples; comparative analysis in different operating condition, performed on the same sample, are, hence, impossible.

By means of our all electrical measurement method, we are able to monitor the resistivity profile in a semiconductor layer. The measurement technique takes advantage of a proper designed electronic test device that permits to control the operating conditions during the measurements. Moreover, the same device can be monitored before and after ion implantation giving unambiguous information on the sole effect of the implantation process. Also, the same test device can be used to measure the recombination lifetime profile thus allowing the complete electrical characterization of the implantation process.

Fig.11 displays the effective doping evaluated by our technique on STD device and helium implanted devices with doses 10^{11} cm^{-2} and $2x10^{11}$ cm^{-2}.

The effective doping of the STD device is almost constant and equal to $2x10^{14}$ cm^{-3}.

The dose $2x10^{11}$ cm^{-2} is the same of the sample already analysed with the SRP (Fig.10). From the comparison of Fig.11, it can be seen a discrepancy exists only toward the surface of the device while a good agreement has been found in the rest of the epilayer. Fig. 11 also reports the profile obtained for the dose $1x10^{11}$ cm^{-2}: the effect on the resistivity increase (and hence on the effective doping) is lower but not negligible.
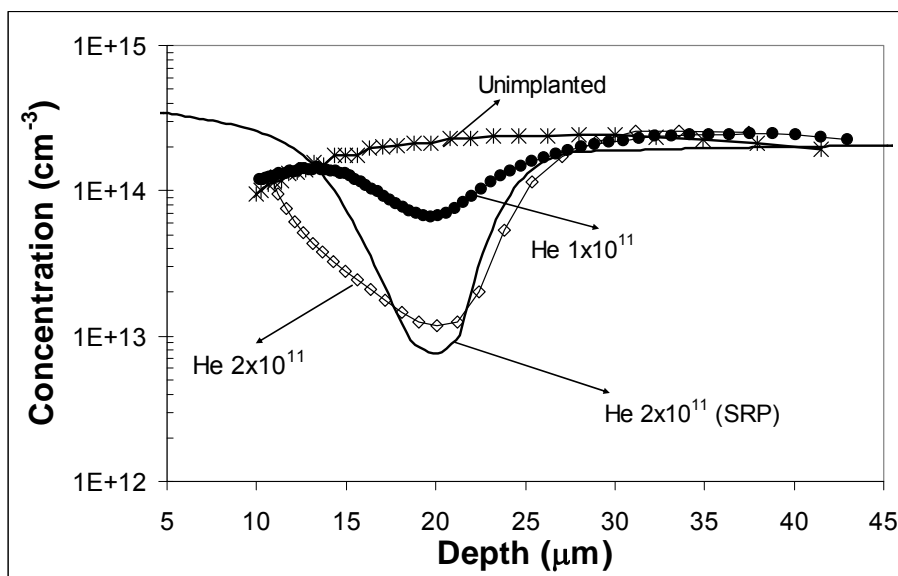
Fig.11 Experimental effective doping concentration obtained on untreated and helium implanted materials. The solid line is the effective doping profile obtained by means of SRP on a sample implanted with an helium dose of 2×10^{11} cm^{-2}; other curves have been obtained by using our technique.

It is interesting to study the effects on the effective doping as a function of both implantation dose and energy.

Fig.12 reports the effective doping profiles (evaluated from resistivity profile data) obtained at room temperature on the same samples implanted with dose 10^{11} cm^{-2} and energy 3.5MeV, 4.4MeV, 5.1MeV and 5.8MeV, the projected range of which are respectively 15μm, 20μm, 25μm and 30μm.

We observe a strong effect of doping compensation that is responsible for the increasing of the on resistance in helium implanted devices. It is worth highlighting that in principle the strong modification of the doping affects the reliability of the lifetime extraction. The minimum of the effective doping is function of the implantation energy: the greater the energy, the higher the concentration minimum is, but at the same time the dispersion around the projected range becomes larger.
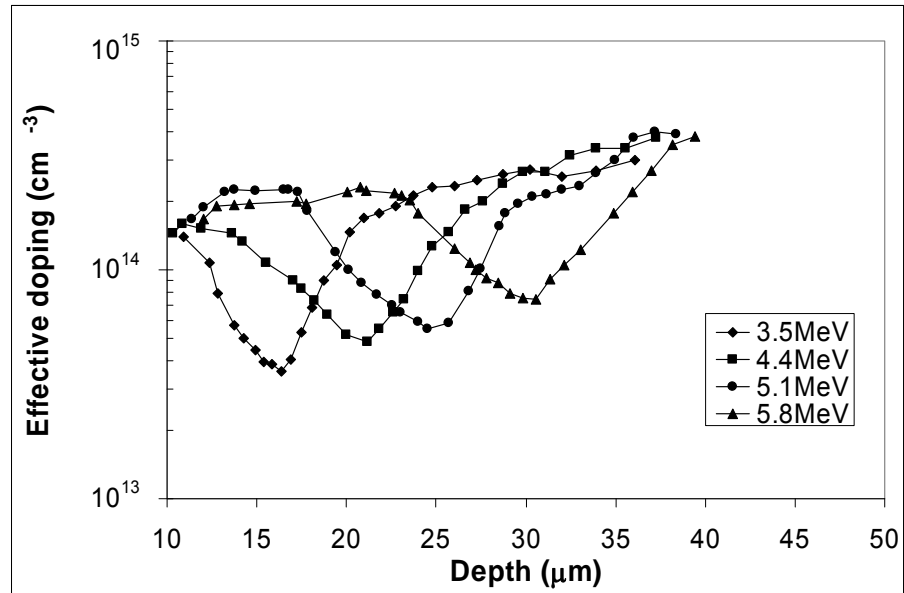
Fig.12 Effective doping profiles evaluated on the devices implanted with 10^{11} cm^{-2} and energy from 3.5 MeV to 5.8 MeV

Also the modification of the effective doping induced on the same samples described above is very interesting. Fig. 13 shows the effective doping profiles for increasing doses. The dose 10^8 cm^{-2} does not affect the layer resistivity, which holds unchanged after the implantation. Increasing the dose up to 10^{10} cm^{-2} a small compensation effect appears, whereas for doses greater than 5×10^{10} cm^{-2} the effect is not negligible anymore.

This fact should be accurately accounted for lifetime tailoring processes design because it is clear that the intrinsic properties of the base material are also changing.
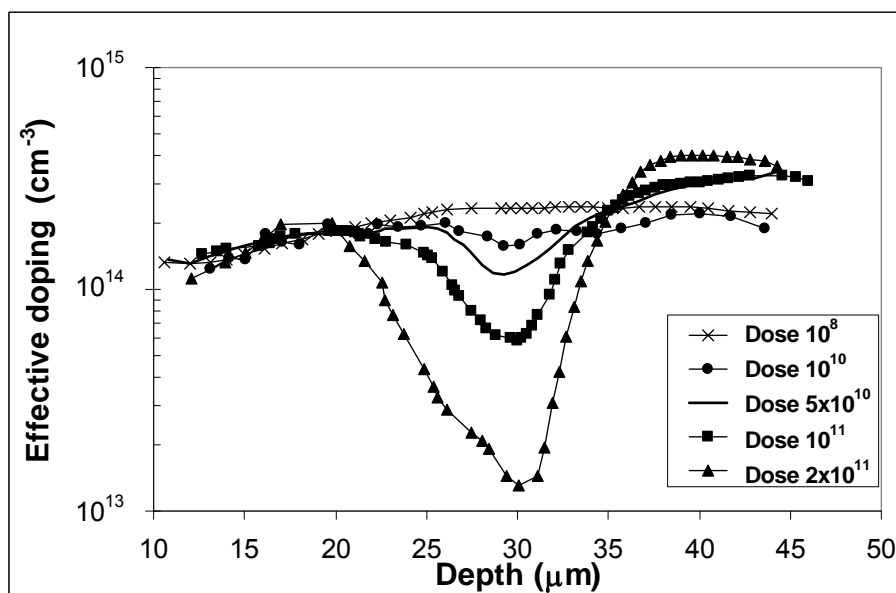
Fig. 13 Effective doping profiles evaluated on the devices implanted with energy 5.8 MeV and dose from $1x10^8$ cm^{-2} to $2x10^{11}$ cm^{-2}

It is very useful the possibility given by our technique to investigate the physical origin of the changes of the resistivity induced by helium implantation varying the device temperature. Fig.14 reports the effective doping profile reconstructed using our technique at increasing operation temperature of a helium implanted device, with dose $2x10^{11}$ cm^{-2} and energy 4.4MeV. The figure clearly shows that effective doping strongly depends on the temperature. The effect is more remarkable at low temperature, while the resistivity tends to recover the nominal value of the layer with increasing temperature and for T=410K the curve coincides with the one measured on the unimplanted sample.

The same results are observed in a helium implanted device with dose 10^{11} cm^{-2} and energy 5.8MeV in a temperature range from 190K to 390K (Fig. 15).

In [35] it is showed the same compensation effect related to the helium implantation on the N-doped silicon layer. They find out that the effective doping reduction around the penetration depth tends to vanish increasing the annealing temperature. For temperatures greater than 430°C the introduced states are not acceptor-like anymore
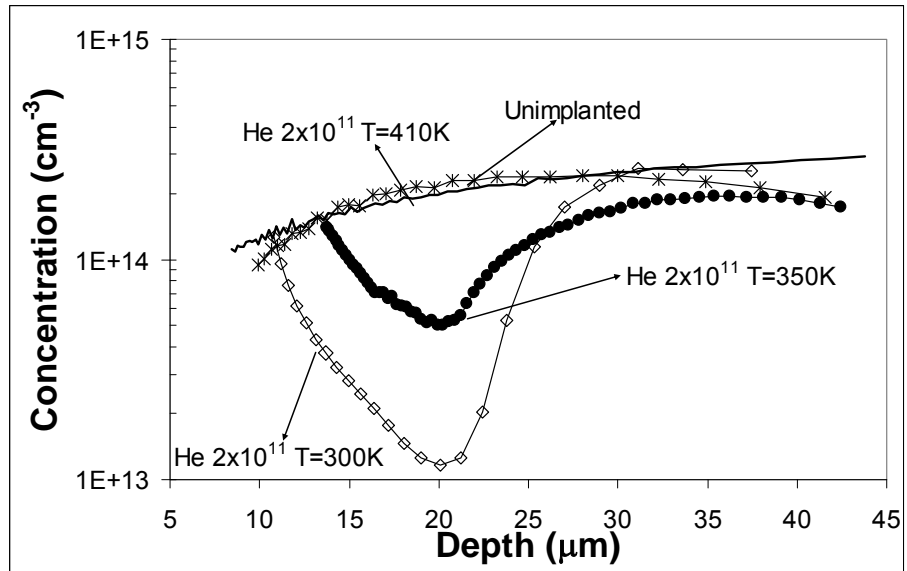
Fig.14 Effective doping profiles obtained for the sample implanted with dose 2×10^{11} cm^{-2} measured at three different temperatures. The changes induced by helium implantation vanish when the temperature increases.
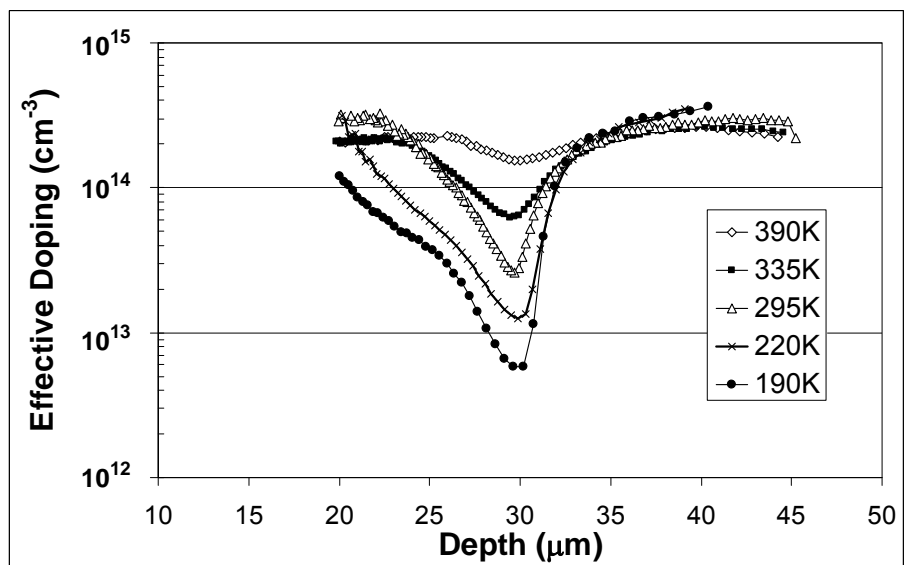

Fig. 15 Shape of the effective doping as a function of the measurement temperature evaluated on the device implanted with dose 10^{11} cm^{-2} and energy 5.8 MeV

but their nature change and a doping increasing is revealed. Nevertheless, at these temperatures most implantation-related defects are completely annealed and thereby the effectiveness of the centres on the recombination lifetime reduction drastically decreases. Such annealing temperature is suitable only if helium implantation is just used to locally modify the doping concentration. If the aim is to control the recombination lifetime, lower annealing temperatures have to be used.

Nevertheless, even though in [35] they observe the same compensation effects, they are not capable to study the dependence of this effect on the operating temperature, but just on the annealing temperature. Our technique allows us to measure the effective doping reduction in the typical temperature range of power devices (25°C-125°C), when the device works at high injection level. We notice that in this temperature range the effect is totally reversible, indicating that it is due to some trap level in the energy bandgap of the silicon epilayer. The observed disappearance of the resistivity variation for high temperatures indicates the crossing of the trap energy level by the Fermi level that makes ineffective the trap capability. Hence, the temperature at which the above disappearance occurs gives an estimation of the energy level of the trap centre. The compensation effect, which determines a reduction of the effective doping, suggests that the centre responsible of this behaviour is an acceptor-like, as observed in [35].

3.4   Recombination Lifetime

The results found out on the effective doping modifications are useful for the correct estimation of the lifetime profile, by means of the differential measurement technique. Indeed it has been shown in the chapter 2 how the evaluation of the abscissa X within the low-doped region strongly depends on the doping profile. Therefore, knowing the effective doping concentration for each device, we can use this new information for the evaluation of the lifetime profile.

Obviously this is possible because the technique for the resistivity measurement is not destructive and, hence, we can measure both effective doping and recombination lifetime on the same device, for several temperatures. This achievement represents the main point of our measurement technique.

3.41. Room temperature measurements

Firstly we will analyze the effect of helium implantation as a function of the energy implantation, for a given dose 10^{11} cm^{-2}.

The extracted profiles are shown in Fig.16. The shapes we found are almost gaussian, according to the defects distribution of the implantation process. The penetration depth of the energies 3.5MeV, 4.4MeV, 5.1MeV and 5.8MeV are respectively 15μm, 20μm, 25 μm and 30μm and the technique is able to evaluate them with a good agreement. The minimum of the lifetime varies with the energy and its value tends to increase for increasing energies, as well as the width of the profile. We have already observed this effect on the effective doping distribution in Fig 12.
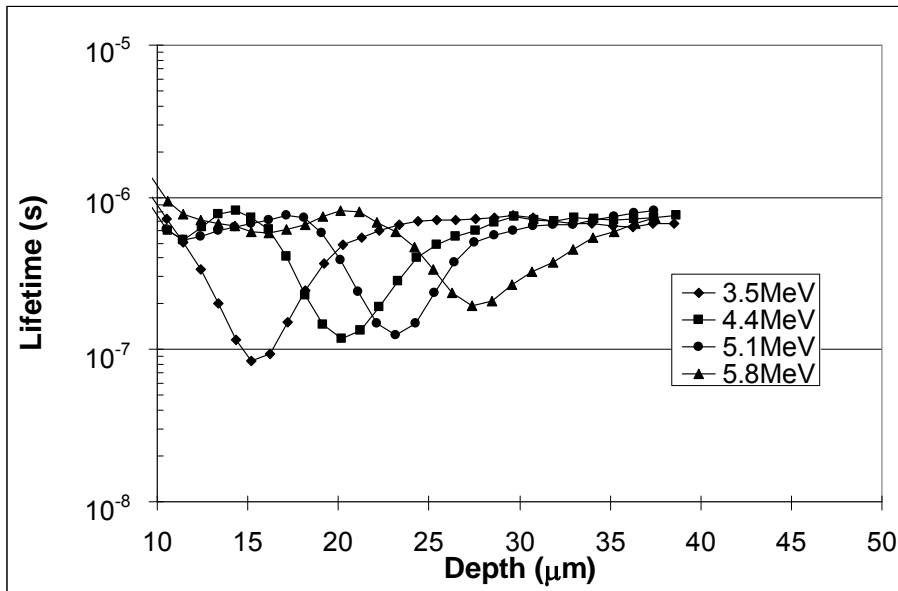
Fig.16 Lifetime profiles measured on the devices implanted with 10^{11} cm^{-2} and energy from 3.5 MeV to 5.8 MeV
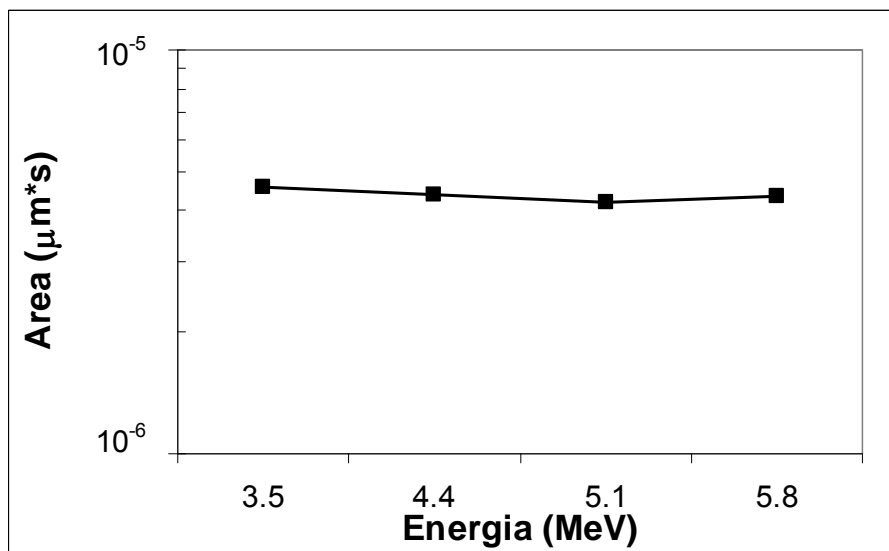

Fig.17 Area enclosed in the lifetime profiles of the Fig. 16, using as reference base value 1μs.

Assuming 1μs as reference value, we can evaluate the area enclosed within the lifetime profile, between the minimum and the reference value (Fig.17). It is really interesting to note that the value of this area is constant changing the implantation energy. This value could be an estimation of the implantation dose which is for all the devices equal to 10^{11} cm^{-2}.

Reporting the width of the profile in correspondence of the lifetime value of 1μs (Fig.18), we find out that the increase is almost linear and the widening is about 2μm for every 10μm of implantation depth.
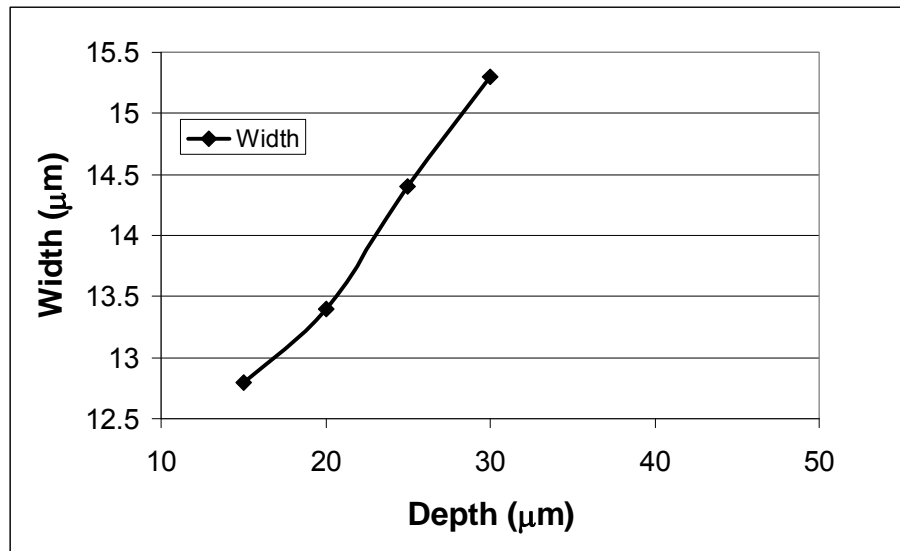

Fig.18 Width of the lifetime profiles as a function of the penetration depth

Although the energy range is not so wide, the curves of Fig. 17-18 could be useful to draw a rule to predict the minimum lifetime value and the profile width even for energies greater than 5.8MeV.

Fig.19 shows the lifetime profiles obtained for a fixed energy of the helium beam (5.8 MeV) and by varying the total dose from 10^8 cm^{-2} to 2×10^{11} cm^{-2}. The lifetime of the unimplanted material is about 100μs with a decrease toward the epilayer-substrate transition due to the presence of a small buffer layer. The figure shows that also with the lower dose a significant effect of the helium implantation is

obtained. In fact, the lifetime profile decreases of about one order of magnitude without the evidence of a localised low lifetime region. A possible explanation is that the very high lifetime of the untreated material is indicative of a defect free high quality material in which also the low concentration of defects induced by helium ions that travel across has a macroscopic effect.

The dose of 10^{10} cm^{-2} causes a further and almost uniform decrease of one order of magnitude. Nevertheless, in the dose range from 10^8 cm^{-2} to 10^{10} cm^{-2} we note a reduction of the lifetime, without any compensation effect on the effective doping, as shown in Fig.15.

Then, from a dose of 10^{10} cm^{-2} onwards, lifetime starts to locally reduce around the penetration depth. The minimum is reached with the higher dose of $2x10^{11}$ cm^{-2}: in this case the lifetime becomes about three order of magnitude lower than the one of the untreated material.

This experiment suggest that helium ions create active lattice defects along their path also prior of the stopping range and that only using high doses, in the range 10^{10}-$2x10^{11}$ cm^{-2}, a separate low lifetime region is clearly visible.
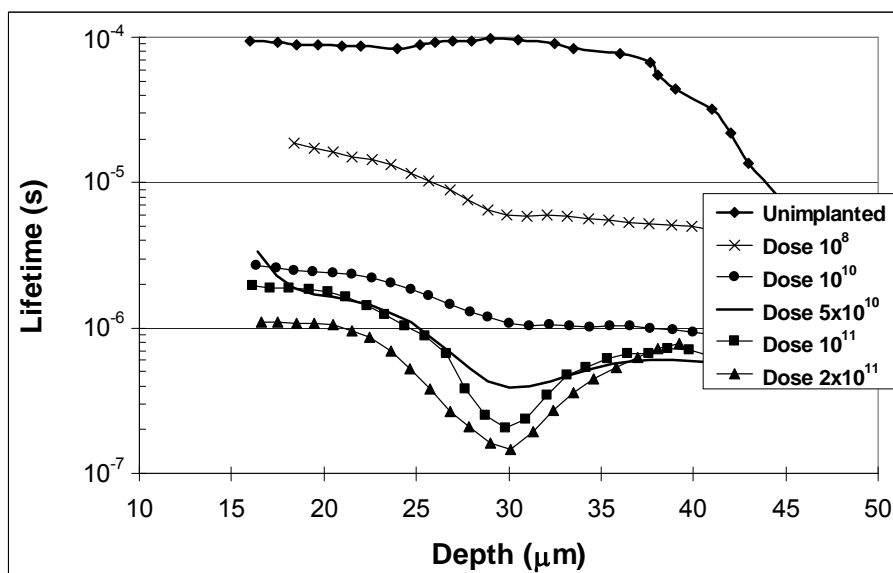

Fig. 19 Lifetime profiles measured on the devices implanted with energy 5.8 MeV and dose from 10^8 cm^{-2} to $2x10^{11}$ cm^{-2}

The measured lifetime profiles show how helium implantation involves a noteworthy localized reduction of the recombination lifetime, even though the lifetime reduces in whole low-doped region compared to the unimplanted device. The quality of the starting material is very high and its features degrade fast when the implanted ions go through the lattice.

However, the displayed profiles represent a remarkable result, because in literature there are not works which shows how helium implantation locally modify the recombination lifetime respect to the unimplanted device. Many techniques are only able to extract directly the recombination centers by observing the temperature dependence of some physics parameters (e.g. emission velocity in DLTS), but they can not measure the lifetime value around the damaged region.

The lifetime profiles at room temperature are interesting, because allow showing the effect of the helium implantation on the recombination lifetime tailoring.

Nevertheless, a more complete analysis requires measurements at different temperature, in order to extract information about the nature of number and the nature of the introduced recombination centers.

3.4.2 Lifetime measurements as a function of the operating temperature

Temperature dependent experiments have been performed on samples implanted with dose of 10^{11} cm^{-2} and beam energy 5.8MeV. Fig.20 shows the lifetime profiles measured in the temperature range 190K-390K.
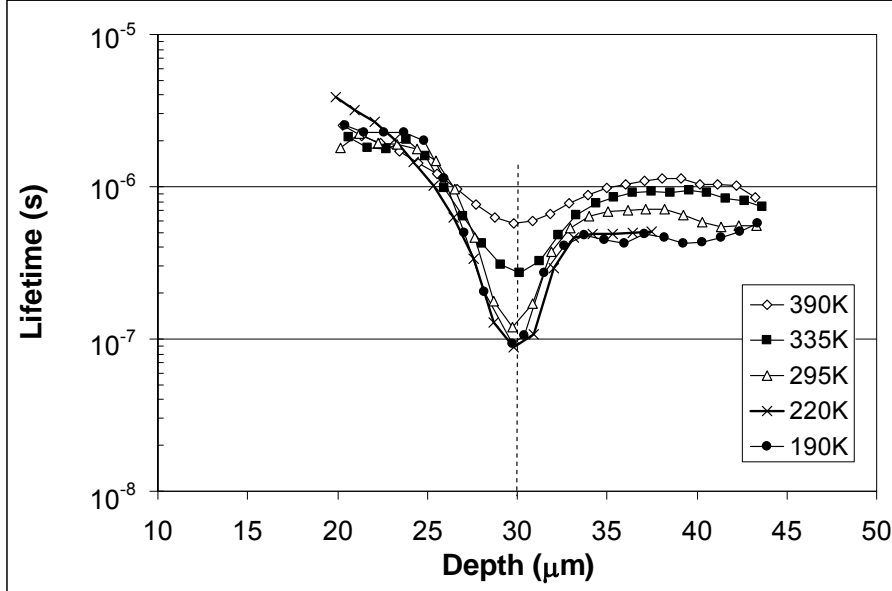
Fig. 20 Lifetime profiles at different temperatures measured on device implanted with dose 10^{11} cm^{-2} and energy 5.8 MeV

As can be seen the lifetime in the low lifetime region increases when the temperature increases. This fact gives a strong evidence that recombination centres involved in the recombination process are far from silicon midgap. As it is well known, in fact, the dependence of the lifetime on the temperature T (and the injection level) is the one of Eq.12 in the chapter 2, from which it is clear that the dependence on T only appears when the Fermi level crosses the energy level of the recombination centre. The more E_t is close to E_i, the more the temperature dependence appears at higher temperatures.

Based on the validity of Eq.12 and assuming that each recombination centre present within the bandgap acts independently from the others, the total lifetime can be written as:

$$\frac{1}{\tau} = \sum_i \frac{1}{\tau_i} \qquad (5)$$

It is worth noting how the temperature dependence of the lifetime around the projected range is very pronounced, whereas in the external regions the lifetime is almost unchanged.

This evidence let us suppose that helium implantation introduces recombination centers in the middle of the forbidden gap and, hence, the lifetime in this region changes considerably with the working temperature. In the external region there are only the centers of the starting material and due to the weak dependence on the temperature, they could be supposed to lie near the midgap.

3.5 Extraction of the recombination centres distribution

As already described in the chapter 2, we can study the nature of the recombination centers tracing the Arrhenius diagram for each depth along the layer. Let concentrate our attention on what happens at a depth of 30μm along the semiconductor layer, as indicated from the line drawn in Fig.20. The intercepts of this line with the measured lifetime profiles allows us to construct the plot shown in Fig.21 that represents the temperature dependence of the lifetime at the point x (circles). Using the procedure illustrated in section 2.4 the curve of Fig.21 has been interpreted using Eq.12 in the chapter 2, thus obtaining the relevant parameters of the recombination centers present at the point x. In this figure the marked full line is the analytical fit of the experimental points (circles).

As it was expected the figure shows that the lifetime is constant at low temperatures and starts to increase at the temperature where the Fermi level crosses the energy level of the recombination centre present in the material. It is worth noting that at low temperatures, when the normalised lifetime becomes constant, the constant value is given by

$$\tau \times T^{-1/2} \propto \frac{1}{\sigma N_t} \qquad\qquad (3)$$

where σ is the capture cross-section of the recombination center and N_t is its concentration. Hence, from plots like that of Fig.21, it is also possible to obtain for each centre the product σN_t that represents the effectiveness of the centre. Moreover, if the capture cross section is known, it is possible to calculate the absolute number of defects N_t.
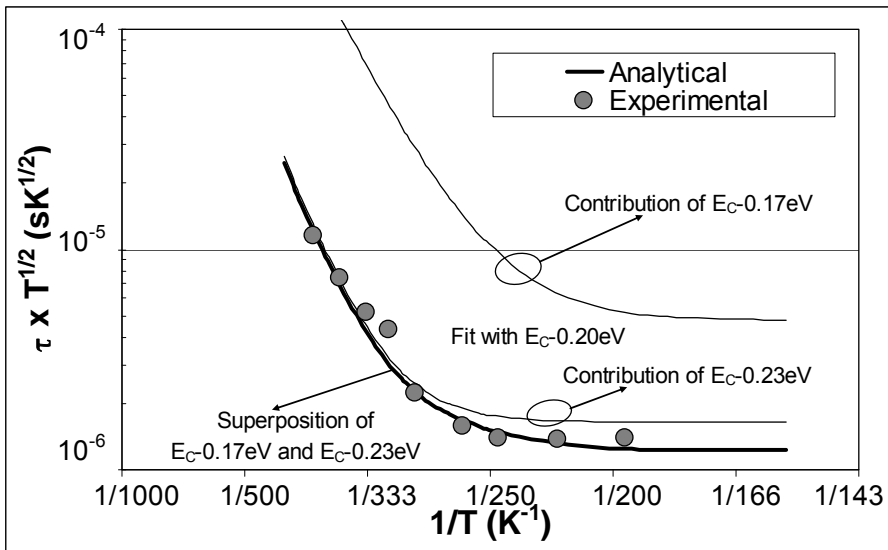

Fig.21 Arrhenius plot extracted from the profiles of Fig. 20 at the depth of 30μm

However, as shown in the figure, a single trap process does not describe the whole set of the experimental points because the value of the constant part and the knee of the curve are correlate. Indeed the fit of the experimental points has been obtained from the superposition of two independent recombination centers, E_C-0.23eV and E_C-0.17eV (the contribution of each of them is indicated with the thin full lines); in particular we find that, at room temperature, the lifetime is dominated by a recombination centre whose energy level lies at E_C-0.23eV.

In the Fig.22 are reported two "error curves" (dashed lines) obtained using E_C-0.23eV +/-0.03eV as energy level. As can be seen the fit of experimental data is totally wrong in these cases.

The analysis described above with reference to Fig.21 for the depth x=30 μm has been repeated at various points along the epitaxial

layer thus obtaining the identification of the centers present along the entire epitaxial layer and their concentration.
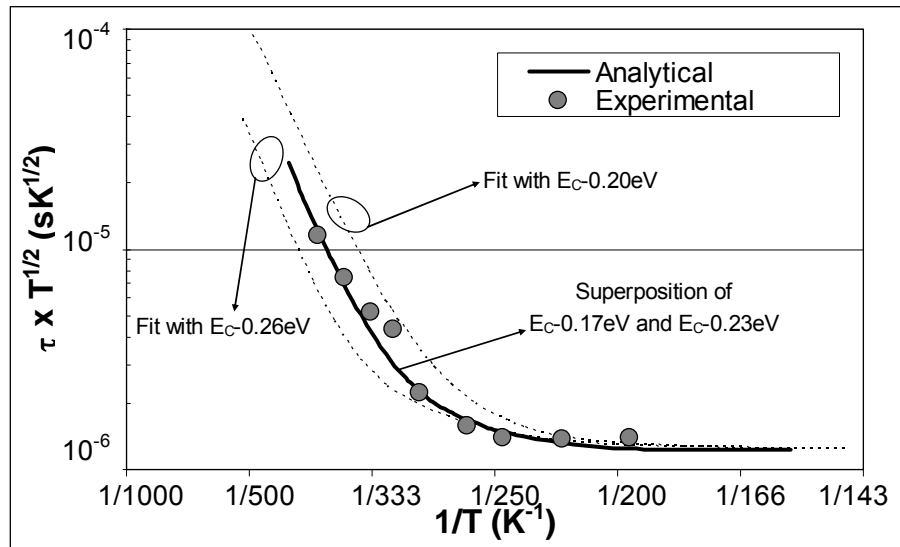

Fig.22 Arrhenius plot extracted from the profiles of Fig. 20 at the depth of 30µm, with "error curves"

Fig.23 shows the distribution of the most relevant recombination centers that have been identified. In the entire epilayer we have identified the same centers founded at the penetration depth.

In Fig.23 the concentration profiles for E_C-0.23eV and E_C-0.17eV are compared with the primary damage induced by helium implantation evaluated by the Montecarlo simulator TRIM [36]. TRIM can evaluate the distribution of the vacancies, that are primary defects, created when atoms are dislodged from their equilibrium position by implanted ions. As said, this defects are very unstable and tend to recombine each other or with other impurities. Our characterization method permits to interpret the temperature behaviour of the lifetime in terms of energy levels of recombination centers. Based on relevant results reported in the literature, we can identify the physics nature of the defects knowing their energy level.
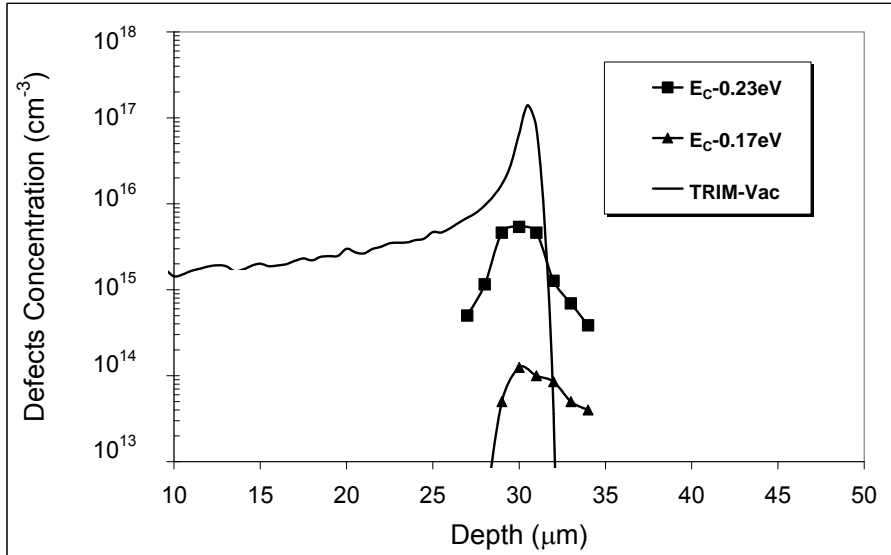
Fig.23 Comparison between the primary defects shape evaluated by TRIM and the secondary defects ones evaluated by means of our technique

In particular the energy levels we found, Ec-0.17 eV and Ec-0.23 eV have been elsewhere [37] attributed to the oxygen-vacancy complex (A-center) and to the double negatively charged level of the divacancy V_2^{--} respectively. The values of the capture cross section of the two centers are [37]:

E_C-0.23eV -> $\sigma = 2x10^{-15}$ cm^2
E_C-0.17eV -> $\sigma = 2x10^{-14}$ cm^2

As seen, the extracted recombination centers are related to the combination of vacancies with other vacancies (divacancy) or with oxygen (A-center), which is the dominant impurity present in silicon.

Therefore the characterization technique allows us to obtain the distribution of the secondary defects and we can compare it with the vacancies profile evaluated by TRIM simulation. The position of the peak defects coincides but experimental curves seem to be wider than that predicted by TRIM. Fig.23 also shows that the concentration associated to E_C-0.17eV is more than one order of magnitude lower that that associated to E_C-0.23eV thus confirming that the latter dominates the recombination mechanism.

Other works [38,39] reveal the presence of the same recombination centers after helium implantation. Nevertheless, they find also a deeper level E_C-0.42eV, that is the single negatively charged divacancy. Being a deep centre, it affects the low level injection lifetime and the generation lifetime, while its effect at high injection level is low. At high injection level, the recombination lifetime is strongly affected by the A-center and V_2^{--}.

3.5.1 ATLAS simulation

The concentration profile of Fig.23, with energy level and capture cross-section of the centers, allows having a complete description of the helium-related defects and represents to final results to which we have been aiming. Indeed by using all the extracted information we are able to describe more accurately the recombination centres introduced by helium into a device simulator, aiming at studying the impact on the power diodes behavior.

In order to verify the reliability of the extracted defects concentration and energy levels, we tried to evaluate the lifetime profile by using it as input parameter for the device simulator

In particular we described the elementary cell of our test structure by means of an ATLAS mesh, making use of the doping profile measured on the real device. Afterwards we introduced the defects concentration recalling an ascii file with the in-depth profile of the centres as well as obtained in Fig.23. Obviously the energy levels of the two centers are E_C-0.17eV and E_C-0.23eV. The base lifetime is been set equal to 1μs.

Fig.24 displays the measured lifetime profile on the STD device implanted with dose 10^{11} cm^{-2} and the lifetime curve obtained from a simulated experiment using the above mentioned parameters.

The agreement of the two curves is a further evidence of the coherence of our results, since the defects distribution of Fig.23 allows the same lifetime measured on the real device to be obtained.
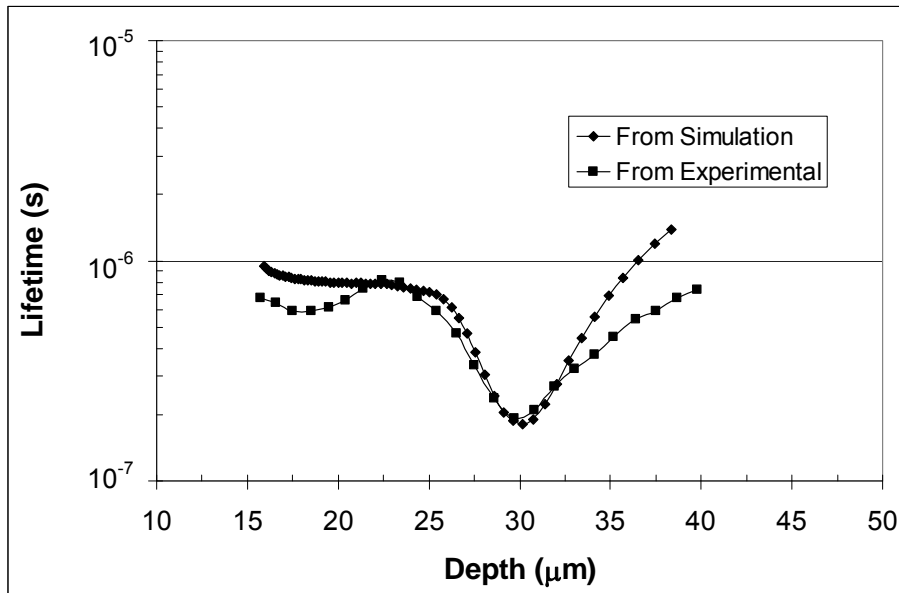
Fig.24 Comparison between the lifetime profile measured on the device implanted with dose 10^{11} cm^{-2} and energy 5.8 MeV and this one evaluated with ATLAS simulation using the defects profile of Fig. 23

3.6   Combined effect on recombination lifetime and effective doping

It is worth observing the effects on both recombination lifetime and effective doping as a function of the temperature on the same diagram. Fig.25 shows the profiles measured on the sample implanted with an energy beam of 4.4 MeV and dose of $2x10^{11}$ cm^{-2} for two different temperatures (300K and 410K) As can be seen, at room temperature the variation of the effective doping is very pronounced but at T=410K the nominal value ($2x10^{14}$ cm^{-3}) of the untreated material is recovered. On the other hand the lifetime profile is still variable at 410K, even if the minimum low lifetime value has increased. The results of   Fig.25 indicates that great care must be taken in the design of power devices operating at varying temperatures because of the strong variation of such basic parameters.
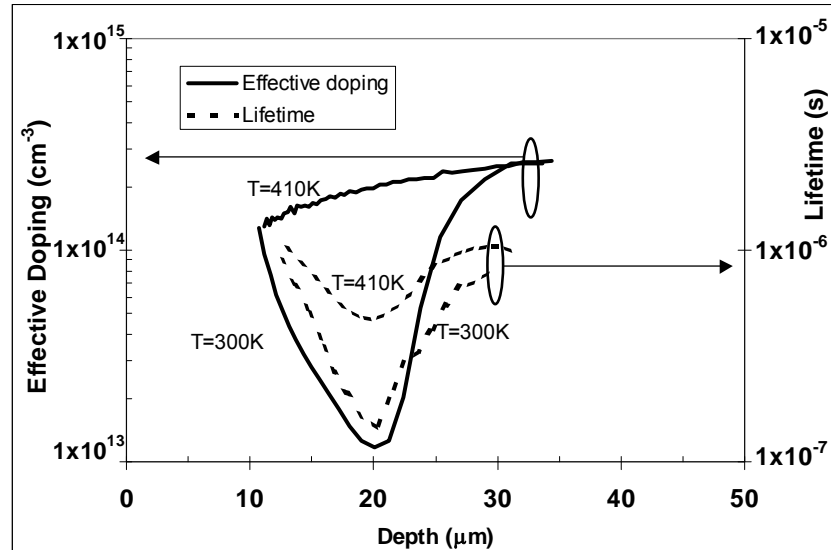

Fig. 25 Effective doping and lifetime profiles measured at two different temperatures on the sample implanted with helium in dose $2x10^{11}$ cm^{-2}

3.7 Application on helium implanted power diodes

For the sake of concreteness previous results have been used to reproduce the turn-off behavior of a fast recovery power diode. The diode has been implanted with helium in the anode region with a dose of 10^{11} cm^{-2} and energy 2.3MeV.The reverse recovery curves have been recorded at two temperatures, 298K and 428K respectively; they are reported in Fig.26 using the full lines. The curve with the higher reverse peak corresponds to the higher temperature. The increasing of the reverse peak indicates that the lifetime has increased with the temperature. Again, this fact implies that the recombination center dominating the recombination process in this range of temperatures has an energy level far from the midgap. As can be seen from the figure the two experimental curves are perfectly reproduced by the simulated experiment (dashed lines) done by using the energy level and the spatial trap distribution found in the previous section.
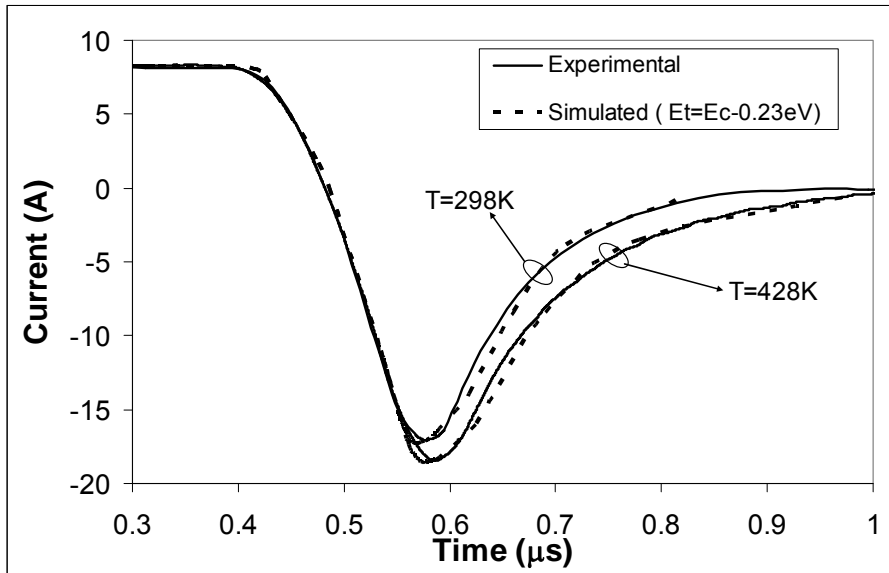

Fig.26 Comparison between the reverse recovery waveforms measured on Helium implanted diode with energy 2.3 MeV and dose 10^{11} cm^{-2} and these ones evaluated with ATLAS simulation using the defects distributions of Fig. 16 extracted with our technique

3.8   Final comments

By means of the improvement proposed for the measurement technique, we have been able to investigate the nature of the defects related to helium implantation. The good knowledge of the effects on recombination lifetime and effective doping compensation let us extract a valid model which describes effectively the defects distribution around the penetration depth in silicon implanted layer.

By using this model in a physically-based simulator, now we are able to study the behavior of power diodes with a local control of the lifetime and design a device with desired features.

Chapter 4

Dynamic Avalanche

In the modern switching applications a freewheeling diode in parallel to the switch is needed, in order to avoid abrupt current variations that could damage the circuit components.

Power diodes have also the task of sustaining large reverse voltages when they are reverse biased. The maximum voltage sustained across the depletion region depends on the impact ionisation onset, which starts as soon as the electric field reaches its critical value, which is around 10^5 V/cm in silicon semiconductor devices. [51]. One of the most valuable features for these devices is just the breakdown voltage, which represents an operation limit for the circuit. The breakdown voltage is inversely proportional to the doping concentration: the higher the needed breakdown voltage, the lower the doping concentration is, with the consequent drawback of increasing the series resistance in forward mode.

Power diodes could be supposed to be never under avalanche multiplication condition if the voltage across the device is less than the breakdown value. Nevertheless during the ON-OFF switching it could happen that impact ionisation starts inside the device even though the breakdown voltage has not been reached yet. In stressful conditions this effect can lead even to the destruction of the device.

During the turn-OFF the analysis is more complex because the drift region is filled with the charge carriers stored in the forward biasing that have to be swept out and their distribution is obviously time dependent. Reverse voltage is sustained across the depletion region, but the presence of the carrier excess, in particular working conditions as forward current, di/dt, temperature, can lead the electric field to reach the critical value although the voltage is less than the static breakdown value [40]. In this event carriers reach the saturation

velocity and the ionization impact process begins with the consequent generation of the new charge carriers. The effect is called *dynamic avalanche* and, together with the snappy recovery, is one of the main failure mechanism in power devices [41,42,43]. Many published works study the phenomenon, but, although the causes have been identified, on the other hand it has not been understood clearly how improving the dynamic ruggedness of the device, without worsening the static parameter, as ON-state voltage drop and leakage current.

The generation of the new free carriers due to dynamic avalanche determines an unwanted increase of the current while the diode voltage rises and, therefore, the device exhibits a negative differential resistance (NDR) behavior.

As shown in [42] the onset of the dynamic avalanche can cause the destruction of the device, due to the formation of filaments, where the current density reaches very high values [44]. The dynamic avalanche does not determine necessarily the destruction of the device: as described in [45] the electron generation can partly compensate the concentration of the mobile carriers in the depletion region and, therefore, the gradient of the electric field reduces. In this case the phenomenon becomes self-limiting.

Usually the impact ionisation starts near the PN junction, which is the first to deplete; for hard switching conditions also the depletion region of the NN+ transition extends in the drift layer [46]. This is a critical operating condition: when the two depleted regions merge, the plasma region vanishes abruptly, causing dangerous voltage overshoots for the device and the other circuit components. As final effect the reverse recovery can become snappy in the final instants, leading to oscillations and system instability. In [46] we can see how the dynamic avalanche becomes very dangerous when avalanche multiplication appears also at NN+ transition.

Due to the increase of the switching frequency, the slew rate di/dt has to be high but, just when switching conditions become particularly stressful the dynamic avalanche appearance is more probable [40]. Also undesired voltage spikes in the circuit could cause the avalanche multiplication onset during diode urn-OFF.

As shown in [42] the higher the charge concentration in the drift region during reverse recovery, the higher the probability to have

dynamic avalanche is. The stored charge has to be swept out as soon as possible, but we could incur in the snappy recovery phenomenon, with the danger to have large voltage overshoots [47,48]. Therefore we have to find the right trade-off between the need to obtain a soft recovery and the one to avoid the onset of the dynamic avalanche [49].

It is necessary to understand the physics of the phenomenon and improve the ruggedness of the device, in order to avoid either its destruction or a further power loss.

4.1   Static breakdown

In this section we recall briefly the basic theory of the static breakdown. Fig. 1 reports the reverse IV characteristic of a power diode. For applied voltage less than the breakdown value, the leakage current flows through the device. As the breakdown voltage is reached, avalanche multiplication takes place and the current increases. In Fig.2 we show the electric field shape for the five points indicated in Fig.1.

For voltages less than the breakdown value the electric field exhibits the typical triangular shape. When the intensity reaches the critical value (about 2.2×10^5 V/cm) at the PN junction the avalanche multiplication starts and new free carriers (holes and electron) are generated. The electric field pushes the negative charges toward the NN+ transition and positive ones toward the PN junction. Here, at the junction, we can write the slope of the electric field as:

$$\frac{dE}{dx} = \frac{q}{\varepsilon}\left(N_D + p + p_{gen}\right) \tag{1}$$

where N_D is the doping of the bulk and p_{gen} is the number of the generated holes for unit of volume.
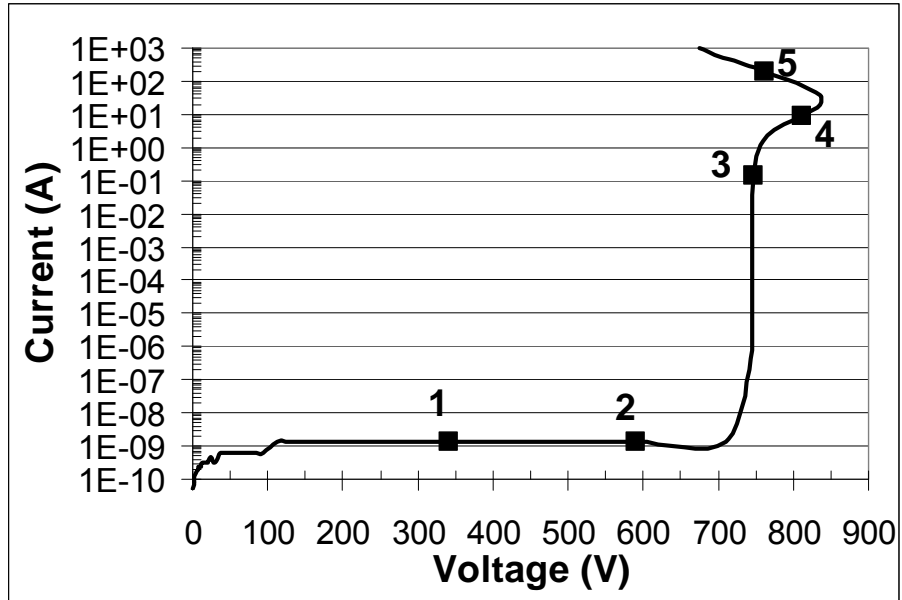
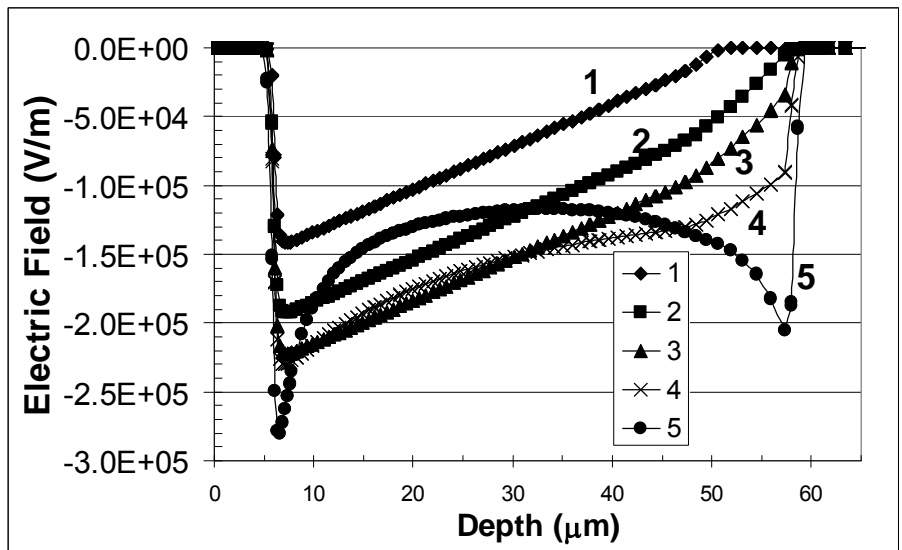**Fig.1 Reverse IV characteristic of a power diode**

Fig.2 Electric field strength in the five points of the IV characteristic of Fig.1

Therefore, due to the holes generated and accelerated toward the junction, the slope of the electric field increases: the area under the

electric field also increases and we observe a positive differential resistivity behavior in the I-V characteristic.

For higher current level, a depleted region appears also at the transition NN+ where the slope of the electric field is:

$$\frac{dE}{dx} = \frac{q}{\varepsilon}\left(n + n_{gen} - N_D\right) \qquad (2)$$

In this case n_{gen} is the number of the electrons generated for unit of volume. Therefore the slope increases in this region and the electric field assumes an U-shaped form. The area under the electric field reduces and in these conditions a negative differential resistance branch appears.

4.2   Dynamic avalanche

The above analysis only concerns the static behaviour, when there are no charge carriers in the drift region. Nevertheless we know that power diodes for switching applications have to switch fast from the ON-state to the OFF-state. When the junction is forward biased, a large current flows and the device works at high injection level. The minority carrier number is much greater than the doping concentration and, respecting the neutrality law, the majority carriers concentration is equal to the minority one. As known, this effect is called conducibility modulation and allows the series resistance to be reduced in forward mode. Generally the series resistance is large, due to the low doping concentration, needed to have a high breakdown voltage.

When drift region is filled with charge carriers, we can define a new effective doping N_{eff} evaluated as [46]:

$$N_{eff} = \left|N_D + p - n\right| \approx \left|N_D + \frac{J_p - J_n}{q v_{sat}}\right| \qquad (3)$$

and, therefore, for large current values the effective doping is greater than the bulk concentration N_D.

When the On-Off switch starts, the charges stored in the drift region have to be removed before the current flow becomes zero. During the transient the reverse voltage is applied while there are still charge carriers in the drift region and, consequently, the previous analysis about the onset of the static avalanche breakdown is no longer valid.

4.2.1 Time evolution of charge carriers and electric field

To better understand how dynamic avalanche affects the switching, it is worth observing how charge concentration and electric field strength vary as a function of the time during the reverse recovery.

In normal conditions (recalling section 1.1 of the chapter 1) when the switching starts, the charge concentration decreases near the PN junction and a depleted region, where the reverse voltage is sustained, extends. The shape of the electric field is almost triangular. At the end of the transient, the drift region is depleted of charge carriers and the electric field is still triangular.

Under particular operation conditions it could happen that the electric field reaches the critical value during the transient and carriers acquire enough energy to create a new electron-hole couple and impact ionisation starts.

Below we show ATLAS simulations where impact ionization model has been either enabled or disabled. The thickness of the drift region of the simulated diode is 58μm and the doping concentration $2x10^{14}$ cm^{-3}, to which corresponds a breakdown voltage of about 700V.

In Fig. 3 we show the two reverse recoveries evaluated on the same structure, with or without impact ionization model.
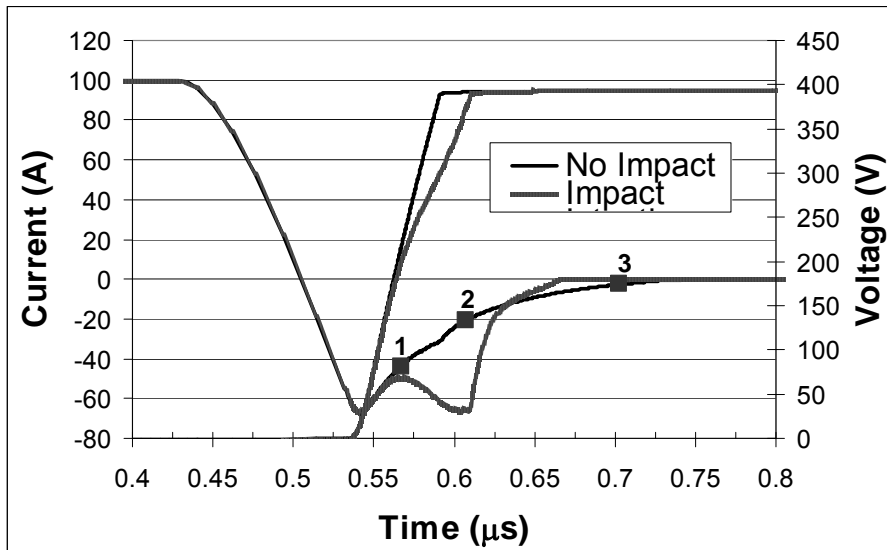
Fig.3 Comparison between the simulated reverse recoveries with or without impact ionization model enabling

In the simulation with impact model we observe an evident current tail, whereas the other simulation shows the typical shape of reverse recovery. Since the two simulations differ just because of impact ionization model enabling, we can conclude that the effect is due to the generation of new charge carriers. It is worth noting that the voltage across the diode is always less that 700V.

In Fig.4-5 we report the shapes of carriers concentration and electric field in three time instants of the reverse recovery. At first drift region is filled with charge carrier; minority carrier concentration is much greater than bulk doping and, thereby, the diode works at high injection level. At the instant time 1, after the reverse current peak, the depleted region starts to expand and charge concentration progressively reduces: electric field and charge distribution are almost the same in the two simulations and electric field assumes the typical triangular shape. At the instant 2, the current tail appears: the electric field reaches the value of 2.7×10^5 V/cm and hole concentration near the junction is enhanced respect that one evaluated in the simulation without impact model. The excess charge carriers are generated by avalanche multiplication and, as already seen in the static case (Fig.2), the slope of the electric field increases according with Eq.1, which is

valid also during the switching. On the contrary, disabling impact model, the electric field continues to assume the triangular shape.
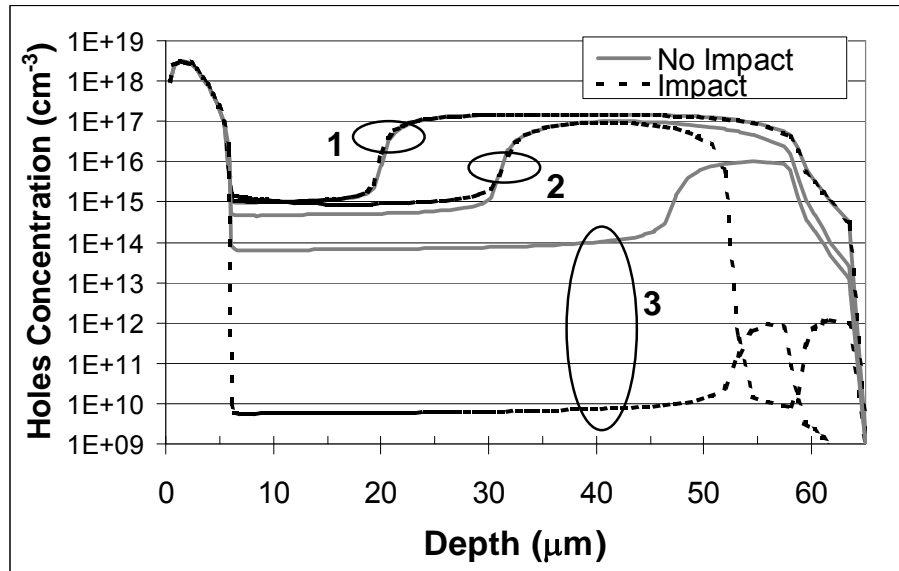

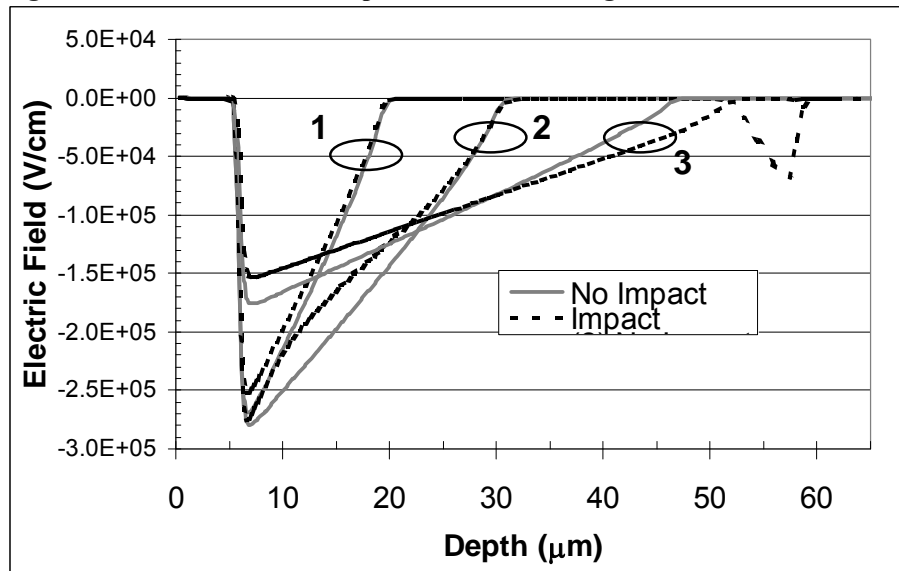**Fig.4 Hole concentration in the points indicated in Fig.3**

Fig.5 Electric field strength in the points indicated in Fig.3

Due to carriers generation, the rate dV/dt reduces and the voltage across the diode is lower (Fig.3). Therefore, respect to the simulation without impact model, the current increases and the voltage reduces.

The electric field speeds up the holes toward the PN junction and the electrons toward the NN+ transition. Due to impact ionisation generation, a larger number of electrons reaches the edge of the plasma region, where they recombine with the holes presents here. The recombination rate is enhanced at the border of the plasma region which vanishes faster and, in fact, at the instant time 3, we see that the depletion region width is larger in the simulation with impact ionisation model. This explains why, when dynamic avalanche appears, the diode exhibits a snappy behaviour, as described also in [42]. For high reverse current also the NN+ transition starts to deplete and plasma region can vanish more abruptly, causing dangerous voltage overshoots for the device and the other circuit components. Therefore this is not a negligible effect.

From above simulation we can say that the typical effects of the dynamic avalanche onset are:

- Appearance of a current tail, due to the new charge generated by impact ionization.
- Reduction of the rate dV/dt of the diode voltage
- Snappy behaviour in the final state of the switching

4.2.2 Dependence of dynamic avalanche onset on charge carriers distribution

The mode how the electric field reaches the critical value, with the consequent dynamic avalanche onset, is strictly related to both the initial charge distribution and recombination velocity during the turn-off.
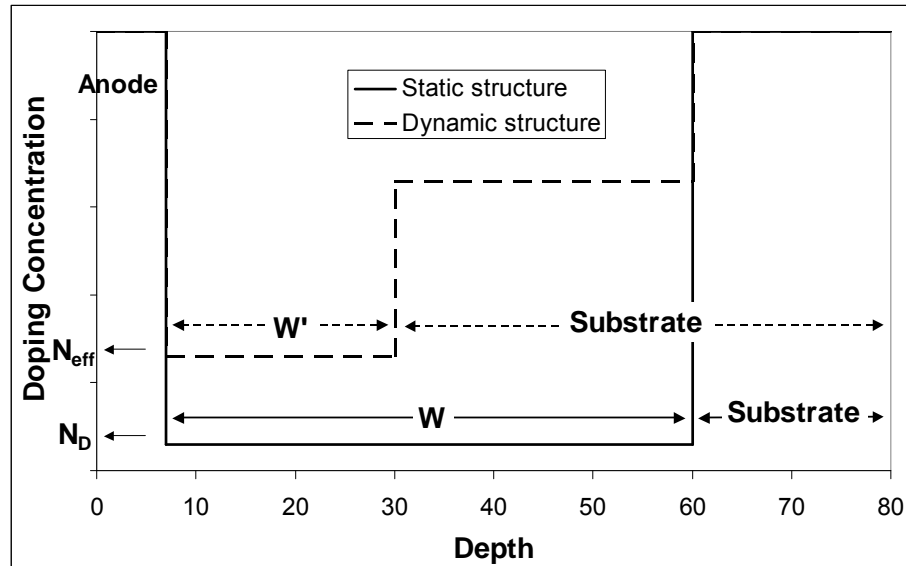
Fig.6 Schematic of the diode structure for the evaluation of the dynamic breakdown voltage

As already described, in direct biasing the diode works at high injection level and the doping in the drift region is equal to the effective doping, which is greater than the bulk doping. After the reverse peak current, the device exhibits its blocking capability and the current decreases. The PN junction starts to deplete and we can imagine the drift region split in two regions: the one in the bottom, still filled with carries, and the other one where the carrier concentration progressively reduces.

In each time instant, we can imagine the diode as a new device (Fig.6) with these new characteristics:

- The drift region has the thickness w' equal to the width of the depletion region which is establishing at the PN junction side, with a doping concentration equal to the effective doping N_{eff}

- Since the carrier concentration in the bottom is so high to retain this region to have a very low resistivity, we can consider it as a substrate region with high doping concentration

In Fig.6 w e N_D are respectively the thickness of the drift region and the bulk doping of the real diode, to which corresponds the breakdown voltage V_{BR}, while w' ed N_{eff} are referred to the new diode which has a breakdown voltage V_{BR}' less than V_{BR}.

The new diode has the typical structure of a punch-through diode and then we can evaluate its breakdown voltage V_{BR}' as [50]:

$$V_{BR}^{'} = E_{CRIT} w' - \frac{q N_{eff} w'^2}{2\varepsilon_S} \qquad (4)$$

where E_{CRIT} is the critical value of the electric field.

The new diode, so regarded, has got a thinner low-doped region and a greater doping value and, therefore, its breakdown voltage V_{BR}' is less than the one of the real diode. Considering the diode with these new time-dependent characteristics, we can repeat the same analysis made for the static breakdown even in dynamic conditions: for each time instant we have to consider a breakdown voltage V_{BR}' dependent on the removal speed of the charges.

After the reverse current peak, the voltage across the diode is rising and it could happen that in a certain time instant the space charge region has not reached yet the thickness needed to avoid the avalanche multiplication onset. The voltage is applied to a narrow and high doped depleted region and thereby at the PN junction the field can reach the critical value: therefore new carriers are generated by ionization impact even thought the voltage is lower than static breakdown value.

With reference to the Fig.7, we can see that at the showed time instant a current tail appears. Charge carriers shape at the same instant is depicted in Fig.8. The depletion region is extending from the PN junction and the doping concentration is reducing. At this instant, we can suppose the drift region has got a thickness of 20μm (w'), whereas, being the hole concentration 6.5×10^{14} cm^{-3}, the effective doping is $N_D + p = 8.5 \times 10^{14}$ cm^{-3} (N_{eff}). The breakdown voltage V_{BR}' of this structure is 206V. From Fig.7 we can see that the voltage across the diode is 286V, greater than the equivalent dynamic breakdown voltage V_{BR}'. We can conclude that the diode is under avalanche

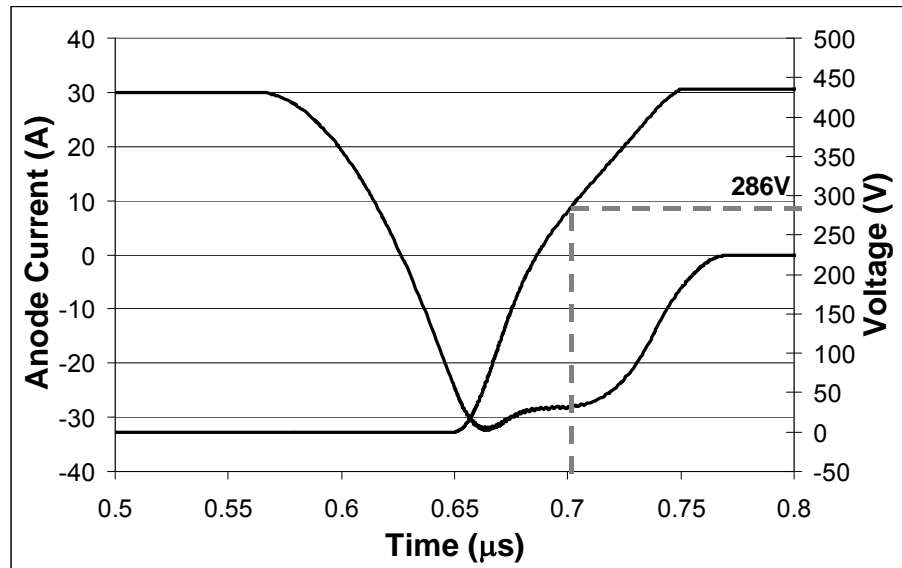multiplication condition till the diode voltage holds less than the dynamic breakdown value.

Fig. 7 Simulated reverse recovery, where dynamic avalanche takes place
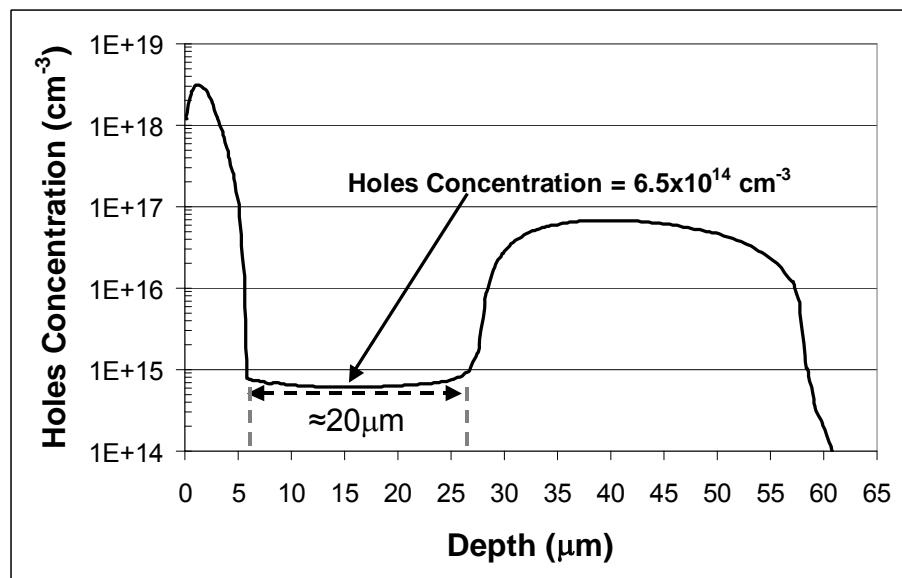

Fig.8 Hole concentration at the instant when voltage across the diode reaches 286V in Fig.7

If recombination rate is greater than generation rate, charge carrier concentration continues to reduce and the thickness of the depleted region increases and so VBR' rises. When VBR' overcomes the value of the voltage across the diode, the charge generation due to impact ionization ends and current decreases quickly.

Using again ATLAS simulations, we can further verify our proposed approach.

In Fig.9 the applied reverse voltage is 200V and forward current 16A. The circles represent the breakdown voltage V_{BR}' evaluated from Eq.4, using the charge concentration of the device for each time instant. In this case the diode voltage is always less than V_{BR}' and impact ionization does not start. But, with the same forward current, if we apply a reverse voltage of 440V, we can see (Fig.10) that the voltage across the diode becomes greater than V_{BR}' and electric field reaches the critical value. From this time instant onwards, diode switches under dynamic avalanche conditions. The new charge generation determines the appearance of a current tail and the dV/dt reduces.
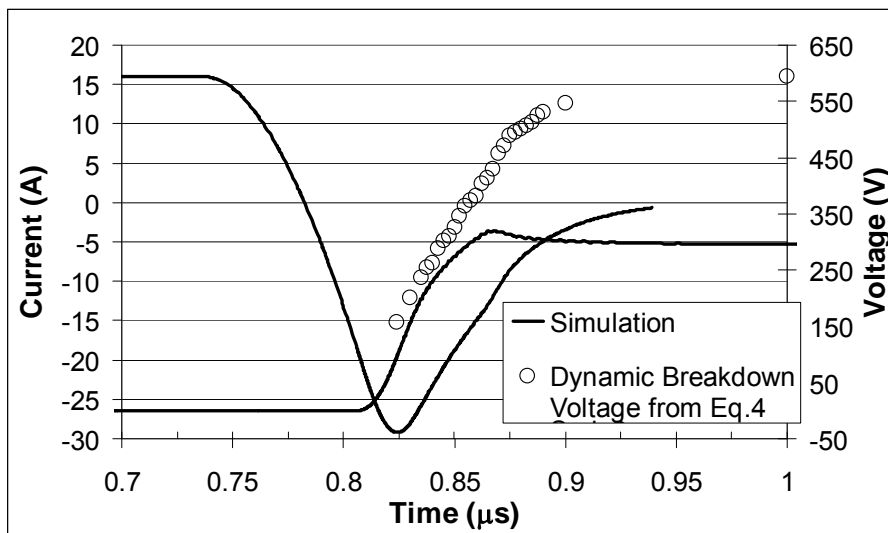
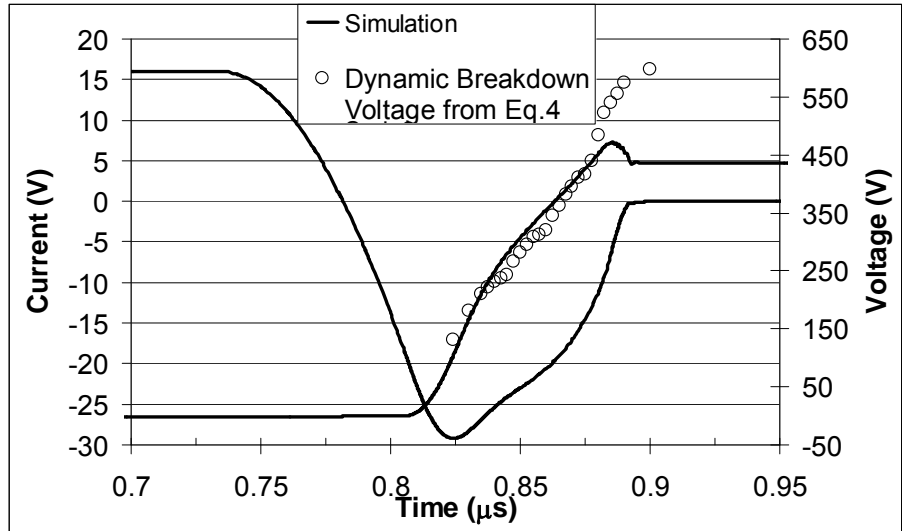**Fig.9 The dynamic breakdown voltage is always greater than the voltage across the diode**

Fig.10 The voltage across the diode overcomes the dynamic breakdown voltage and dynamic avalanche starts

The effect becomes more drastic for a forward current of 40A. In this case (Fig.11) avalanche multiplication starts at a lower reverse voltage and carrier concentration near the junction is so enhanced that, in the initial phase, V_{BR}' reduces unlike observed in Fig.10 and, consequently, the tail current si more emphasized.
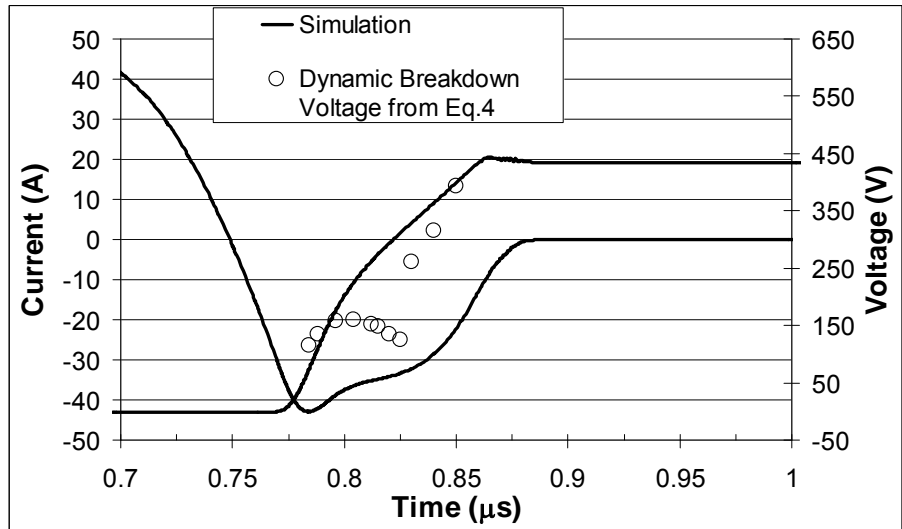

Fig.11 For high charge concentration, diode voltage becomes greater than the dynamic breakdown value at low voltage

Therefore during the switching we can not define a single breakdown voltage, but a series of values function of the time. In the power applications, in forward biasing the devices work at high injection level and, therefore, the effective doping in the low-doped region results enhanced. All the stored charge has to be extracted before the diode exhibits its blocking capability in the reverse mode. During the switching charge carriers recombine each other and, therefore, effective doping reduces and depletion region extends inside the drift region. In each time instant we can consider the diode evolves in a sequence of static conditions: for each of this state we can think the device as a new diode whose drift region has got a doping level equal to the effective doping and a thickness equal to the depletion region width. From the static point view a lower breakdown voltage corresponds to this "new" diode and, therefore, if the voltage across the device results greater than this value, the electric field reaches the critical value and impact ionization starts.

4.3 Experimental   measurements   on unimplanted power diodes

In this section we present experimental reverse recoveries measurement on power diodes whose breakdown voltage is 700V. The doping profile of the diodes is showed in Fig.12: the drift region has got a thickness of 58μm and the doping concentration is 2×10^{14} cm^{-3}. The active area is 3.46×10^{-2} cm^{-2}. Diodes have been diffused with platinum at 880°C and 920°C.

Fig.13 plots the reverse recovery of the diode diffused with platinum at 880°C for a forward current of 16A , di/dt about 750A/μs and two reverse voltages. Applying 200V we observe the typical reverse recovery waveform. As shown in the section 1.1 of the chapter 1 current reaches a negative peak and after it drops to the leakage value, while the voltage rises roughly with the same rate dV/dt. Applying a higher value (440V) a bump appears as voltage across the diode is about 280V. Starting from the same time instant, the rate

dV/dt reduces. These effects have been demonstrated to be related to the dynamic avalanche onset. When the phenomenon extinguishes current gradually reduces. Due to this effect, the dynamic power loss increases, whereas the reverse recovery time seems to be not considerably worsened. Since for this forward current the onset of the dynamic avalanche is about 280V, applying a reverse voltage of 200V there is not charge carriers generation and any current tail is observed.
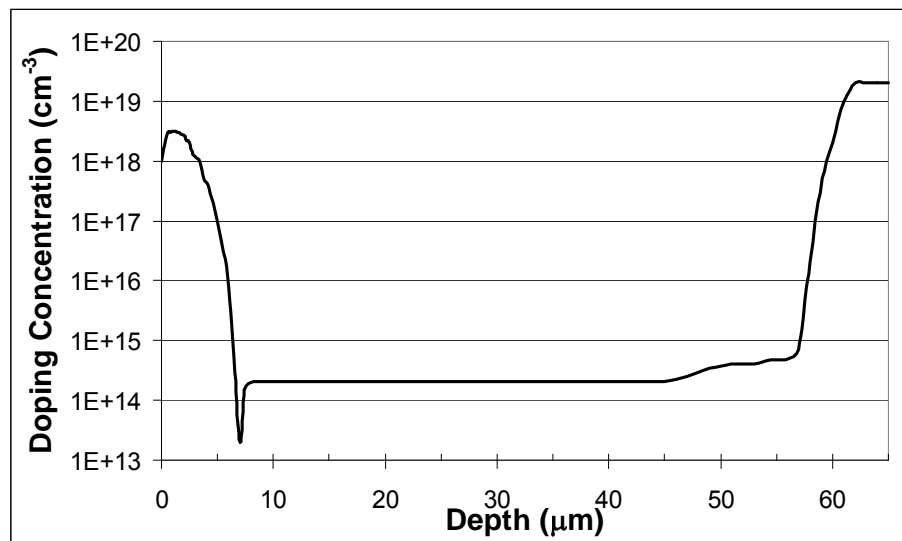

Fig.12 Net doping concentration of the experimental diode

In Fig.14 we have measured the turn-off with a forward current of 43A, reverse voltage of 440V and di/dt about 650A/μs. Immediately after the reverse current peak, current does not reduce to zero, but there is an unexpected increase and current reaches a value greater than the first reverse peak. From the time instant when current tail appears onwards, the voltage continues to rise up to 440V with a slope lower than the initial one.
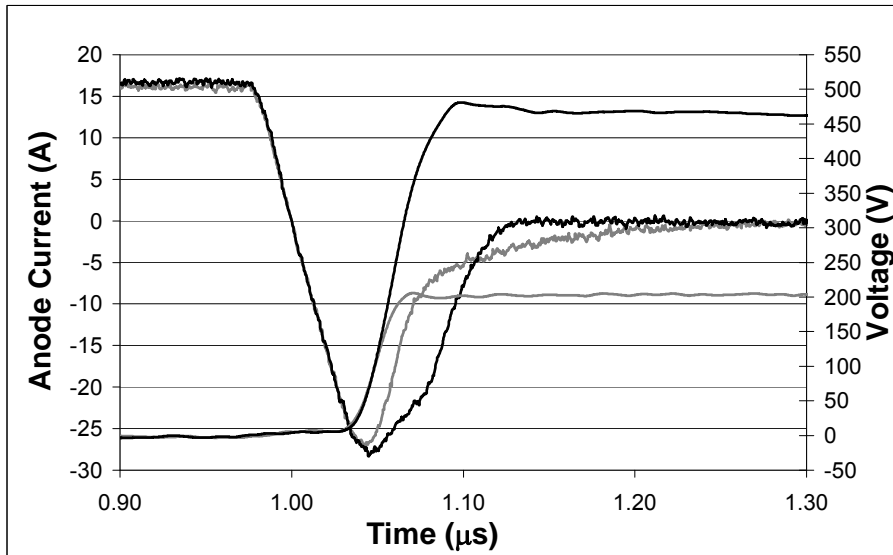
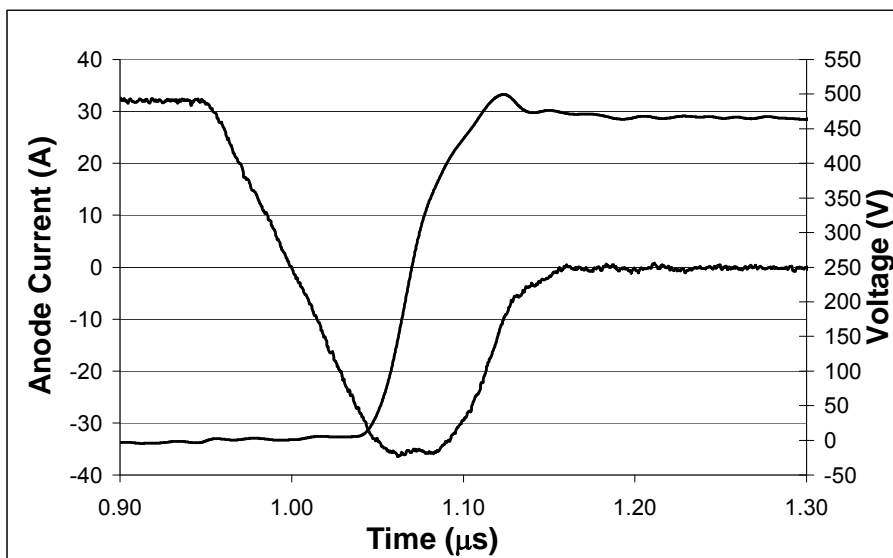**Fig.13 Reverse recoveries of Pt880 for I$_F$=16A and reverse voltages 200V and 450V**

Fig.14 Reverse recoveries of Pt880 for I$_F$=43A and reverse voltage 450V

We can say that these power diodes, diffused with platinum at 880°C, are affected by avalanche multiplication onset during the

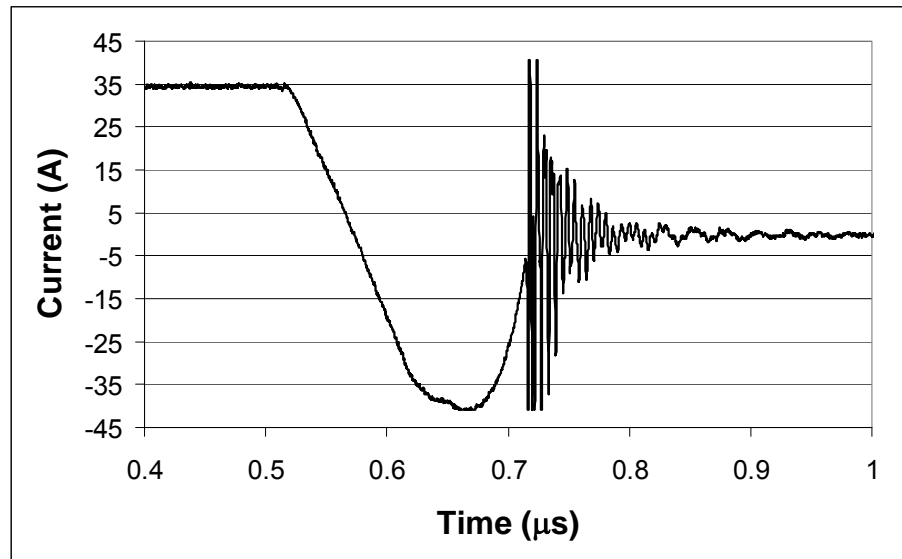transient even though the voltage across the diode is always less than the breakdown value.

Fig.15 For stressful switching condition recovery can become snappy and oscillations appear

It is worth observing how increasing the rate di/dt, in the final instants of the switching oscillations appear. We observed in section 4.2.1 that when dynamic avalanche intensity increases, NN+ transition starts to deplete and at the same time, due to the electrons generated at the PN junction and accelerated toward the cathode, the recombination rate at the left side of the plasma region increases. Therefore the two depletion regions merge and snappy phenomenon occurs [47]. The sudden disappearance of charge carrier in the drift region involves a fast reduction of the diode current, which causes oscillations because of the stray inductance, as showed in Fig.15. The system becomes unstable and more stressful conditions can lead to the diode destruction. Fig.16 shows the package of a destroyed diode as a consequence of the this effect.

Fig.16 Package of a destroyed diode because of snappy phenomenon

The diode diffused with platinum at 920°C exhibits roughly the same problems. Nevertheless since the stored charge is lower due to the reduced recombination lifetime, the effects seems to be less dangerous.

In Fig.17 we report the reverse recoveries measured applying a reverse voltage of 200V and 450V for a forward current of 16A. In this case after the reverse peak the current reduces and the tail appears only when the current has reached a value less than the 40% of the reverse peak. In the device diffused at 880°C we observed the current tail appearance immediately after the reverse peak (Fig. 13).

Increasing the forward current (30A) the device exhibits the same behaviour (Fig.18): the dynamic avalanche onset takes place while the current is already dropping to zero.
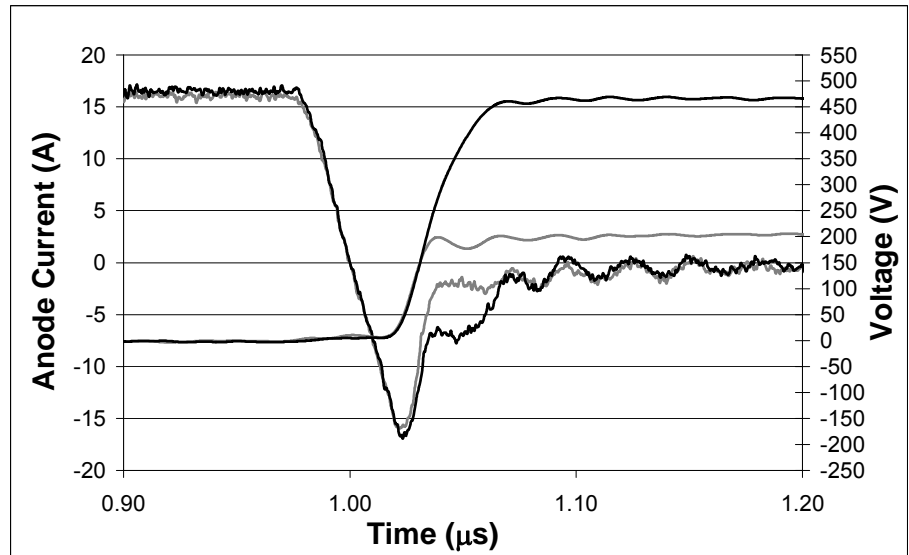
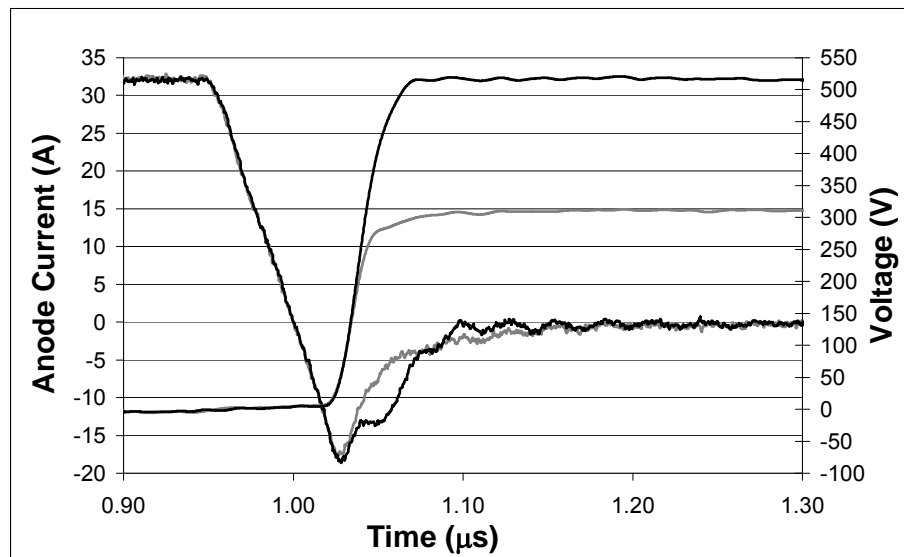**Fig.17 Reverse recoveries of Pt920 for I$_F$=16A and reverse voltages 200V and 450V**

Fig.18 Reverse recoveries of Pt880 for I$_F$=30A and reverse voltages 200V and 500V

4.4 ATLAS simulations

As observed, the dynamic avalanche onset is strictly related to the charge distribution into the drift region and the mode how carriers are swept out. Therefore we could try to modify the ruggedness to this phenomenon controlling opportunely the recombination velocity of the charge carriers. In order to achieve the best trade-off between static and dynamic performances, we recurred to helium implantation technique.

In the Chapter 3 we studied carefully the effects of helium implantation on recombination lifetime and effective doping and the analysis allowed us to identify the dominant recombination centers and their concentration around the penetration depth. By using the extracted model, we have tried to study how helium implantation modify the behaviour of power diodes under dynamic avalanche conditions. The aim is to reach a good comprehension of the phenomenon and manufacture experimental samples, based on the results of the simulations and more resistant to this phenomenon.

The doping profile of the simulated diodes is the same of the real one, measured by SRP and shown in Fig.12.

The thickness of the drift region is 58μm, the doping concentration $2x10^{14}$ cm^{-3} and the junction depth about 7μm. The active area $3.46x10^{-2}$ cm^2.

4.4.1 Effect of the defects localization on the dynamic avalanche

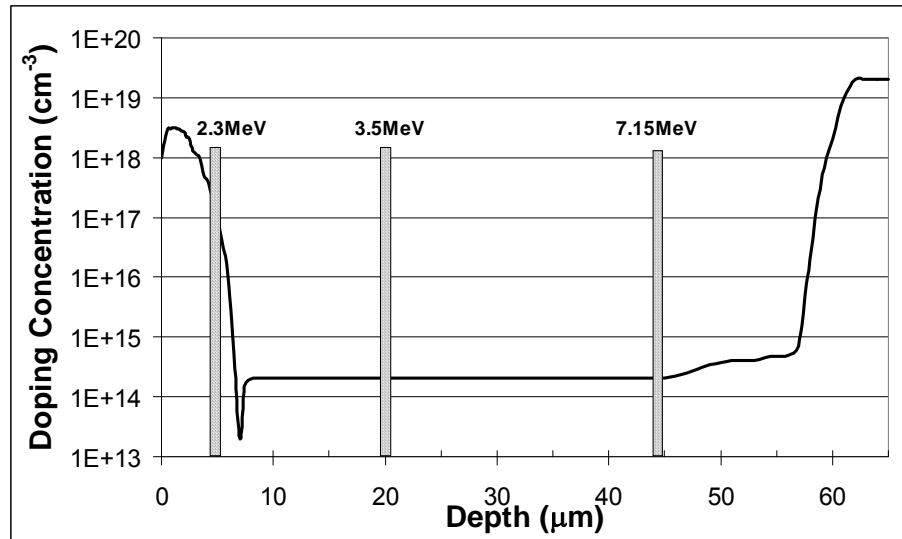The positions of the damage taken into consideration in this work are showed in Fig.19

Fig.19 Position of the defects in ATLAS simulations

The implantation energy needed to lie the damage at the indicated positions in Fig.19 are resumed in Table I:

Depth (μm)	Implantation Energy (MeV)
5	2.3
20	3.5
44	7.15

Table I Energies needed to place the defects at the showed positions

In the work we will refer to the different devices as indicated below:

- D1 (Unimplated)
- D2 (defects lied at 5μm)
- D3 (defects lied at 20μm)
- D4 (defects lied at 44μm)

The helium defects profile has been described using the results obtained by means of the differential technique in the chapter 3 (Fig.): the energy level is E_C-0.23eV, which is the dominant centre, while the

distribution is the same of Fig., with the peak localised in the above indicated positions.

Simulations have been obtained by means of a Mixed-Mode simulation. This kind of simulation allows a circuit to be described by means a SPICE-like netlist, giving the possibility to insert a physically-based model for one or more devices, using an ATLAS mesh. Obviously for the diode under analysis we used the physical description, while the chopper circuit has been described by means a simple SPICE netlist.

Fig.20 shows both the current and voltage waveforms during the TURN-OFF of a diode with a constant defects concentration.
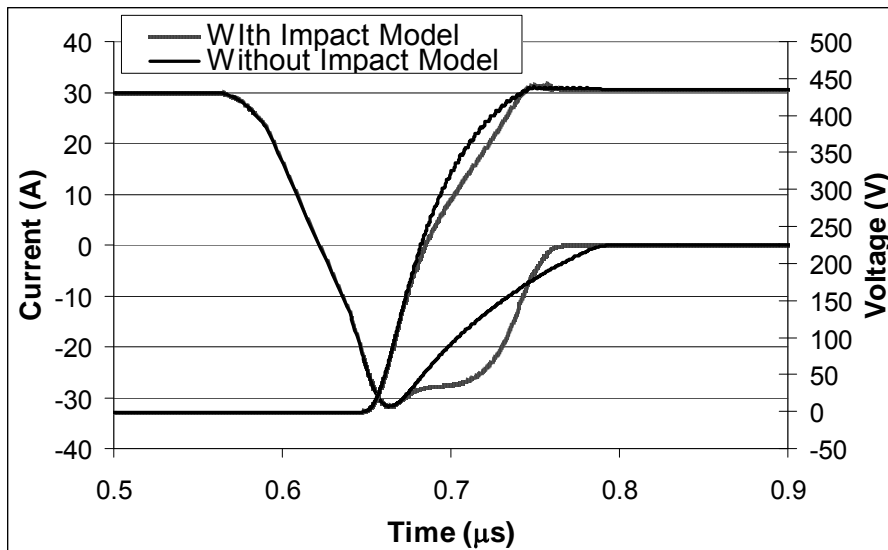

Fig.20 Comparison between the simulated reverse recoveries of a diode with a constant lifetime with or without impact ionisation model

Enabling the ionization impact model, a current tail appears and the rate dV/dt decreases, as already shown. We are sure that this device is affected by dynamic avalanche and all the consideration have been done in the section 4.2.1.

Fig.21 shows how reverse recovery waveforms change introducing a localised lifetime control at the positions showed in Fig.19.
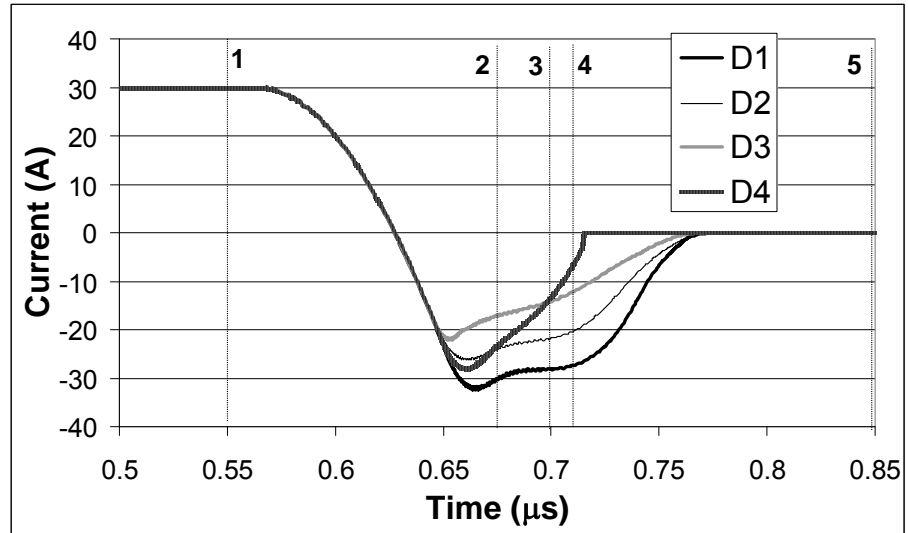
Fig.21 Comparison between the reverse recoveries of the untreated diode and the devices with defects lied at the positions of Fig.19

We can observe how all the positions allow the reverse peak to be reduced. However introducing the defects into the anode region, the device is still strongly affected by avalanche multiplication, how simulations in Fig.22 show, where as usual the impact ionisation has been either enabled or disabled. The simulation without impact ionisation model does not exhibit any current tail. Diodes where defects lie into the drift region and near the buffer layer are a little affected by this phenomenon, as illustrated in Fig.23 for the device D4.
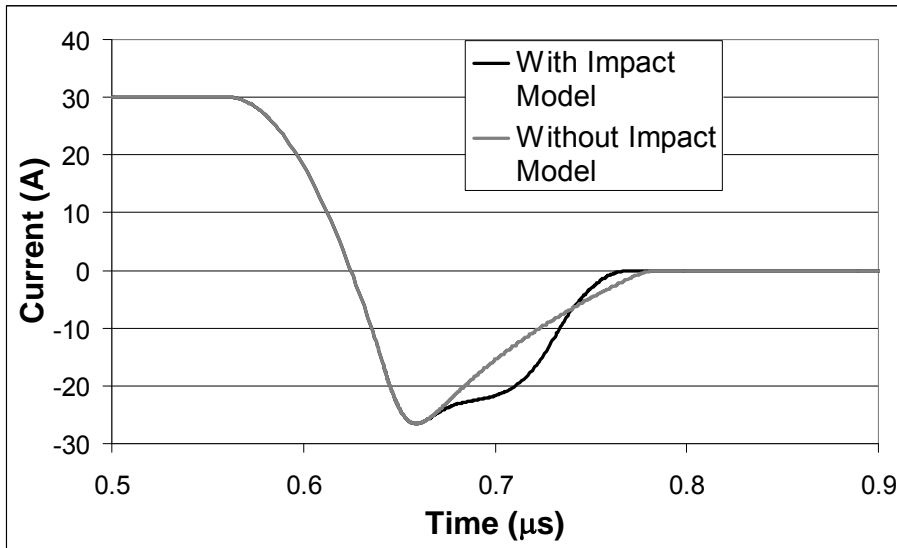
Fig.22 Comparison between the simulated reverse recoveries of a diode with defects at 5μm with or without impact ionization model
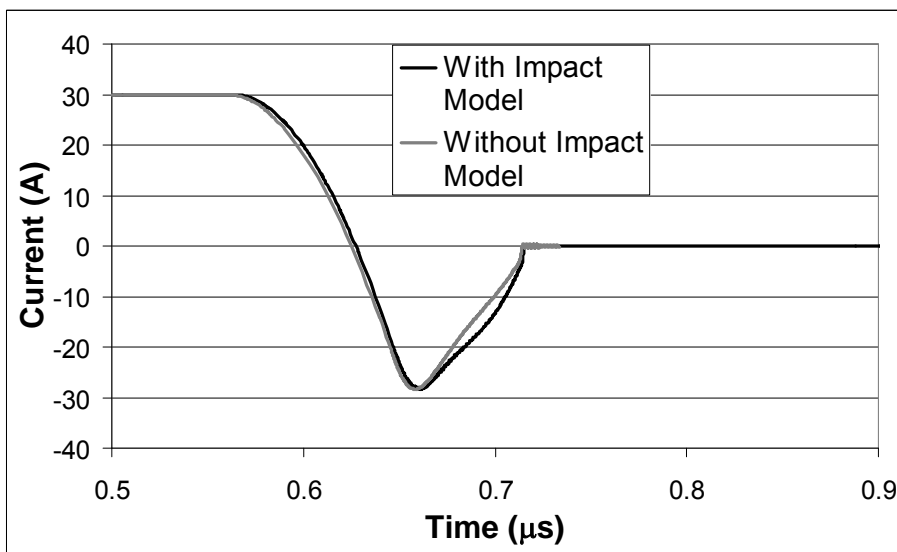

Fig.23 Comparison between the simulated reverse recoveries of a diode with defects at 44μm with or without impact ionization model
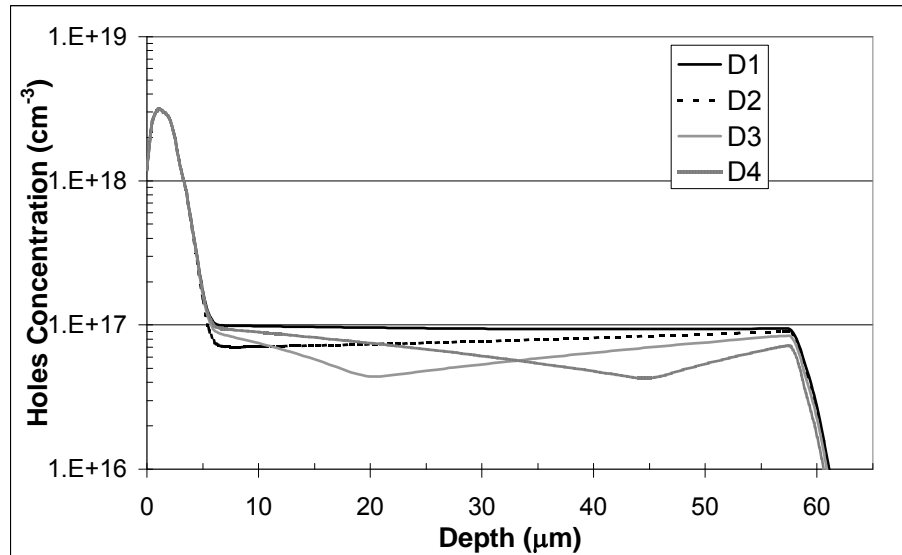
Fig.24 Hole concentration at the time instant 1 of Fig.21

We can observe how charge distribution and electric field shapes change varying the position of the defects. In particular we identified six relevant time instants.

Initially a constant current flows through the device. In the untreated device and in the device with the defects in the anode region carrier concentration is almost constant along the epilayer, whereas in the other two devices a decrease of the charge concentration is observed around the maximum of the damage (Fig.24). The recombination centers in the anode region allows the carrier concentration to be considerably reduced near the junction in respect to the other devices, but in the device D2 the carrier concentration is lower along the whole drift region.

At the time instant 2 (Fig.25) the depletion region starts to expand. All the devices have already reached the minimum of the current, which is now decreasing toward zero value. Among implanted devices, in the diode with defects in the middle of the epilayer (D3) the depletion region is extending faster than other ones, due to the lower carrier concentration in the drift region (Fig.25). Respect to the first instants, at this moment the device damaged in the anode (D2) shows a depletion region less extended than the one of the device with defects in lied in the back (D4). In fact at this instant the border of the

plasma region is about 20μm far from the position of the defects and their effect on the recombination rate at the border of the plasma region becomes more and more negligible.

The electric field shape is almost triangular in all the devices (Fig.26), even though it is reaching the critical value.
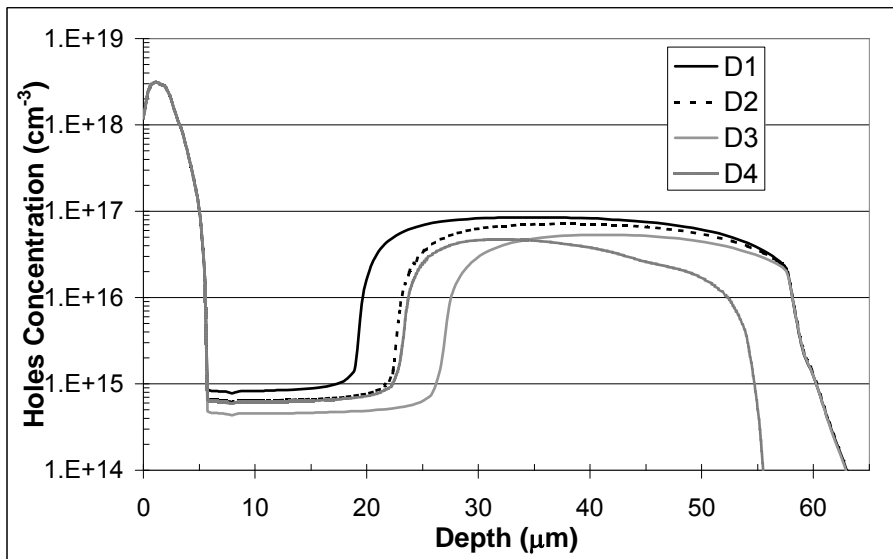

Fig.26 Hole concentration at the time instant 2 of Fig.21
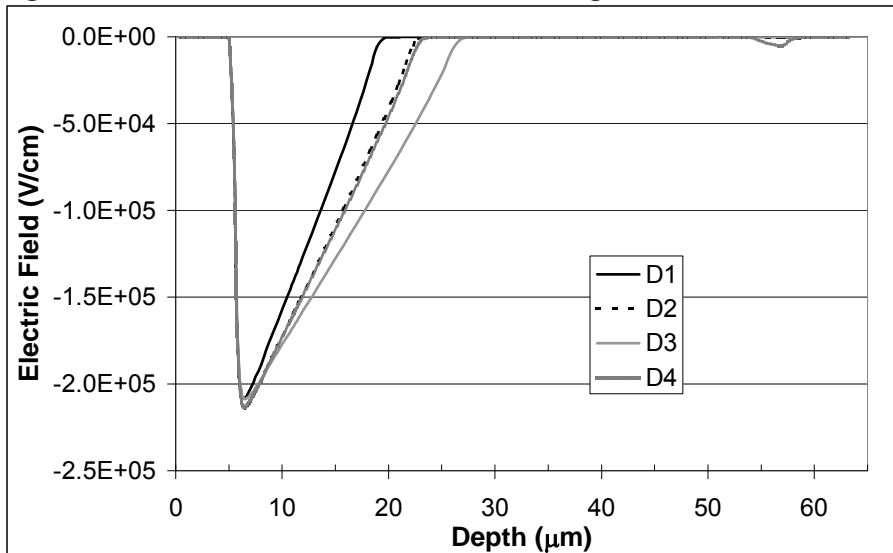

Fig.26 Electric field strength at the time instant 2 of Fig.21

At the instant 3 all the devices are under ionisation impact condition, because the electric field strength near the junction has overcome the critical value (about 2.2x10^5 V/cm), as shown in Fig.28. The device D4 has the widest depletion region. Moreover defects lied at 40μm increase the charge removal speed also near the NN+ transition (Fig.27), which starts to deplete and where a certain amount of the diode voltage is sustained. Indeed a low intensity electric field appears also in the back of the device. This effect could be dangerous under more critical switching condition, whether the electric field reaches the critical value also at the NN+ transition while PN junction is still under avalanche multiplication condition. Electrons generated at the PN junction are accelerated toward the NN+ transition; in the event that the electric field has reached the critical value, these electrons can create a new hole-electron pair. The new generated holes are accelerated by the electric field toward the PN junction where they can acquire enough energy to create other hole-electron pairs. Therefore there is a positive feedback which can lead to the device destruction.
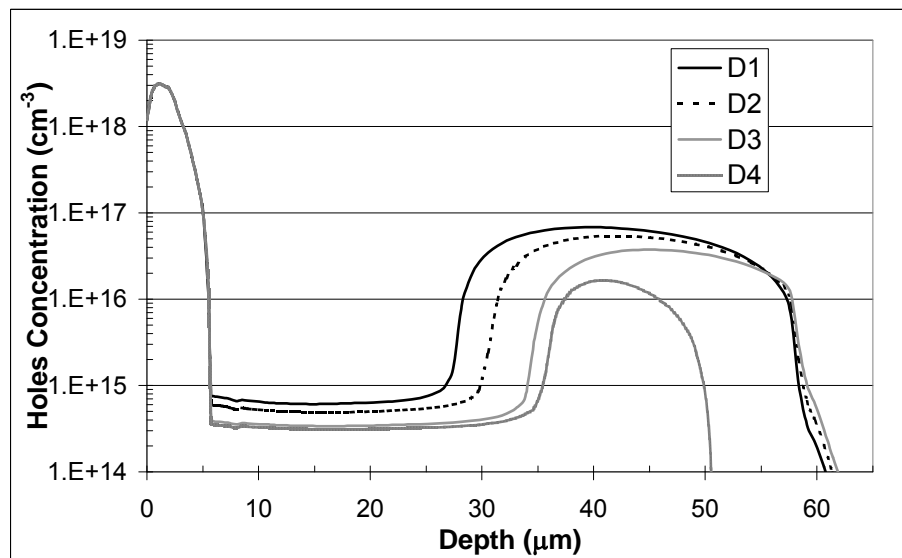

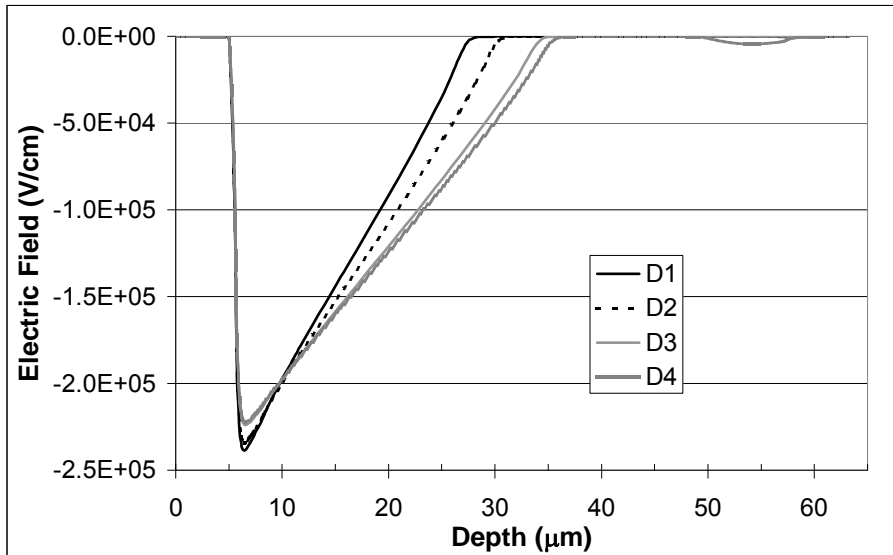**Fig.27 Hole concentration at the time instant 3 of Fig.21**

Fig.28 Electric field strength at the time instant 3 of Fig.21

At the instant 4 it is worth noting how the electric field strength in the devices D4 becomes less than 2×10^5 V/cm (Fig.30) and thereby this diode is no longer under dynamic avalanche condition. Respect to the instant 3, in D4 there are no longer two depletion regions (Fig.29). In fact the depletion region which is extending from the PN junction and the one which is extending from the NN+ transition merged, causing a sudden disappearance of charge carriers. Obviously this effect can lead the switching to be snappy, causing dangerous voltage overshoots. Therefore this is not the more suitable condition. Other diodes are still under dynamic avalanche condition and only one depletion region is observed.
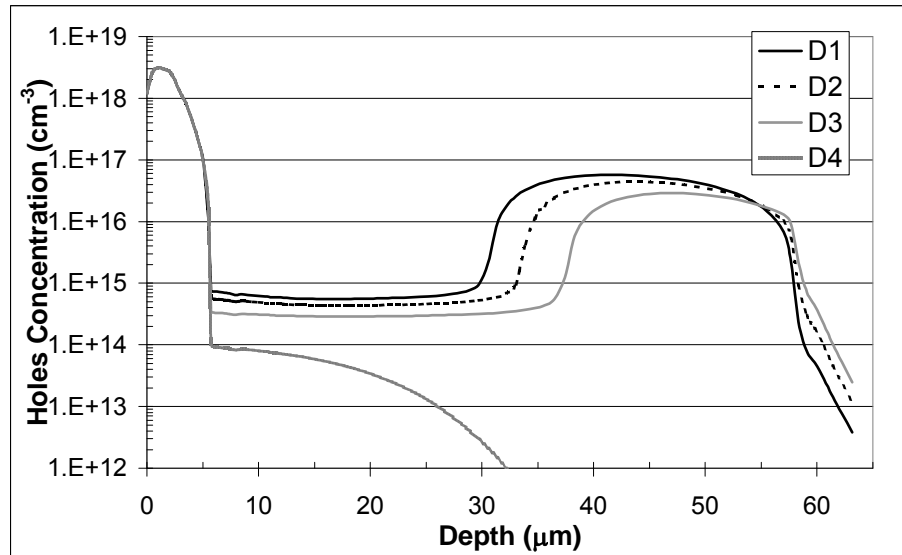
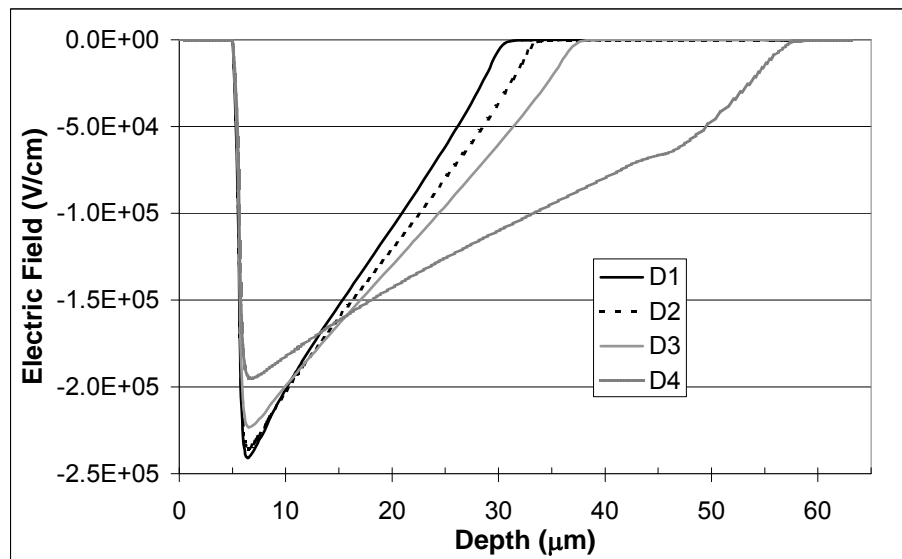**Fig.29 Hole concentration at the time instant 4 of Fig.21**

Fig.30 Electric field strength at the time instant 4 of Fig.21

At the final instant 5, dynamic avalanche is extinguished and current is already zero in all the diodes. Minority carrier are reached the equilibrium concentration (Fig.31) and the electric field shape is triangular in all the devices (Fig.32).
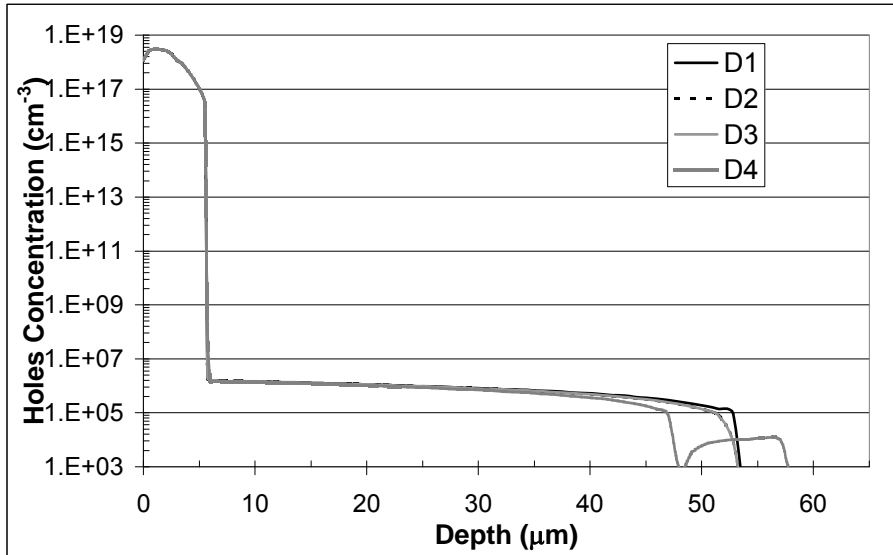
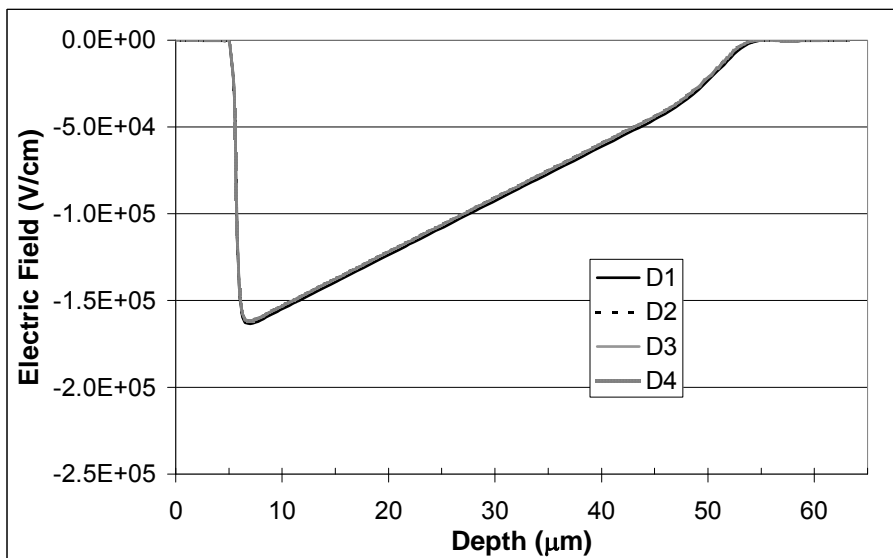**Fig.31 Hole concentration at the time instant 5 of Fig.21**

Fig.32 Electric field strength at the time instant 5 of Fig.21

In order to have a better overview of the incidence of the different defects positioning on the switching, we show the time-dependence

evolution of electric field, hole concentration and generation rate, which have been evaluated in the N- region, near the PN junction.

In Fig.33 we report also the value of the critical electric field, which is 2.2×10^5 V/cm. In all the devices the electric field strength overcomes the critical value and, thereby, all of them work under dynamic avalanche condition. Nevertheless due to the presence of defects this condition is verified for different periods of time. In D4 electric field is greater than the critical value just for 15ns and in D3 for 29ns. After 15ns, in D4 the two depletion regions join and the voltage is suddenly sustained within a wider depleted region. Therefore the intensity of the electric field near the junction decreases fast. It is worth noting that unimplanted device keeps under ionisation impact condition for 63ns.
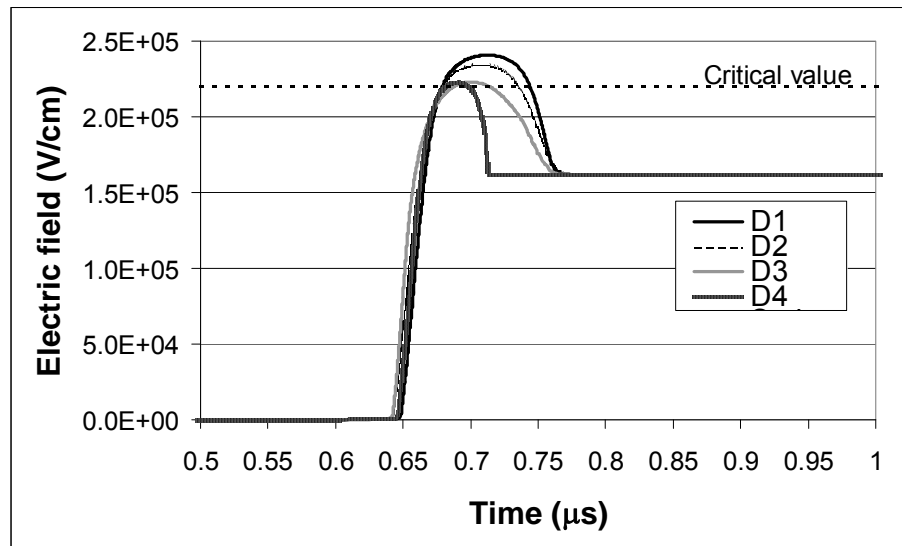
Fig.33 Electric field strength of the diodes of Fig. 21 as a function of the time (evaluated near the PN junction)

In Fig.34 the generation rate near the PN junction is depicted. In the devices D3 and D4 the maximum of the generation rate is reduced of about a factor 6. From the hole concentration evolution (Fig.35) we can see how charges disappear with the same time-dependence law in D1 and D2, whereas in D4 they disappear abruptly when the two depletion regions merge each other.
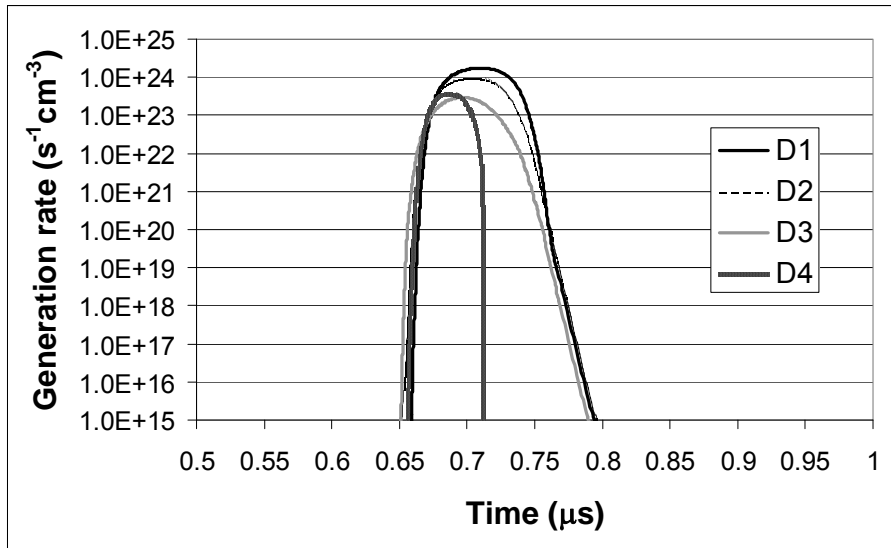
Fig.34 Generation rate of the diodes of Fig. 21 as a function of the time (evaluated near the PN junction)
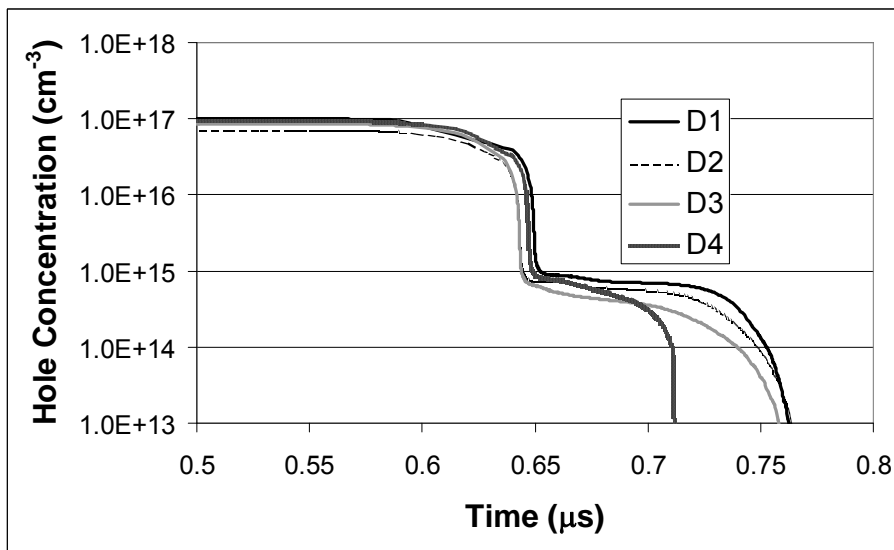
Fig.35 Hole concentration of the diodes of Fig. 21 as a function of the time (evaluated near the PN junction)

    If on the one hand recombination centers in the N- region allow
the dynamic avalanche onset to be reduced, on the other hand the
presence of defects involves an increase of the forward voltage drop,
as depicted in Fig.36. Nevertheless, if our aim is to avoid the diode
reaching the impact ionisation condition, this drawback must be
accepted.

**Fig.36 Forward IV characteristic of untreated diode and diodes with defects
lied at the positions of Fig.19**

4.5 Experimental measurements on helium implanted power diodes

Based on the results of simulations showed in the previous section 4.4, we manufactured devices with local lifetime control implanting helium in diodes previously diffused with platinum at 880°C and 920°C.

Many doses have been used, but in this works we present only the results on devices implanted with dose 10^{11} cm^{-2}.
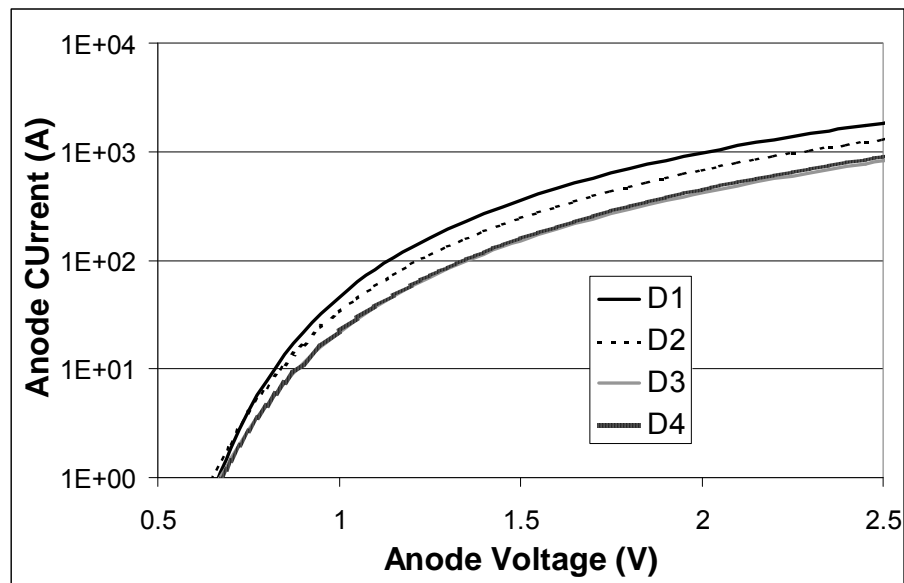
The energies, as already reported in TableI, are 2.3MeV, 3.5MeV and 7.15MeV.

In the section 4.3 we showed how Pt880 diode suffer of dynamic avalanche, as well Pt920, even though in latter device the phenomenon starts at higher reverse voltage.

First of all, we analyse Pt880 diodes. In Fig.37 we report the reverse recovery waveforms for forward current 30A, reverse voltage 300V and di/dt 700A/μs. In this conditions any current tail appears and waveforms have got the typical shape. It is worth observing how the unimplanted device and the one implanted in the back (Pt880_D4) exhibit the same reverse current peak, because defects do not affect carrier concentration and recombination rate in the first instants of the switching near the PN junction.
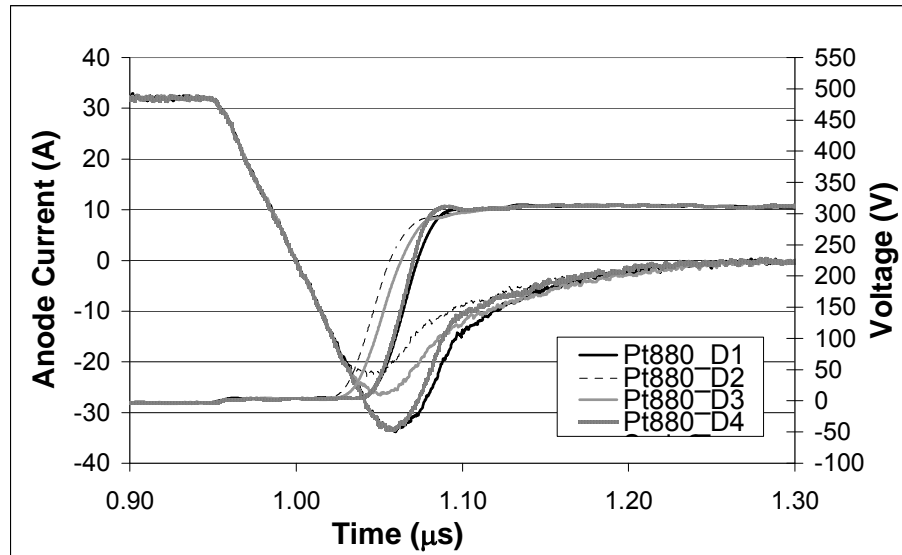
Fig.37 Experimental reverse recoveries of Pt880 implanted by Helium, for I$_F$=30A and reverse voltage 300V

Increasing only the reverse voltage (Fig.38), in the unimplanted device we can observe the appearance of a new reverse peak, after the first one. This is a clear effect of the dynamic avalanche onset. The peak appears when the diode voltage is about 330V and this explain why in Fig.37 we do not observe any current tail, because the maximum reverse voltage is 300V. It is very interesting to observe again the comparison with the device implanted with energy 7.15MeV. The reverse current peak is again the same in this condition, but helium implantation allows the current tail to be avoided. The voltage shape is also interesting: since the two devices reach the same reverse peak, the voltage starts to rise at the same time instant. Nevertheless when the current tail appears in the unimplanted device, the rate dV/dt reduces in this diode, while it holds constant in the implanted device. As observed in the section 4.2.1 the reduction of the rate dV/dt is another effect of the dynamic avalanche onset. Therefore we have manufactured a diode which has got the same reverse current peak of the untreated device without being affected by ionisation impact. However we have to consider that the reverse recovery is snappy, due to the depletion of the NN+ transition and some oscillations appear at the of the switching.
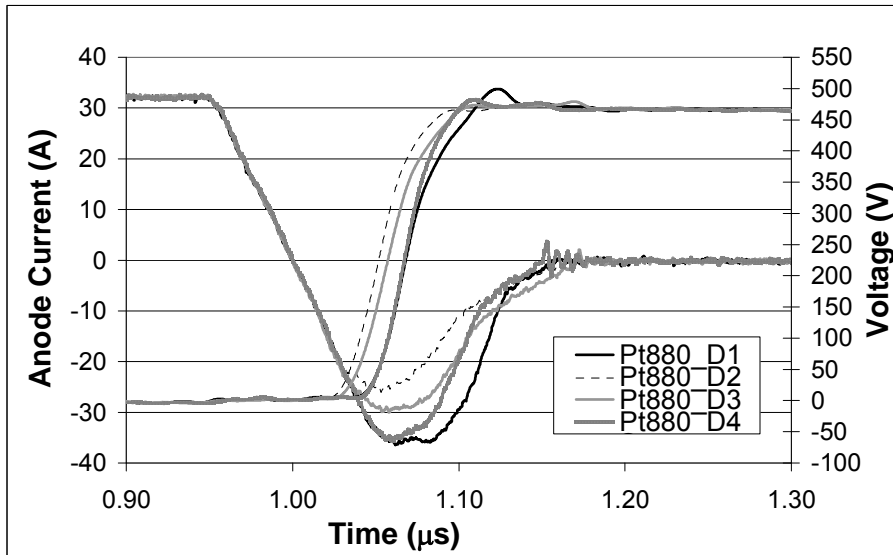
Fig.38 Experimental reverse recoveries of Pt880 implanted by Helium, for I$_F$=30A and reverse voltage 450V

Diodes implanted with energy 2.3MeV and 3.5MeV exhibit a lower reverse current peak and they are less affected by dynamic avalanche respect to the unimplanted device. It is worth noting how the reverse recovery time is not considerably reduced, but rather it keeps almost unchanged.

Diodes diffused with platinum at 920°C show a behaviour similar to simulation of Fig.21.

With a forward current of 30A, reverse voltage of 300V and di/dt 700A/µs (Fig.39) the untreated diode and the implanted ones do not work under dynamic avalanche conditions, as well as diodes diffused at 880°C. In this case the diode implanted with the energy 3.5MeV shows the lowest reverse current peak.

Respect to diodes diffused at 880°C, in these devices the dynamic avalanche onset takes place at higher reverse voltage. Indeed applying a reverse voltage of 500V (Fig.40), the current tail in the unimplanted device is the effect of the new generated charges within the depletion region. As observed in the simulations of Fig.21, the implantation energy of 2.3MeV involves a reduction of the reverse current peak, because defects lied into the anode region reduce carriers concentration near the PN junction. On the other hand as depletion

region extends deeply, recombination centers are too far to affect the recombination rate of charge carriers, which continue to recombine with the same time-law of the unimplanted device. Therefore after the reverse current peak charge carrier distribution becomes roughly the same of the untreated device. Indeed an evident tail appears and current reaches the same intensity of the unimplanted device while avalanche multiplication is taking place. Implanting helium into the anode we can reduce the reverse current peak but it is not effective on the dynamic avalanche limitation.
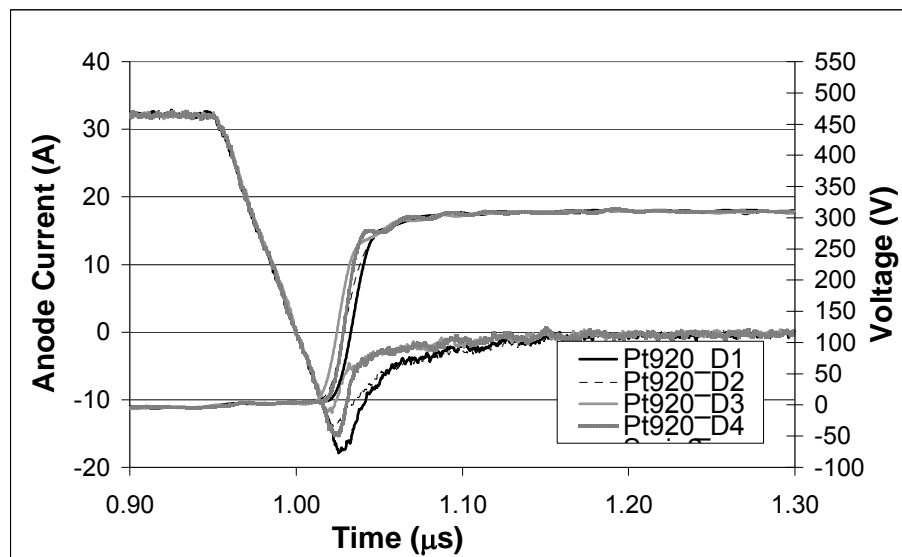
Fig.39 Experimental reverse recoveries of Pt920 implanted by Helium, for I_F=30A and reverse voltage 300V

Implantation energy of 3.5MeV and 7.15MeV are more useful also in these devices: in fact the dynamic avalanche intensity becomes weak and just a small current increase is observed, as shown in Fig. where the comparison between the turn-off at 300V and 500V is depicted for the device implanted with energy 7.15MeV (Fig.41). It is worth noting how snappy phenomenon does not occur in these

devices.

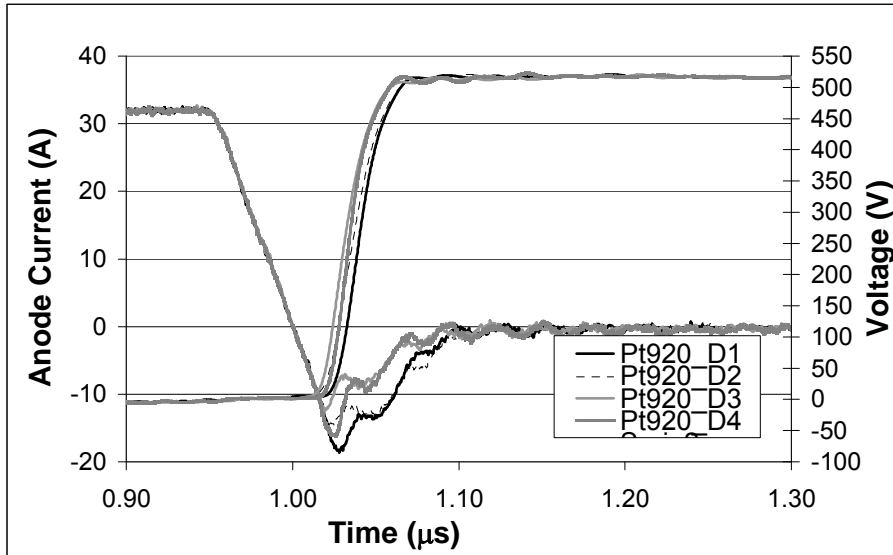**Fig.40 Experimental reverse recoveries of Pt920 implanted by Helium, for I$_F$=30A and reverse voltage 300V**
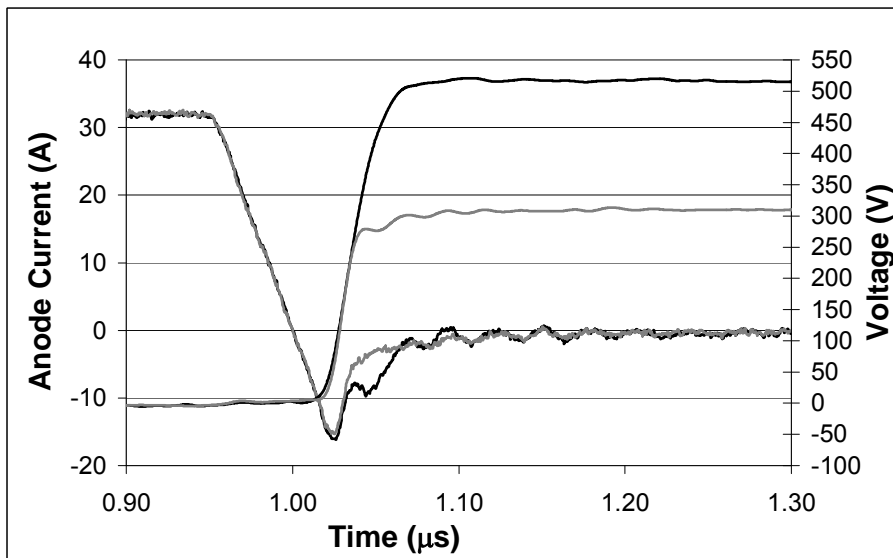
Fig.41 Experimental reverse recoveries of Pt920 implanted by Helium with energy 7.15MeV, for I$_F$=30A and reverse voltages of 300V and 500V

As already said, the presence of defects into the drift region causes a worsen of the static performances, as forward voltage drop and

leakage current. As it can be seen in Fig.42 for the device Pt880, implanting helium into the anode region the leakage current keeps roughly unchanged, compared to the one of the unimplanted device. On the other hand placing the defects into the anode region the leakage current becomes up to 5 times larger, due to the generation centers which lie within the depletion region. If on the one hand the best positions for the dynamic avalanche limitation is the low-doped region, on the other hand defects into the anode do not involve a worsen of the static performances.

Therefore the implantation energy has to be chosen according to the features required for the device to design, taking into account the particular application where the diode is to be used.

Fig.42 Reverse IV characteristics of Pt880 devices implanted by helium, measured at 400K

Conclusions

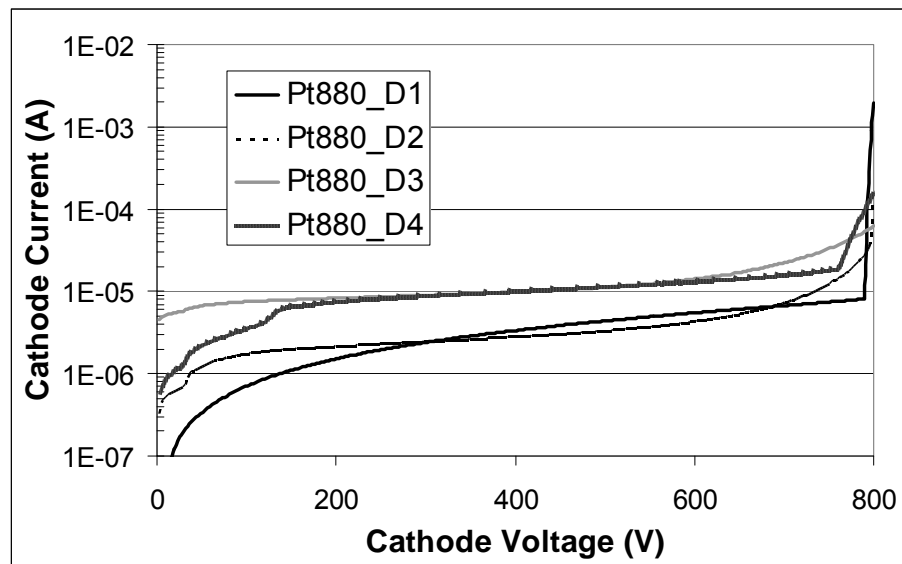The differential technique for the measurement of the recombination lifetime allowed us to have a good comprehension of the effects which helium implantation involves in a low-doped silicon layer. In particular we found out helium implantation not only modifies the recombination lifetime, but causes also a doping compensation around the penetration depth. We proposed an all electrical measurement method which allows the in-depth resistivity profile to be measured for different operating condition (injection level, temperature…), unlike the SRP, which is able to measure the material resistivity only at room temperature. Furthermore SRP involves the device destruction, making impossible the measurement on the same sample of both recombination lifetime and effective doping. We observed how the doping compensation effect vanishes increasing the temperature and therefore it is related to an acceptor-like centre within the bandgap which acts as trap for free carries.

Being a non-destructive technique, we have been able to measure the lifetime profile on the same samples, whose effective doping concentration was previously evaluated. It has been proofed that the knowledge of the local resistivity at different temperatures is essential for the better operation of the technique, whose resolution and precision is enhanced.

Effects of helium implantation have been studied in a wide dose and energy range and by means of the temperature dependence analysis the dominant recombination centers have been detected.

The obtained results are relevant because scientific literature does not propose many works which can show helium implantation effects with such a detail.

The extracted model (energy level and concentration of the recombination centers) has been used in the physically-based simulator ATLAS-Silvaco, in order to use it as a design tool for power diodes with a local control of the recombination lifetime. Recurring to a numeric analysis, we can observe how helium implantation affects power diodes performances, without manufacturing necessarily many

test samples, which would cause a slack and a cost increase of the entire production cycle.

In particular we focused our attention on the dynamic avalanche phenomenon and how a localised lifetime control can reduce this effect, which can lead even to the device destruction. Dynamic avalanche consists in the impact ionization onset during the reverse recovery, even though the diode voltage does not reach the static breakdown value. We showed that during the switching we have to define a new dynamic breakdown voltage which is function of the effective doping concentration and depletion region width for each time instant.

Helium implantation increases the recombination rate and if the damage is placed into the low-doped region dynamic avalanche effect is considerably reduced. Indeed for each time instant the effective doping concentration is lower and depletion region extends faster, leading to an increase of the dynamic breakdown voltage.

Experimental test diodes have been manufactured using the implantation energy needed to lie the damage at the same depth of the simulations. The measurements have shown that the behaviour of the experimental samples is in good agreement with the one observed with the simulator. Implanting helium into the drift region, dynamic avalanche ruggedness enhances, but on the other hand both forward voltage drop and leakage current increase. Placing the defects into the anode, static performances are less worsened but dynamic avalanche can reach the same intensity observed in the unimplanted device. Therefore the right trade-off is to be found, according to the required features of the power diode to design.

References

[1] E. Napoli, P. Spirito, A.G. M. Strollo, F. Frisina, L. Fragapane, D. Fagone, "Design of IGBT With Integral Freewheeling Diode", *IEEE Electron Device Letters*, vol.23, no. 9, September 2002

[2] S. Pendharkar and K. Shenai, "Optimization of the anti-parallel diode in an IGBT module for hard-switching applications," *IEEE Trans. ElectronDevices*, vol. 44, pp. 879–886, May 1997.

[3] H. Benda, E. Spenke, "Reverse recovery processes in silicon power rectifiers", Proceedings of IEEE, vol. 55, no. 8, August 1967

[4] M. T. Rahimo, N. Y. A. Shammas, "Freewheeling Diode Reverse-Recovery Failure Modes in IGBT Applications", *IEEE Trans. On Industry Applications*, vol. 37, no.2, March/April 2001 661

[5] V. K. Khanna, "Carrier lifetimes and recombination–generation mechanisms in semiconductor device physics", *Eur. J. Phys.* 25 (2004) 221–237

[6] S. Sze, "Semiconducto devices, physics and technology", John Wiley & Sons, Inc. 2nd Edition

[7] H. Zimmermonn, H. Ryssel, "The Modeling of Platinum Diffusion in Silicon under Non-equilibrium Conditions" *J. Electrochem. Soc.*, Vol. 139, No. 1, January 1992

[8] U. M. Rosele, "Fast diffusion in semiconductors", *Ann. Rev. Mater. Sci.* 1988. 18 : 257-82

[9] H. Zimmermann, H. Ryssel, "Observation of inverse U-shaped profiles after platinum diffusion in silicon", *Appl. Phys. Lett.*, Vol. 59, No. 10, 2 September 1991

[10] M. Valdinoci, L. Colalongo, A. Pellegrini, M. Rudan, "Analysis of Conductivity Degradation in Goldplatinum-Doped Silicon", *IEEE Trans. On Electron Devices*, vol. 43, no. 12, December 1996 2269

[11] B.J. Baliga, E. Sun, "Comparison of gold, platinum, and electron irradiation for controlling lifetime in power rectifiers", *IEEE Trans. Electron Devices,* ED-24, 685-688 (1977)

[12] R.O. Carlson, Y.S. Sun, H.B. Assalit, "Lifetime control in silicon power devices by electron or gamma irradiation", *IEEE Trans. Electron Devices,* ED-24, 1103-1108 (1977)

[13] P. Hazdra, J. Vobecky, N. Galster, O. Humbel, T. Dalibor, "A new degree of freedom in diode optimization: arbitrary axial lifetime profiles by means of ion irradiation", ISPSD 2000, May 22-25, Toulouse, France

[14] P. Hazdra, K. Brand, J. Rubes, J. Vobecky, "Local lifetime control by light ion irradiation: impact on blocking capability pf power P-i-N diode", *Microelectronic Journal*, 32 (2001) 449-456

[15] J. Vobecky, P. Hazdra, O. Humbel, N. Galster, "Crossing point current of power P-i-n diodes: impact of lifetime treatement", *MIEL 2000*, vol.2 14-17 May, 2000 Nis, Serbia

[16] P. Hazdra, J. Vobecky, K. Brand, "Optimum lifetime structuring in silicon power diodes by means of various irradiation techniques", *NIM B*, 186 (2002) 414-418

[17] A. Veron, M. Ohanisian, D. Ciocea, C. Mitroi, C., "Spin-on dopants as lifetime modifier sources in fast recovery epitaxial diodes processing", *Semiconductor Conference, 1997. CAS '97 Proceedings., 1997 International*, Page(s): 225-228 vol.1

[18] J. Vobecky, P. Hazdra, J. Homola, "Optimization of power diode characteristics by means of ion irradiation", *Electron Devices, IEEE Transactions on*, vol. 43, issue 12, Dec. 1996 Page(s):2283 – 2289

[19] D.K. Schroder, "Semiconductor material and device characterization", John Wiley & Sons, Inc., 1990

[20] D.V. Lang, Deep-level transient spectroscopy: A new method to charactrize traps in semiconductors, Appl. Phys. A 26 (1981) 191

[21] P. Spirito, G. Cocorullo, "A measurement technique to obtain the recombination lifetime profile in epi layers at any injection level", *Electron Devices, IEEE Transactions on*, vol. 34, Issue 12, Dec 1987 Page(s):2546 – 2554

[22] P. Spirito, G. Cocorullo, "Measurement of recombination lifetime profiles in epilayers using a conductivity modulation technique", *Electron Devices, IEEE Transactions on,* vol. 32, Issue 9, Sep 1985 Page(s):1708 – 1713

[23] S. Daliento, A. Sanseverino, P. Spirito, "An improved model for extraction of strongly spatial dependent lifetimes with the AC lifetime profiling technique", *Electron Devices, IEEE Transactions on,* vol. 46, Issue 8, Aug. 1999 Page(s):1808 – 1810

[24] S. Daliento , L. Mele, P. Spirito, B.N. Limata, "All electrical resistivity profiling technique for ion implanted semiconductor

materials", *Materials Science and Engineering B,* vol. 124-125, 5 December 2005, Pages 310-313

[25] ATLAS Users Manual. Santa Clara, CA: Silvaco International

[26] S. Daliento, L. Mele, P. Spirito, L. Gialanella, B. N. Limata , Lifetime and resistivity modifications induced by helium implantation in silicon: experimental analysis with the ac profiling technique, Journal of Applied Physics, accepted

[27] A. Sanseverino, P. Spirito, "The effect of recombination centers on the lifetime dependence upon temperature and injection level", *Power Electronics and Applications*, 1993, Fifth European Conference on, 13-16 Sep 1993 Page(s):58 - 62 vol.2

[28] R.E. Whan, "Investigation of oxygen-defect interactions between 25 and 700K in irradiated germanium", *Physical Review,* vol.140 no. 2A, October 1965

[29] A. Hallén N. Keskitalo, L. Josyula, B. G. Svensson, "Migration energy for the silicon self-interstitial", J. Appl. Phys., vol. 86, Issue 1, pp. 214-216, July 1, 1999

[30] G. D. Watkins, "Radiation Damage in Semiconductors", (Dunod, Paris, 1964), p. 97.

[31] S. Coffa, V. Privitera, F. Priolo, S. Libertino, G. Mannino, "Depth profiles of vacancy- and interstitial-type defects in MeV implanted Si", *J. Appl. Phys.* 81 (4), 15 February 1997

[32] G. D. Watkins, "Lattice Vacancies and Interstitials in Silicon", *Chinese Journal of Physics* vol. 15, no. 2 summer, 1977

[33] S.-H. Yoon, K.-D. Kwack, B.-G. Ko, J.-G. Park, J.-Y. Kim, H. Ruh, "Oxygen precipitation and secondary defects in silicon by high energy ion implantation and two-step annealing", Journal of Applied Physics, vol.86 no. 5, Septmber 1989

[34] P. Spirito, S. Daliento, A. Sanseverino, L. Gialanella, M. Romano, B.N. Limata, R. Carta, L. Bellemo, "Characterization of recombination centers in Si epilayers after He implantation by direct measurement of locl lifetime distribution with the ac lifetime profiling technique", *IEEE Electron Devices Letters*, vol. 25, no. 9, September 2004

[35] R. Siemieniec, H.-J. Schulze, F.-J. Niedernostheide, W. Südkamp, J. Lutz, "Compensation and doping effects in heavily helium-radiated silicon for power device applications", *Microelectronics Journal* Volume: 37, Issue: 3, March, 2006, pp. 204-212

[36] www.srim.org

[37] B.G. Svensson, B. Mohadjeri, A. Hallen, J.H. Svensson, J.W. Corbett, "Divacancy acceptor levels in ion-irradiated silicon", *Phys. Rew. B*, Vol. 43, Number 3 (1991)

[38] D.C. Schmidt, J.F. Barbot, C. Blanchard, P. Desgardin, E. Ntsoenzok, G. Blondiaux, "Studies of deep levels in He+ -irradiated silicon", *Applied Physics A* 65, 1997

[39] P. Hazdra, J. Rubes, J. Vobecky, "Divacancy profiles in MeV helium irradiated silicon from reverse I-V measurement", *Nuclear Instruments and Methods in Physics Research B* 159 (1999) 207-217

[40] A. Mulay, M. Trivedi, K. Shenai, "Dynamic Avalanching Considerations in Optimization of Reverse Conducting Diode in IGBT Modules", 1998 *IEEE BCTM*

[41] M.T. Rahimo, N.Y,A Shammas, "Reverse Recovery Failure Modes in Modem Fast Recovery Diodes", *Proc.. 22nd International Conference on Microelectronics (MIEL 2OOO)*, vol. 2, Nis, Serbia, 14-1 7 MAY, *2000*

[42] Munaf T. Rahimo, N. Y. A. Shammas, "Freewheeling Diode Reverse-Recovery Failure Modes in IGBT Applications", *IEEE Transactions on industry applications*, vol. 37, no.2, march/april 2001 661

[43] M. Domeij, J. Lutz, D. Silber, "On the Destruction Limit of Si Power Diodes During Reverse Recovery With Dynamic Avalanche", *IEEE Trans. On Electron devices*, vol. 50, no. 2, February 2003

[44] F.-J. Niedernostheide, H.-J. Schulze, "Studies on dynamic avalanche and current filaments in high-voltage diodes", *Physica D: Nonlinear Phenomena,* vol. 199, Issues 1-2, 1 December 2004, Pages 129-137

[45] H. Schlangenotto, H. Neubrand, *Arch. Elektrotech.* 72 (1989), p. 113.

[46] Martin Domeij, B. Breitholtz, Josef Lutz, M. Oèstling, " Dynamic avalanche in Si power diodes and impact ionization at the nn+ junction", *Solid-State Electronics* 44 (2000) 477-485

[47] R. Siemieniec, J. Lutz, R. Herzer, "Analysis of Dynamic Impatt Oscillations caused by Radiation Induced Deep Centers", *ISPSD 2003*, April 14-17, Cambridge, UK

[48] R. Siemieniec, J. Lutz, R. Herzer, "Analysis of dynamic impatt oscillations caused by radiation induced deep centres with local and

homogenous vertical distribution", *IEE Proc.-Circuits Devices Syst.*, Vol. 151, No. 3, June 2004

[49] J. Lutz, "Fast Recovery Diodes - Reverse Recovery Behaviour and Dynamic Avalanche", *Proc.. 24th International Conference on Microelectronics (MIEL 2004)*, vol. 1, Nis, Serbia, 16-19 May 2004

[50] B. Jayant Baliga, Modern power devices, A Wiley-Interscience publication, 1987

[51] S. Pendharkar, M. Trivedi, K. Shenai, "Dynamics of Reverse Recovery of High-power P-i-N Diodes," *IEEE Trans. Electron Devices*, vol. 43, no. 1, pp.142-149, 1996.